Developing a Framework to Design a Building Envelope Integrated with PCM

Arash Bastani

A Thesis

In the Department

of

Building, Civil and Environmental Engineering

Presented in Partial Fulfillment of the Requirements

For the Degree of

Doctor of Philosophy (Building Engineering) at

Concordia University

Montreal, Quebec, Canada

August 2014

CONCORDIA UNIVERSITY
SCHOOL OF GRADUATE STUDIES

This is to certify that the thesis prepared

By: Arash Bastani

Entitled: Developing a Framework to Design a Building Envelope with PCM Wallboards

and submitted in partial fulfillment of the requirements for the degree of

Doctor of Philosophy (Building Engineering)

complies with the regulations of the University and meets the accepted standards with respect to originality and quality.

Signed by the final examining committee:

_____ Chair
Dr. J. Paquet

_____ External Examiner
Dr. A.M. Malkawi

_____ External to Program
Dr. A. Dolatabadi

_____ Examiner
Dr. Z. Chen

_____ Examiner
Dr. R. Zmeureanu

_____ Thesis Co-Supervisor
Dr. F. Haghighat

_____ Thesis Co-Supervisor
Dr. J.A. Kozinski

Approved by: _____
Dr. F. Haghighat , Graduate Program Director

August 22, 2014 _____
Dr. A. Asif, Dean
Faculty of Engineering and Computer Science

ABSTRACT

Developing a Framework to Design a Building Envelope Integrated with PCM

Arash Bastani, Ph.D

Concordia University, 2014

While space conditioning load contributes largely to the grid critical peak, shifting it partially or entirely to the off-peak period could have significant economical impact on both energy supply and demand sides. This shifting technique is accomplished by storing energy during off-peak periods in order to be utilized during peak periods. The building envelope integrated with phase change material (PCM) can provide latent heat thermal energy storage (TES) distributed in its entire surface area and inhibit the enhanced thermal mass in light weight buildings. Selecting the most appropriate PCM wallboard based on its thickness and thermo-physical properties, is the main target; yet, there is a lack of an appropriate design tool. Accordingly, this dissertation focuses on the development of a design framework to quantify and qualify the application of PCM wallboards in a building envelope in order to efficiently shave and shift the demand peak.

In this study, the non-dimensionalized analysis was conducted, and the dimensionless numbers influencing the thermal behavior of a PCM wallboard were identified. Moreover, the correlations between the dimensionless parameters and the performance of the PCM wallboard were determined through a comprehensive parametric study. Consequently, these correlations were presented as the design framework to select and size a PCM wallboard. The tool consists of a number of charts

identified as the extension of the well-known Heisler chart of transient temperature and heat transfer for materials that undergo the phase transition.

Finally, the developed design framework was applied to select and size three PCM wallboards for an existing residential house, and TRNSYS simulation software was used to study the thermal performance of the house furnished with the PCM wallboard. The application of PCM wallboards was evaluated for both charging and discharging periods at three different outdoor climates: cold, very cold, extremely cold. It was observed that the tool can appropriately size the wallboards to efficiently store energy and postpone the peak. In addition, the wallboard with the thickness identified by the framework provides the longest shift of load compared to other simulated sizes of the same material. Moreover, the building refurbished with either one of those PCM wallboards was able to have longer shift of load and lower daily energy consumption than the conventional gypsum board.

ACKNOWLEDGMENTS

First and foremost, I would like to express my deepest gratitude to my supervisor, Dr. Fariborz Haghighat, for his continuous motivation, inspiration and support throughout my study. I am grateful for the invaluable advice, both professional and personal, which he gave me over these years. I also want to thank my co-supervisor, Dr. Janusz Kozinski, for his advice and support throughout my study. His guidance was invaluable and greatly contributed to my success in my research.

I also gratefully acknowledge my supervising committee: Dr. Radu Zmeureanu, Dr. Ali Dolatabadi, and Dr. Zhi Chen for their knowledgeable advice. This thesis owes an enormous debt to them due to their intellectual contributions.

I would like to acknowledge the Hydro-Quebec research laboratories (Laboratoire des Technologies de l'Energie) in Shawinigan, Quebec, for providing the data and information of the residential building. Special thanks are due to Mr. Alain Moreau whose recommendations made the building simulation feasible. In addition, my sincere appreciation is given to Dr. Frederic Kuznik and Dr. Kevyn Johannes from the Thermal Science Center of Lyon (INSA) for providing the PCM simulation type in TRNSYS.

I am also grateful for the financial support by the Natural Science and Engineering Research Council of Canada (NSERC) discovery grant, Concordia Research Chair and Public Works and Government Services of Canada.

I would like to thank all my colleagues in the energy and environment research group at Concordia University for stimulating exchange of ideas and creating a

supportive atmosphere. I would like to extend my gratitude to my best friends, Arash Amirkhany, Maziar Dehghani, Arash Rakhshanpoor, Laurent Magnier, Parham Mirzaei, Hamid Kholafaei, Kian Alaeddinin Omid Ashrafi, and Nazanin Hashemi for their unconditional support and love.

Last but not least, I wish to express my warmest appreciation and love to my wonderful parents, Masoomeh and Pirooz, my kindhearted sister, Parastoo, my trustworthy brother and friend, Kaveh, and my beloved friend and brother-in-law Arash Soleimani for their continuous inspiration and support. I am indebted to their unconditional love and encouragement. To my lovely family, this thesis is dedicated.

TABLE OF CONTENT

LIST OF FIGURES

LIST OF TABLES

LIST OF SYMBOLS

English Symbols	Description
x	Space coordinate [m]
C	Specific heat capacity [J kg^{-1} K^{-1}]
k	Thermal conductivity [W m^{-1} K^{-1}]
t	Time [s]
L	Latent heat [J kg^{-1}]
s	Interface position [m]
H	Volumetric enthalpy [J m^{-3}]
T	Temperature [°C]
l	Thickness of PCM wallboard [m]
f(T)	Liquid fraction
h	Overall room heat transfer coefficient [W m^{-2} K^{-1}]
A_1	Coefficient as a function of *Bi*

Greek Symbols	Description
ρ	Density [kg m^{-3}]
α	Thermal diffusivity [m^2 s^{-1}]
λ_1	Coefficient as a function of *Bi*
ΔT	Melting range

Dimensionless Parameters	Description
Ste	Stefan number
Bi	Biot number
Fo	Fourier number
X	Dimensionless space coordinate
θ	Dimensionless temperature
ψ	Dimensionless temperature constant

Subscript	Description
f	Fusion
ref	Reference
s	Solid/Solidification
m	Melting
l	Liquid
in	Indoor
ex	Exterior
low.Op.Temp.	The lowest operating temperature
High.Op.Temp.	The highest operating temperature
pc	PCM indicator
op	Operating temperature indicator
∞	Ambient
i	Initial
hl	Half liquefied
fl	Fully liquefied
ss	Steady state

Abbreviations	Description
PCM	Phase Change Material
TES	Thermal Energy Storage
IEA	International Energy Agency
TABS	Thermally-Activated Building Systems
TMA	Thermal Mass Activation
DSC	Differential Scanning Calorimeter

CHAPTER 1 INTRODUCTION

1.1 BACKGROUND

Nowadays, the growth of energy usage raises concerns over exhaustion of energy resources, heavy environmental impact (ozone layer depletion, global warming, etc.) due to the excessive green house gas emission and supply difficulties. According to Perez-Lombard et al. (2008), in 20 years the primary energy consumption has grown by 49% and CO_2 emissions by 43%, with an average annual increase of 2% and 1.8%, respectively. Considering different sectors as the final energy consumers, the building sector is one of the main consumers. According to Natural Resources Canada (2011), Figure 1.1, more than 30% of the total secondary energy was used by residential and commercial/institutional buildings. This fact implies that the building sector contributes largely in total energy consumption. Particularly, in extremely cold/hot climate areas, space heating/cooling results in high energy consumption. The data from National Resources Canada (2011), Figure 1.2, also shows that space heating accounts up to 63% of the total energy used in non-industrial buildings.

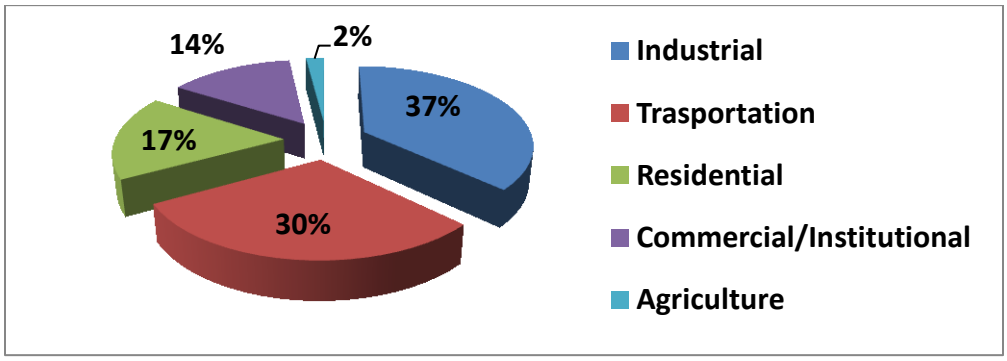

Figure 1.1 Total secondary energy used by the sectors in Canada, 2009 (Natural Resources CANADA, 2011)

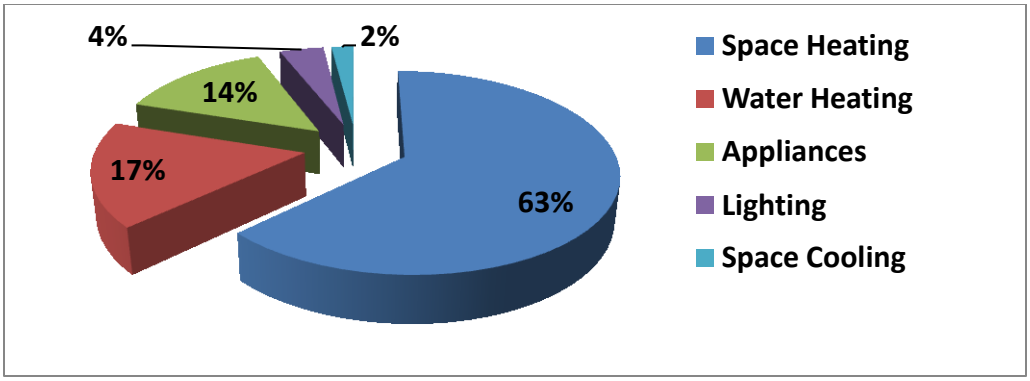

Figure 1.2 Distribution of residential energy use, 2009 (Natural Resources CANADA, 2011)

Extracted from this data, electricity is an exclusive source of energy for space conditioning in buildings. Its total usage varies during a day due to the combination of activities in industrial, commercial, and residential sectors. This results in peak (mostly in early morning) and off-peak periods. In Quebec, Canada, 70% of residential buildings and 60% of the commercial and institutional sector utilize electricity for space conditioning (HydroQuebec, 2007). 80% of the total load of all-electric households during peak hours results from space conditioning. Also, the combined space heating load of the non-industrial buildings accounts for almost 40% of the total electric utility peak during winter peak hours (Leduc et al., 2011). According to Hydro Quebec (2011), during the peak period in winter the electricity cost for the supply side is 10 $/kW and will be increased up to 40 $/kW in 2015.

Taking this information into account, shifting a significant portion or the entire space conditioning energy consumption to off-peak periods would have significant economical impact for both supply and demand side. The shifting of the demand from peak periods to off peak periods can result in a significant reduction of a building's

operational costs of the demand side (Khudhair and Farid, 2004). Meanwhile, the capital investment in the equipment that generates power in peak periods may reduce on the supply side.

Herter et al. (2007) reported that automated control strategy is an effective demand response to reduce the peak load while preserving the occupant thermal comfort. In the last decade, there were a number of studies investigating the application of control strategies along with building thermal mass and thermal storage to reduce the space conditioning load in peak hours (Braun and Lee, 2006a; Braun and Lee, 2006b; Lee and Braun, 2008a; Lee and Braun, 2008b; Liu and Henze, 2006a; Liu and Henze, 2006b; Peng and Haves, 2006). Yang and Li (2008) investigated the relationship between a building thermal mass and its air conditioning cooling load in order to characterize the best design of the building thermal mass to effectively reduce and shift the load during peak hours by night conditioning. Moreover, Leduc et al. (2011) compared different control strategies for heating season in Quebec, Canada to shift and shave the heating load during peak hours. Their evaluation concludes that preheating the building envelope thermal storage during night time with set-point temperature at 25°C and set back during peak hours is the most efficient strategy to shave and shift the heating load.

Common in all the relevant research, the thermal energy is stored as sensible heat during off-peak hours for later application during peak hours. However, potentially, the efficiency of the shifting method can be improved if the thermal energy storage is in the form of latent heat. Latent heat storage results from the absorption and release of the heat of fusion when a material undergoes a phase change phenomenon. It is more preferred

than sensible heat storage due to its high-energy storage density and its nearly isothermal nature which occurs around the fusion temperature of a phase change material (PCM). According to Dutil et al. (2011), the latent heat stored in a PCM wallboard is comparable to sensible heat stored in a concrete wallboard when its temperature increases for 200°C. Therefore, this high latent heat capacity storage can be accompanied by an appropriate control strategy to extend the shifting period and improve the building thermal performance efficiency.

Beside the application of PCM in hot water tank (Nkwetta et al., 2014) and mechanical ventilation system (El-Sawi et al., 2014), it can also be integrated in a building envelope to improve its thermal storage efficiency. Many studies which tackled the application of PCM wallboards in a building envelope are summarized and analyzed in detail in the next chapter of this dissertation. The medium can be located either in the ceiling, on the floor or in wall sections. Furthermore, its location will differ in relation to the insulation layer based on climate conditions, for instance, it is more efficient to place it between the insulation and indoor space for cold climate regions. Nevertheless, there is a lack of a general framework to select and size a PCM wallboard which can be employed along with an appropriate control strategy to shift and shave the peak load.

1.2 OBJECTIVES

The objectives of this study are:

- Characterizing the parameters influencing the thermal performance of PCM wallboards with regard to the storage and release of latent heat energy

- Developing a framework to quantify and qualify the application of a PCM wallboard in a building envelope
- Investigating the effective design parameter of the PCM wallboards for a real residential house utilizing the developed design framework

1.3 THESIS OUTLINE

Chapter 2 contains the fundamentals of heat transfer in PCM and the critical reviews of previous studies on the application of PCM wallboards in a building envelope. Chapter 3 reports the development of numerical model to simulate the thermal behavior of a PCM wallboard, and the non-dimensionalization procedure of the problem formulation. It then presents the characterization of the effective parameters on the thermal performance of a PCM wallboard. At the end of this chapter, the validation procedure is described. Chapter 4 describes the developed framework to size a PCM wallboard for a building to shift its space conditioning load to off-peak periods. The framework is based on a number of parametric studies conducted on the impact of the effective parameters on the thermal performance of a PCM wallboard. Chapter 5 discusses the application of the developed framework to size three PCM wallboards for an existing residential building. This chapter includes the evaluation of the design framework and the impact of the designed PCM wallboards on the shift of space heating load. Finally, Chapter 6 summarizes the conclusions of this research and makes recommendations for future studies.

CHAPTER 2 LITERATURE REVIEW

2.1 APPLICATION OF PCM AS A THERMAL STORAGE

The energy efficiency of buildings can be improved by reducing the mismatch between supply and demand of the energy. In passive solar designed buildings, the energy density is time-dependant and the source of energy, i.e. solar energy, is intermittent. The mechanically air conditioned buildings also intermittently consume energy whose expenditure depends on the building occupant's activities and behaviours. The application of thermal energy storage (TES) can be a promising method to improve the energy efficiency of a building for both heating and cooling processes. Indeed, TES is utilized to redeem the mismatch between the time that energy is required (i.e. peak period) and the time with the most economically favorable supply of energy (i.e. off-peak period).

Generally, the building thermal mass can act as a medium to store thermal energy, help decrease the external heat flow and prevent the indoor temperature swing (Russell and Surendran, 2001). Nowadays, thermally-activated building systems (TABS) integrate building structures as the thermal energy storage to flatten the peak load and to shift it to off-peak periods. The systems range from cooling to heating and exploit the dynamic thermal behaviour of building elements: Building envelope to store space conditioning thermal energy during off-peak periods and releasing it during peak periods. The thermal energy can be stored either as sensible or latent heat. The International Energy Agency (IEA) presented an overview of the application of TABS in the context of the Annex 44, "Integrating Environmentally Responsive Elements in Buildings", and characterized

thermal mass activation (TMA) into two categories: internal TMA and external TMA (IEA ANNEX 44, 2009). Lehmann et al (2007) and Gwerder et al. (2008) investigated the application of the TABS with control strategies to store thermal energy in conventional building materials as sensible heat to enable the reduction of energy consumption during the peak hours. Beside the conventional building material i.e. concrete and brick, the incorporation of PCM in building elements provides the opportunity to store both sensible and latent heat. Latent heat is more preferred than sensible heat storage due to its high-energy storage density and its nearly isothermal nature which occurs around its fusion temperature. Therefore, the combination of a PCM layer in a building envelope and a control strategy to manage the charging and discharging of the PCM can provide a storage capacity to reduce and shift the space conditioning load to off peak periods.

2.2 PCM WALLBOARD AND ITS MANUFACTURING FOR BUILDING APPLICATIONS

The latent heat storage is the main reason to utilize PCMs in building applications. Compared to the conventional materials used for their sensible heat storage, PCMs have the advantage to store larger amounts of thermal energy in much smaller mass. The storage capabilities can be used for both heating and cooling applications. For cooling applications, PCM stores energy when it is solidified and releases its energy during melting process. For heating applications, however, it acts in reverse. Therefore, integrating PCM in building thermal elements improves building thermal capacity. To have a desired integrated PCM, the following specifications are important;

- Suitable thermo-physical parameters including latent heat, specific heat, thermal conductivity, fusion temperature and melting range
- Physical stability including no-phase segregation, high thermal cycle and small volume change
- Safe application including non-toxic off-gassing and inflammability
- Non-corrosive properties and compatibility with conventional building materials

It is worth to emphasize that any PCM wallboard needs to be mechanically stable to be properly applied in a building envelope which was studied in details by Hawes (1991).

Generally, PCMs are classified in three groups: inorganic compound, organic compound and eutectics of organic and/or inorganic compounds. Each group has advantages and disadvantages which are explained in detail in (Mehling and Cabeza, 2008). Organic PCMs possess some general advantages such as chemical and thermal stability, non-corrosiveness, almost no sub-cooling and self-nucleating. They can provide a latent heat storage density between 120 kJ/kg and 240 kJ/kg and have a melting temperature in a range of 20ºC to 80ºC. The phase change phenomenon occurs in a relatively wide range of temperatures in organic PCMs. Some of their notable disadvantages are inflammability, relatively low heat of fusion and low thermal conductivity. Paraffin and fatty acids are the common organic compounds used as PCM in building applications. On the other hand, inorganic PCMs are not flammable; they can provide a high storage of latent heat and thermal conductivity. The common inorganic PCMs are salt hydrates which have a latent heat density between 170 kJ/kg and 450 kJ/kg

and a melting temperature in the range of 18ºC to 90ºC. The main disadvantages of these PCMs are sub-cooling, corrosiveness, phase segregation and thermal as well as chemical instability. Eutectic PCMs are a mixture of either organic, inorganic or a combination of both compounds. These materials have latent heat storage capability between 120 kJ/kg and 230 kJ/kg and a melting temperature in the range of 18ºC to 80ºC. The common PCMs in building applications and their physical properties are discussed in (Farid et al., 2004; Kuznik et al., 2011; Zalba et al., 2003).

The application of PCM as a TES in buildings was reviewed by previous researchers (Baetens et al., 2010; Khudhair and Farid, 2004; Verma et al., 2008; Zhang et al., 2007). One way to improve the thermal inertia of a building is to integrate PCM layers in its envelope. Due to the considerably large surface area of a building envelope, integrating PCM in the envelope can provide a TES with a large capacity. Regular building wallboard can be a medium to accommodate PCMs. The wallboard enhanced with PCM can provide TES distributed in the whole surface area of the building shell and prevent the enhanced thermal mass in light weight buildings. To manufacture PCM wallboards, three methods can be utilized: direct integration, impregnation, and encapsulation. In direct integration, PCM powder is mixed with common building material during the manufacturing procedure (Feldman et al., 1991); while in impregnation, the conventional wallboards are immersed in hot molten PCM (Kaasinen, 1992; Shilei et al., 2007). Although, these two methods can be implemented easily, the leakage of the liquefied PCM from the enhanced wallboard represents a major issue (Schossig et al., 2005). To avoid this problem, the encapsulation of PCM inside the conventional building wallboard was elaborated as a manufacturing technique. In this

method, capsules in various sizes are filled with PCM and integrated in the conventional wallboard during its manufacturing process. Hawlader et al. (2003) documented two methods to produce encapsulated PCM wallboards and investigated the effect of different parameters such as the distribution of capsules on the thermal performance of the PCM layer. The encapsulation of PCM in the wallboard inhibits both direct contact between PCM and the conventional wall component and the possible leakage of PCM at the liquid state. Moreover, by providing high surface/volume ratio, the encapsulation results in increasing the heat transfer area (Farid et al., 2004). However, the interaction between the containers and the wallboard material may lead to corrosion problems (Verma et al., 2008) or a decrease in the mechanical strength of the wallboard (Cabeza et al., 2007). Recently, the encapsulation technique was improved and new types of PCM wallboards, called shape-stabilized PCM, were produced (Xu et al., 2005). They consist of macromolecule material as the container and paraffin as the dispersed PCM. Paraffin is micro-encapsulated in the supporting material and decreases the chance of leakage during the phase transition. Regarding the mechanical stability of PCM wallboards, (Hawes, 1991)

2.3 Modeling of Phase Change Phenomenon in PCM Wallboards

Unlike an experimental study, numerical analysis can be conducted faster and more cost-efficiently to investigate a phenomenon. The validated model can always be employed for parametric studies and offers more general applications than an experimental work. The modeling of PCM is employed to simulate the phase change procedure inside the material and predicts its thermal performance. The main difficulty in

modeling a PCM occurs during its melting and/or solidification state. When the temperature of the PCM reaches its melting temperature range, the material gradually changes from one phase to another one. This creates an interface between both phases which gradually moves toward one of the phases based on whether PCM is absorbing or releasing the latent heat. The displacement rate of this interface depends on the rate of absorption and release of latent heat. The moving interface between the phases leads to the moving boundary problem. The location of this boundary is unknown as a priori, and it is part of the solution. Thus, the system has a non-linear nature which creates certain challenges in the modeling procedure.

Having complete knowledge of the thermo-physical properties of a PCM and how they change during phase transition is essential in the simulation and analysis of the thermal dynamic of the PCM and its latent heat storage. There are three methods for measuring the thermo-physical properties of a PCM wallboard:

- Differential scanning calorimetry (DSC) (Kuznik and Virgone, 2009b)
- T-history method (Marín et al., 2003)
- Guarded hot-plate (Darkwa and Kim, 2005)

These techniques provide the heat of fusion, melting temperature range (solidification temperature and melting temperature), and specific heat capacity of the material as a function of temperature.

The general energy balance equation is employed to model the heat transfer phenomena in PCM. This equation consists of advection and diffusion terms. The

advection term includes both unsteady and natural convection terms. With regards to PCM wallboards, assuming no convection heat transfer inside the liquid zone of PCM is widely accepted. Comparing the heat transfer characteristic length inside an encapsulated or impregnated PCM with the whole wall section thickness, assuming a negligible convection heat transfer is acceptable. By neglecting the convection heat transfer, the general energy balance equation is reduced to the heat equation;

$$\frac{\partial(\rho CT)}{\partial t} = \vec{\nabla}\left(k\vec{\nabla}T\right) \tag{2-1}$$

where ρ [kg.m^{-3}] is the density, C [J.kg^{-1}.K^{-1}] is the specific heat capacity, k [W.m^{-1}.K^{-1}] is the thermal conductivity, and t [s] is time. Unlike the case dealing with one phase, heat capacity changes notably with temperature, particularly, during the phase change procedure.

Although some researchers conducted two dimensional simulations (Ahmad et al., 2006a; Alawadhi, 2008; Carbonari et al., 2006), assuming a unidirectional heat transfer through a PCM wallboard is widely utilized, due to the large surface of a wall comparing to the thickness of a PCM layer.

Dutil et al. (2011) documented the available numerical technique and solving schemes in modeling PCMs. To model a wallboard enhanced with PCM two methods have been proposed to treat the changing parameters in addition to the moving interface inside the PCM. The main difference between these methods is the way they deal with the medium phase variation. Herein, these methods are called: single liquid-solid

interface method, and enthalpy method. These methods are employed to characterize the thermal behaviour of a PCM wallboard integrated in a building envelope.

2.3.1 The single liquid-solid interface method:

In this method, the PCM during the phase change procedure consists of two phases: liquid and solid, and the border between two phases is treated as a two dimensional interface (the moving interface). The heat equation governs the temperature distribution in each single phase separately, and the moving interface is treated as the energy balance in the moving boundary follows the Stephan condition (Dutil et al., 2011);

$$L\rho\left(\frac{ds(t)}{dt}\right) = k_s\left(\frac{\partial T_s}{\partial n}\right) - k_l\left(\frac{\partial T_l}{\partial n}\right) \quad (2\text{-}2)$$

where L [J.kg^{-1}] is the latent heat of the PCM, $s(t)$ [m] is the interface position, and $\partial/\partial n$ is the derivative following the normal vector at any point of the interface. Halford and Boehm (2007) applied this method to simulate a wall with an encapsulated PCM layer. They assumed one dimensional heat transfer to study the effect of the location of the PCM sandwiched between two insulation layers.

This method does not detect the temperature variation between two phases and would be more suitable for materials with a single melting temperature. However, due to the different physical properties of both phases, discontinuity may occur in this numerical technique.

2.3.2 The enthalpy method:

In this method, PCM is treated with three separate zones during the phase change procedure: solid, liquid, and mushy zone. The mushy zone is a transient zone between solid and liquid. In this zone PCM exists within the wallboard in both the solid and liquid phase simultaneously. The governing equation for this model is re-configured to consider enthalpy as the variable. This equation is identical for both phases; the single interface is replaced and treated as the mushy zone between the two phases. The creation of the mushy zone and the rate of change of its volume and thickness are governed by the rate of absorption/release of the latent heat. Generally, the equation for enthalpy method is;

$$\frac{\partial H(T)}{\partial t} = \vec{\nabla}(k\vec{\nabla}T) \tag{2-3}$$

where H [J.m^{-3}] is the volumetric enthalpy of the material as a function of temperature. It consists of both sensible and latent heat. While the sensible heat is a product of heat capacity, density and temperature, the latent heat is quantified by the rate of change of the liquid fraction as follows;

$$H(T) = h(T) + \rho L f(T) = \int_{T_f}^{T} \rho C_p dT + \rho L f(T) = \int_{T_r}^{T} \rho C_p(T) dT \tag{2-4}$$

Here, T_f [°C] is the fusion temperature, T_r [°C] is the reference temperature, and *f(T)* is the liquid fraction as a function of temperature.

$$f(T) = \begin{cases} 0 & T < T_f \ Solid \\ ]0,1[& T = T_f \ Mushy \\ 1 & T > T_f \ Liquid \end{cases} \tag{2-5}$$

Thus, the governing equation for the whole PCM system is:

$$\frac{\partial h(T)}{\partial t} = \vec{\nabla}\left(k\vec{\nabla}T\right) - \rho L\frac{\partial f}{\partial t} \quad (2\text{-}6)$$

Here, the phase-change phenomenon occurs in the mushy zone, and the absorption/release rate of the latent heat is quantified by the rate of change of the liquid fraction in this zone. Mirzaei and Haghighat (2012) applied this method to simulate the thermal dynamic of a PCM wallboard. This method has another variation in which the absorption/release of the latent heat is not quantified by the rate of change of the liquid fraction. The function presents the evolution of the heat capacity is utilized to measure the enthalpy at each point with its specified temperature. The heat capacity equation can be calculated experimentally (Kuznik and Virgone, 2009a), or theoretically (Kondo et al., 2000). Some studies, also, resemble the trend of the evolution of the specific heat capacity with Gauss function or linear function (Diaconu and Cruceru, 2010).

This method prevents the discontinuity of the former method and its possible numerical instability. However, the procedure to quantify the rate of change of liquid fraction may have a negative impact on the accuracy of the method.

2.4 Related Building Design

PCM wallboards can have various applications based on their phase change temperature intervals: While a PCM with a melting temperature over 50ºC is employed for active layers such as radiant floors; in passive design and leveling the heat load, materials with intermediate melting range (20 ºC-30ºC) are utilized (Khudhair and Farid, 2004). In passive design, the storage medium receives energy from exposure to solar

radiation, long wave radiation from other surfaces and internal loads. For cooling, heat transfer occurs between the storage medium and the cold, night time outdoor air by convection and the sky by radiation. Enhancing the thermal capacity of a building envelope using PCM wallboards in passive design results in a shift of required energy consumption and reduction of heating energy consumption (Zhou et al., 2007). On the other hand, for cooling season, the coolness of the outdoor air at night can be stored in PCM layers to shift and reduce the cooling load during the next day. Unlike the passive design, PCM wallboards can be installed in a building envelope accompanied by an auxiliary heater/cooler to create a thermally active layer with high thermal capacity. Many scientists investigated various applications of PCM wallboards, layers in building envelopes and proposed different design criteria. The PCM wallboards can be located in walls, ceilings and/or floors (Farid and Chen, 2001; Heim and Clarke, 2004; Koschenz and Lehmann, 2004; Voelker et al., 2008). These investigations were conducted either experimentally or numerically. Generally, the experiments were conducted to provide the required data for validation. However, numerical studies were conducted to simulate the effect of various parameters for a wider range of applications in order to study the impact of PCM on a building thermal performance in different weather and operational conditions. In addition, these investigations were carried out either to determine the characteristics of a single PCM wallboard (Ahmad et al., 2006b; Koschenz and Lehmann, 2004; Weinläder et al., 2005) or to assess the effects of PCM wallboard on the entire building thermal performance (Darkwa and O'Callaghan, 2006; Heim, 2010)

2.4.1 PCM layer on the floor and in the ceiling:

Farid and Chen (1999) investigated the application of a PCM layer integrated in an under floor electric heating system as an active layer for domestic space conditioning. They suggested a set of design parameters for the PCM layer to efficiently store energy to heat the space uniformly during the day while the heater was operated only 8 h during the off-peak period. The PCM that was used was a wax with a melting temperature of 40°C. They simulated the phase-change using the effective heat capacity technique. They only considered the floor in their simulation, and there was no heat transfer through the walls or the ceiling. They claimed that the proposed design can shift 7.2 MJ/m^2day of electricity to the night time.

Lin et al. (2004; 2005) presented the application of shaped-stabilized PCM accompanied by an electrical heater on the floor as an active layer. They investigated the shift of space heating to the night time by storing energy in the PCM layer. They conducted a parametric study to find the optimum design parameters of PCM to achieve thermal comfort during the day by heating the PCM for 9 h in off-peak periods. Their design shifted 50% of the total heating load to the night time. Following this study, they investigated the impact of the melting temperature range, thermal conductivity, layer thickness and heat of fusion of the shaped stabilized PCM on the indoor temperature swing in a passive solar design (Xu et al., 2005). Their observations confirmed, similar to those of other researchers, that the suitable melting temperature of the PCM layer is equal to the average room temperature in a sunny day. Selecting the suitable melting temperature shaved the peak indoor temperature up to 10ºC. They also found that the

latent heat and the conductivity of the PCM layer should be larger than 120 [$kJ.kg^{-1}$] and 0.5 [$W.m^{-1}K^{-1}$], respectively.

Ceron et al. (2011) experimentally investigated a new tile which included PCM to furnish the floor to save energy during both heating and cooling seasons. They tested a mixture of paraffinic composition inside the tile. They found that the application of this new tile stabilizes the room temperature in the winter and absorbs the heat inside the room in the summer time when the PCM melting point is less than average room temperature. Moreover, the results showed that the tiles receiving direct solar radiation are more effective in heating the space in the winter time.

Pasupathy and Velraj (2008) numerically and experimentally investigated the application of inorganic eutectic PCM in a roof slab. Double layer PCM was suggested for year-round thermal management in passive design. Like Diaconu and Cruceru (2010), they suggested higher melting temperature for the outer PCM layer. To completely melt and solidify in a cyclic manner, the outer PCM layer needs to have a melting temperature of at least 6-7ºC higher than the average ambient temperature. The thickness of this layer also needs to be at least 4 cm to prevent the fluctuation of the ceiling surface temperature. In another work, they proposed the application of the PCM layer accompanied by a water pipe as the external heat extractor (Pasupathy et al., 2008). The suggested design was interesting for summer time when the outdoor temperature does not decrease sufficiently to solidify the PCM. Both the experiment and the numerical analysis were conducted in two identical test rooms in which all surfaces were insulated except for the roof. The

results showed that the required water capacity to cool down the PCM layer is very large, which is impractical.

2.4.2 PCM wallboards

Neeper (2000) studied the thermal dynamics of a gypsum wallboard impregnated with fatty acid and paraffin waxes which were subject to diurnal variation of the indoor and outdoor temperature as interior or exterior wallboard in passive solar design. He investigated the effect of PCM fusion temperature, phase change temperature range and PCM latent heat. He suggested a PCM with fusion temperature equal to the average room temperature and a narrow melting range (around 2º).

Kuznik et al. (2008a) experimentally and numerically investigated a commercial micro-encapsulated PCM wallboard in a full size cell inside an environmental chamber. The 5 mm PCM doubled the stored energy inside the envelope. In another study, they experimentally assessed the effect of a PCM copolymer wallboard on the thermal performance of the same fully controlled test cell (Kuznik and Virgone, 2009b). The PCM layer was located on the inner section of the wallboard. The controlled cell could provide consistent conditions for three consecutive days with three different conditions resembling summer, winter and mid-season conditions. The experimental results showed that the decrement factor varied between 0.73-0.78 in different seasonal conditions which shows that the shave of indoor temperature fluctuation resulted from the PCM wallboard. Nevertheless, not a significant shift in the peak indoor temperature was observed as a result of the application of the PCM layer.

Halford and Boehm (2007) studied the performance of a PCM layer sandwiched between two insulation layers. The simulation was conducted based on a sinusoidal temperature change on the outdoor boundary location while they kept the indoor temperature constant at a predetermined magnitude during the peak and off-peak periods. They evaluated the impact of outdoor mean temperature, peak/off-peak indoor temperature, and the thickness of inner side insulation on the magnitude of heat flux to the indoor space. They concluded that the application of the PCM layer could result in peak load reduction up to 25%. One of their notable results was the effect of the thickness of insulation on the level of efficiency of the latent heat storage. The work concluded that installing inappropriate thickness of insulation may result in losing the latent heat storage capability of the PCM layer.

Kuznik et al. (2008b) investigated the optimum thickness of a wallboard consisting of encapsulated paraffin in a polymeric material. The objective of the optimization was to have the highest energy storage capacity with the least possible PCM thickness. The enthalpy method with effective heat capacity was deployed as the modeling technique. They concluded that when the thickness of the PCM layer is sufficiently thin, the stored energy depends proportionally on the thickness of the layer. Also, when the PCM layer is sufficiently thick, increasing the thickness of the layer does not have any impact on the storage capacity (semi-infinite layer). Thus, the optimum design thickness for a PCM layer can be said to have the highest energy storage capacity. In addition, they found that the variation of the outdoor temperature swing and insulation thickness does not affect the optimum design thickness of the PCM layer. However, increasing the indoor temperature swing resulted in an increase in the optimum design

thickness of the PCM wallboard. As a limitation in their work, the simultaneous effect of the thermo-physical properties of the PCM was not considered in characterizing the optimum thickness of the wallboard.

Ahmed et al. (2006b) designed an experimental setup to evaluate the thermal response of PCM wallboards to the thermal solicitations. Also, they employed the enthalpy method with effective capacity using "Heating" software to model the thermal behaviour of PCM wallboards. The experiment was conducted for three wallboards in which PCM was directly incorporated: a polycarbonate panel filled with paraffin granulates, a polycarbonate panel filled with polyethylene glycol (PEG), and a PVC panel filled with PEG. They concluded that the highest storage capacity can be provided with the thickness of wallboard less than 5 cm. As the experiment was carried out only on the wallboard, the result cannot be extrapolated for a real application. Therefore, in another study, they accompanied the PEG layer with a vacuum insulation panel and mounted them in a cubical cell (Ahmad et al., 2006a). A parametric study was conducted to size the optimum thickness of the PCM layer using TRNSYS. Unlike the former result of their study, they concluded that increasing the thickness of the PCM layer more than 20 mm has no impact on the room temperature. Yet, this effective thickness is only applicable to the tested material and does not represent the other mediums in the market. Indeed, a general framework is required to characterize the best thickness for any PCM wallboard regarding their various thermo-physical properties.

The application of a PCM layer as a thermal shield in building envelopes was optimized by Mathieu-Potvin and Gosselin (2009) based on the layer's position and

fusion temperature. In cold climate regions, they numerically proved that a PCM layer has no shielding performance during heating seasons. Also, the optimal fusion temperature is the one close to indoor temperature.

Diaconu and Crucern (2010) investigated a novel composite wallboard consisting of an insulation sandwiched between two PCM layers to save heating and cooling energy in continental climate areas. A year-round simulation was conducted to model the thermal performance of the wallboard using the enthalpy method with effective heat capacity. The outer PCM layer was proposed to reduce the solar heat flux in the cooling season, while the inner PCM layer was applied to reduce the indoor temperature swing and shift the peak. The design specifies that the outer PCM layer requires a higher melting temperature than the inner PCM layer. They concluded that the suggested two-layer PCM may have a peak load reduction up to 36% for both heating and cooling seasons. The total heating load saving was 12.8%, while the cooling load reduction was only 1%.

2.4.3 All surfaces of a building furnished with PCM wallboard:

Zhou et al. (2007) compared shaped stabilized PCM with a gypsum board impregnated with PCM. The PCM layer was attached to all interior surfaces of the room except the floor. The layer thickness was 30 mm. They found that the optimum melting temperature is equal to the average room temperature, (which was 21°C in their experiment) and the PCM with narrow melting range was more efficient in terms of reducing indoor temperature fluctuations. The impregnated Gypsum board with PCM and

the shaped stabilized PCM shaved the indoor temperature peak by 46% and 56%, respectively.

Castell et al. (2010) proposed the application of macro-encapsulated PCM to reduce the cost of investment and the degradation of the mechanical properties. They experimentally studied the application of macro-encapsulated PCM in bricks. The experiment set-up consisted of two identical cubicles which were equipped with heat pump. They found that the application of PCM could reduce the indoor temperature fluctuations up to 1°C. In addition, the installation of a PCM layer resulted in a 15% reduction of the total energy consumption. However, the gradual increase in the indoor temperature profile proved that the PCM layer did not have an acceptable efficiency in keeping the temperature constant. It is obvious that the PCM did not solidify and melt completely in a periodic manner. Moreover, they did not report any shift of load or parametric studies to improve the application of PCM.

2.4.4 Simulating annual thermal performance of a building equipped with PCM wallboards:

The transient thermal performance of a building can be studied by simulation tools such as BLAST, Energy Plus, TRNSYS and ESPR. Their applications to analyze the building thermal performance equipped with PCM layers were investigated.

Jokisalo et al. (2000) developed a new wall component (type 204) for TRNSYS to simulate a PCM layer in a building envelope. The model can be used to simulate the building thermal performance when a regular layer impregnated with PCM is used in its

wall construction. But the model's prediction has not been validated with experimental data. Schranzhofer et al. (2006) also developed type 241 which is coupled with the multi-zone building model (type 56) in TRNSYS to simulate encapsulated PCM in regular building wallboards. Kuznik et al. (2010) developed type 260 and type 255 to solve heat transfer through a PCM wallboard. The types can be integrated with type 56 of multi-zone building in TRNSYS to simulate building thermal performance equipped with PCM layer in its envelope. They utilized the finite difference numerical method to solve the one dimensional heat equation with apparent heat capacity technique. The numerical scheme is not fully implicit due to the fact that some PCM parameters are used from the previous time step. The modeling tool was validated using the experiment data on two identical cubicles (Kuznik and Virgone, 2009a). The maximum deviation observed between the numerical and experimental results was 1.5ºC.

Heim and Clarke (2004) studied the application of PCM-impregnated gypsum board in an internal room lining in a naturally ventilated passive solar building. They concluded that the stored diurnal solar energy can reduce the required heating energy up to 90% during the autumn and spring. However, the passive heating for winter time requires an improved TES system, and wider analysis is needed. Additionally, the design parameters (its thickness and location) of the PCM did not significantly shave the indoor temperature fluctuation.

2.5 SUMMARY AND LIMITATIONS OF THE FORMER STUDIES

The outcomes of previous bodies of research are summarized in Table 2.1. Generally, the following remarkable conclusions can be extracted from previous findings about the application of PCM wallboards in a building envelope:

- The variation of melting temperature and latent heat of a PCM layer has a significant effect on the thermal performance of a PCM.

- The change of thermal conductivity of a PCM layer does not have a significant effect on its performance.

- A PCM layer in the interior wallboard needs to have a narrow melting range and a fusion temperature near the average room temperature to reduce the room temperature fluctuation more efficiently.

- The PCM wallboard in a wall section has an optimum thickness based on its design specification which provides the maximum thermal energy storage capacity.

- In the case of a design with two PCM layers, the exterior PCM layer needs to have a higher melting temperature than the interior one; its fusion temperature should be higher than the average outdoor temperature.

- The most effective PCM wallboard for a building thermal performance is the one which presents complete phase transition cycle during its thermal dynamics.

Overall, the outcomes of the abovementioned studies emphasize that the best design parameters depends on the design objectives and the environmental conditions. Although these works led to some general suggestions for the application of a PCM in a building envelope, the results are inherently case-specific and cannot be generalized for the design of an integrated building envelope with PCM. All the parametric studies were conducted by changing a single PCM property and presenting its effect on the thermal performance of the wallboard. However, the impact of all those parameters needs to be investigated simultaneously. For instance, changing the latent heat of a wallboard requires the change of the mediums composing the PCM wallboard. This modification alters the other thermo-physical properties of the wallboard. Moreover, among various materials available in the market, each wallboard has its own properties and eventually its own optimal thickness to effectively shift the load to off-peak hours. Thus, a general framework is required to size any possible PCM wallboard in the market based on the design objectives. The procedure to generalize the results, specifically for numerical studies, is to conduct the simulation and parametric studies using dimensionless numbers. Ettouney et al. (2004; 2005) characterized the heat transfer process in PCM applied in double pipe and spherical storage. They provided some correlations for the melting and solidification: Fourier number (*Fo*) as a function of the Stefan number (*Ste*) and Biot number (*Bi*) of the PCM. Those dimensionless numbers display the thickness, heat transfer coefficients and the thermo-physical properties of the materials. Therefore, any possible changes of the characteristics of the materials, which affects the thermal storage/release process inside the PCM, can be evaluated deploying the correlation available between those dimensionless numbers. Yet, a lack of similar correlations for

PCM wallboards requires extensive studies on the application of these materials in a building envelope. The aim of this study is to investigate the application of the PCM wallboard within a building envelope to be able to shift the peak load for space conditioning to the off-peak period. Indeed, the aim is to store energy during the off-peak period for space conditioning during the peak period and to avoid the application of spacing heating/cooling systems at those peak hours. For this purpose, a general framework and a methodology are required to evaluate and size PCM wallboards based on their characteristics in order to determine the required time for it to be charged.

Table 2.1 Summary of the literature review

Ref.	Analysis type	PCM type	Design specifications	Notable results	Energy saving/shifting achievement
Neeper (2000)	•Modeling	•Gypsum impregnated with fatty acid and paraffin waxes	•PCM layer in interior or exterior wallboard with passive solar design	•Melting temperature equal to the average room temperature •Narrow melting range temperature	–
Kuznik and Virgone (2009b)	•Experiment	•PCM copolymer wallboard	•Passive solar design with PCM layer in interior wall	•Decrement factor 0.73-0.78 •Effect of wall orientation	•Peak indoor temperature decreased up to 4.2ºC •Shift of peak indoor temperature for 40 min.
Kuznik et al. (2008b)	•Modeling	•Encapsulated PCM in polymeric material	•PCM interior wallboard	•Optimum thickness of PCM layer with the highest energy storage •Increase of outdoor temperature swing resulted an increase of PCM storage capacity	–
Halford and Boehm (2007)	•Modeling	•Encapsulated PCM wallboard	•PCM sandwiched between two insulation layers	•Increasing the thickness of insulation decreases the PCM effectiveness	•25% reduction in peak load
Ahmed et al. (2006b)	•Experiment •Modeling	•Wallboards with direct incorporation of PCM	–	•Thickness of PCM less than 5 cm for highest storage capacity	–
Diaconu and Crucern (2010)	•Modeling	–	•Wall composites of an insulation sandwiched between two PCM layer	•Exterior PCM layer has higher melting temperature than interior one	•Heating and cooling peak load reduction up to 36% •Total heating load saving =12.8%
Farid and Chen (1999)	•Modeling	•Composite of waxes	•On the floor as active layer with electrical heater	•Electrical heater was working only for 8 hr in off-peak period	•Shift 7.2 Mj/m^2 day of electricity to night time
Lin et al. (2004; 2005)	•Experiment •Modeling	•Shaped stabilized PCM	•On the floor as active layer with electrical heater	•Electrical heater was working only for 9 hr in off-peak period	•Shift 50%of space heating energy to night time

Xu et al., (2005)	•Modeling	•Shaped stabilized PCM	•On the floor as passive solar designs	•Melting temperature equal to the room average temperature •PCM latent heat larger than 120 kJ/kg	•Peak indoor temperature was shaved for 10ºC
Ceron et al. (2011)	•Experimental ly	•Mixture of paraffinic composition	•PCM inside tiles for floor furnishing	•The tiles receiving direct solar radiation are more effective in heating the space	-
Pasupathy and Velraj (2008)	•Experiment •Modeling	•Inorganic eutectic PCM	•Double layer PCM in roof slab for passive solar design	•Higher melting temperature for exterior PCM Melting temperature higher than outdoor average temperature	-
Pasupathy et al., (2008)	•Experiment •Modeling	•Inorganic eutectic PCM	•In roof slab as an active layer with water pipe	•Required water flow is very large and it is not practical	-
Zhou et al. (2007)	•Modeling	•Shaped stabilized •Impregnated gypsum board	•Inner side of all walls and ceiling in passive solar design	•Melting point near room average temperature with narrow melting range	•Shaving the indoor temperature peak up to 56%
Castell et al. (2010)	•Experiment	•Macro-encapsulated PCM	•Inner side of all walls , ceiling and floor	•PCM gradually lost its latent heat storage capacity	•15% reduction of total energy consumption
Heim and Clarke (2004)	•Modeling	•PCM-impregnated gypsum board	•Internal room lining in passive solar design	•Not a significant shave in room temperature	•Heating load reduction up to 90% in fall and spring •Not a significant reduction in winter

CHAPTER 3 PROBLEM FORMULATION AND NUMERICAL MODEL DEVELOPMENT

3.1 INTRODUCTION

To satisfy the thermal comfort inside a built environment, heating and cooling system condition the space. The goal is to minimize their usage during peak hours. Therefore, their application is shifted to the off-peak period as a mean to charge the TES medium during a time of low energy demand. Thus, during peak hours, the stored energy replaces the conditioning system.

As mentioned in the former chapter, the PCM wallboard is a promising latent heat thermal energy storage system that can be used in a building to shave and shift the load. It was also highlighted that a systematic methodology is needed to successfully apply this technology in a building envelope. This methodology needs to size and specify a material based on its thermo-physical properties and provide the most optimal design parameters. One of the unique and decisive characteristics of a PCM wallboard as a thermal storage system is its charging time. The ultimate goal is to fully charge the material during the off-peak period to which the charging procedure is intentionally shifted. Consequently, the best design of a PCM wallboard will be achieved when its thickness and its thermo-physical properties provide a storage system which can be fully charged during off peak hours. The fully charged status of the latent heat thermal storage during the specified period indicates that the full capacity of the storage is achieved.

To obtain the best design parameters of a PCM wallboard, characterizing the impact of the design parameters on its thermal performance is required. Generally, the influential parameters are those which affect the heat transfer rate through the wallboard and the storage capacity. Therefore, the thermo-physical properties of the PCM wallboard, its thickness, and convective heat transfer coefficient characterize its thermal performance. To investigate the impact of these parameters, recognizing the effective dimensionless numbers for such physical phenomenon is required.

3.2 Governing Equations of Heat Transfer in PCM Wallboards

The main difficulty in modeling a PCM is the process of melting and/or solidification. When the temperature of the PCM reaches its melting temperature range, the material gradually changes from one phase to another. Considering T_f [°C] as the fusion temperature of PCM, generally the medium transits from one state to another in a range of temperatures (ΔT) around its fusion temperature. Herein, when the temperature of the material is less than the lower bound of the melting range (solidification temperature T_s), the material is completely solid. Additionally, when the temperature of the material is higher than the upper bound of the melting range (melting temperature T_m), the material is completely liquid. When the temperature of the material is in the melting range, both solid and liquid states coexist. The part of the material in which both solid and liquid coexist is called the mushy zone.

Neglecting convective heat transfer inside the liquid zone, heat transfer through a PCM wallboard can be characterized using the heat equation modified by adding a term

to govern the absorption and release of latent heat during the phase transition (source/sink term) as follows:

$$\rho C \frac{\partial T}{\partial t} = k_{s/l} \frac{\partial^2 T}{\partial x^2} + S \tag{3-1}$$

Here, ρ is the density [kg.m^{-3}], C is the heat capacity [J.kg^{-1}.K^{-1}], T is the temperature [K], t is the time [s], $k_{s/l}$ is the conductivity in solid/liquid [W.m^{-1}.K^{-1}], and the term S is introduced to account for the source/sink of latent heat. It is presented as:

$$S = \rho L \frac{\partial f}{\partial t} \tag{3-2}$$

This equation implies that the rate of absorption and release of latent heat depends on the rate of change of the liquid fraction. By using the chain rule, equation (3-2) is reconfigured as:

$$S = \rho L \frac{\partial f}{\partial T} \frac{\partial T}{\partial t} \tag{3-3}$$

where, L is the PCM latent heat [J.kg^{-1}]. Liquid fraction is assumed to be changed linearly between solidification and melting temperatures. Thus, the liquid fraction as a function of temperature is:

$$f(T) = \frac{T - T_s}{T_m - T_s} \tag{3-4}$$

where, T_s is the solidification temperature and T_m is the melting temperature. In this study, the lower and upper bound of the melting range are called solidification and melting temperatures, respectively.

The PCM wallboard temperature, and consequently its liquid fraction have three states:

$$f(T) = \begin{cases} 0 & T < T_s & Solid & \frac{\partial f}{\partial T} = 0 \\ ]0,1[& T_s < T < T_m & Mushy & \frac{\partial f}{\partial T} \neq 0 \\ 1 & T > T_m & Liquid & \frac{\partial f}{\partial T} = 0 \end{cases} \quad (3\text{-}5)$$

3.3 NON-DIMENSIONALIZING THE EQUATIONS

The following parameters and procedure were used to non-dimensionalize equation (3-1);

$Dimensionless\ space\ coordiante: X = \frac{x}{l}$

$Dimensionless\ PCM\ temperature: \theta_{PC} = \frac{T - T_s}{T_m - T_s}$

$Fourier\ Number: F_o = \frac{\alpha t}{l^2}$

$Stefan\ Number = Ste = \frac{C\Delta T}{L}$ (where ΔT=1°C)

where, l is the thickness of the PCM wallboard, and α is the thermal diffusivity, L is the latent heat and C is the specific heat capacity. Regarding the definition of the Stefan number as the ratio of sensible heat over the latent heat, ΔT is assumed to be 1°C. Therefore, the antecedent of the ratio in Stefan number is the sensible heat stored in a unit of mass of a material when its temperature increases by 1°C.

By substituting equation (3-3) into equation (3-1);

$$\rho C \frac{\partial T}{\partial t} = k \frac{\partial^2 T}{\partial x^2} + \rho L \frac{\partial f}{\partial T} \frac{\partial T}{\partial t} \tag{3-6}$$

Replacing the dimensionless parameters into equation (3-6), it is rearranged as:

$$\left(1 - \frac{\Psi}{Ste} \frac{\partial f}{\partial \theta_{PC}}\right) \frac{\partial \theta_{PC}}{\partial F_o} = \frac{\partial^2 \theta_{PC}}{\partial X^2} \tag{3-7}$$

where,

$$\Psi = \frac{1^{\circ}C}{(T_m - T_s)} = Constant \tag{3-8}$$

The boundary condition is non-dimensionalized as follow:

$$k \frac{\partial T(0,t)}{\partial x} = h(T_{in} - T(0,t)) \tag{3-9}$$

where T_{in} is the room temperature and h is the overall room heat transfer coefficient which consists of both the convective heat transfer coefficient and long wave radiative heat transfer coefficient. To study the effect of the indoor operation temperature, a secondary dimensionless temperature is also introduced as follow:

$$\theta_{in} = \frac{T_{in} - T_{low\ Op.Temp.}}{T_{High\ op.Temp.} - T_{Low\ Op.Temp.}} \tag{3-10}$$

where T_{in} is the indoor air temperature, $T_{Low\ Op.\ Temp.}$ and $T_{High\ Op.\ Temp.}$ are the lowest and the highest operating room air temperatures, respectively. Considering these two operating temperatures, the solidification and melting temperature, the following constants dimensionless values can be expressed as:

$$\Psi_{op} = \frac{T_{High\ Op.Temp.} - T_{Low\ Op.Temp.}}{T_m - T_s} \quad (3\text{-}11)$$

$$\Psi_{PC} = \frac{T_s - T_{Low\ Op.Temp.}}{T_m - T_s} \quad (3\text{-}12)$$

These two constant values show the relationship between the melting range and the indoor operating temperatures. Using those dimensionless parameters, equation (3-9) is modified as follows:

$$\frac{\partial \theta_{PC}(0,Fo)}{\partial X} = Bi\{[\theta_{in}(Fo)\Psi_{Op} - \Psi_{PC}] - \theta_{PC}(0,Fo)\} \quad (3\text{-}13)$$

where;

$$Biot\ number: Bi = \frac{hl}{k}$$

In addition, the no-heat flux boundary condition is:

$$\frac{\partial \theta_{pc}(1,Fo)}{\partial X} = 0 \quad (3\text{-}14)$$

Assuming the wallboard is initially at the same temperature as the room air temperature before charging time ($T_{Low\ Op.\ Temp.}$), the dimensionless initial condition is:

$$\theta_{pc}(X,0) = \frac{T_{Low\ Op.Temp.} - T_s}{T_m - T_s} = -\Psi_{PC} \quad (3\text{-}15)$$

Based on those equations, the thermal performance of a PCM wallboard is defined as;

$$\theta_{PC} = f(Bi, Fo, X, Ste, \Psi, \Psi_{Opt}, \Psi_{PC}) \quad (3\text{-}16)$$

These non-dimensional parameters are used to conduct parametric studies to find the effect of design parameters on the performance of the PCM wallboard. Moreover, the possible correlations between those parameters are practical tools for designing PCM wallboards.

3.4 NUMERICAL METHODS TO SOLVE PHASE TRANSITION PHENOMENON

3.4.1 Numerical scheme:

To simulate the heat transfer through a PCM wallboard, equation (3-1) was solved numerically using the finite difference technique. For internal nodes, the second order partial derivative was selected in terms of central differences with error of $O(\Delta x^2)$ as follows:

$$\frac{\partial^2 T}{\partial x^2} = \frac{1}{\Delta x^2}(T_{i+1} - 2T_i + T_{i-1}) + O(\Delta x^2) \quad (3\text{-}17)$$

In the case of time marching, Crank-Nicolson implicit numerical scheme is adopted to solve the parabolic partial differential heat equation. Crank-Nicolson is the average of two explicit and implicit methods. It is a second order method and is unconditionally stable. For the node *i* in the time step *n*, the equation becomes:

$$-(r_i^n)T_{i-1}^{n+1} + 2(1 + r_i^n)T_i^{n+1} - (r_i^n)T_{i+1}^{n+1} = (r_i^n)T_{i-1}^n + 2(1 - r_i^n)T_i^n + r_i^n T_{i+1}^n \quad (3\text{-}18)$$

where;

$$r_i^n = \frac{k_i^{n-1}\Delta t}{\Delta x^2 \rho(C + Lf')} \quad (3\text{-}19)$$

and,

$$f' = \frac{f_i^{n-1} - f_i^{n-2}}{T_i^{n-1} - T_i^{n-2}} \quad (3\text{-}20)$$

In the boundaries, the forward and backward differences were applied with second order approximation. A code was developed in MATLAB (Matlab, 2010) to solve the system of equations for a PCM wallboard.

3.4.2 Validation of the model:

To validate the accuracy of the developed model, two studies were selected. The cases explained in these studies were replicated, and the results were compared. The first one was a single wall simulation containing PCM with sudden temperature solicitation on the outer sides of the wall, defined as the benchmark (task C) in ANNEX 23 (IEA ANNEX 23, 2013). The second one was a pilot scale cubical whose walls were furnished with a PCM layer in its interior side (Kuznik and Virgone, 2009a).

3.4.2.1 Single wall validation:

For model validation, various case studies for different configurations of the PCM integrated into building walls were proposed in ANNEX Task C (IEA ANNEX 23, 2013). In these case studies, the radiation heat transfer was not considered. The convective heat transfer coefficients for the internal and external were h_{in} = 2.5 [$W.m^{-2}.K^{-1}$] and h_{ex} = 8 [$W.m^{-2}.K^{-1}$]. The thermal properties of PCM, heat capacity and thermal conductivity were changing with temperature and phase transition as expressed in IEA

ANNEX 23 (2013). The internal temperature was set to be constant at 20°C, while the external temperature was initiated at 12°C, increased to and remained constant at 32°C. The various configurations of wall layers were studied by combining different layers with different thickness as listed in Table 3.1.

Table 3.1 Wall designation from (IEA ANNEX 23, 2013)

Wall designation	Material	Thickness (mm)
C30	Concrete (thin)	30
C200	Concrete (thick)	200
I100	Insulation	100
G10	Gypsum	10
P5	PCM	5
P10	PCM	10
P50	PCM	50

Eventually nine case studies were identified as listed in Table 3.2. Here, the model which consisted of either a single PCM layer or a mixture of a PCM layer and a conventional building material was validated. The simulation result of Case 2 as a single 10 mm thick PCM wallboard and Case 4 as a mixture of a PCM layer and a 30 mm concrete were compared with the ANNEX report (IEA ANNEX 23, 2013) and presented in Figure 3.1 and Figure 3.2, respectively.

Table 3.2 Case studies from (IEA ANNEX 23, 2013)

Case	Configuration	
	External Layer	Internal Layer
1	P5	
2	P10	
3	P50	
4	C30	P10
5	P10	C30
6	C200	P10
7	P10	C200
8	I100	P10
9	P10	I100

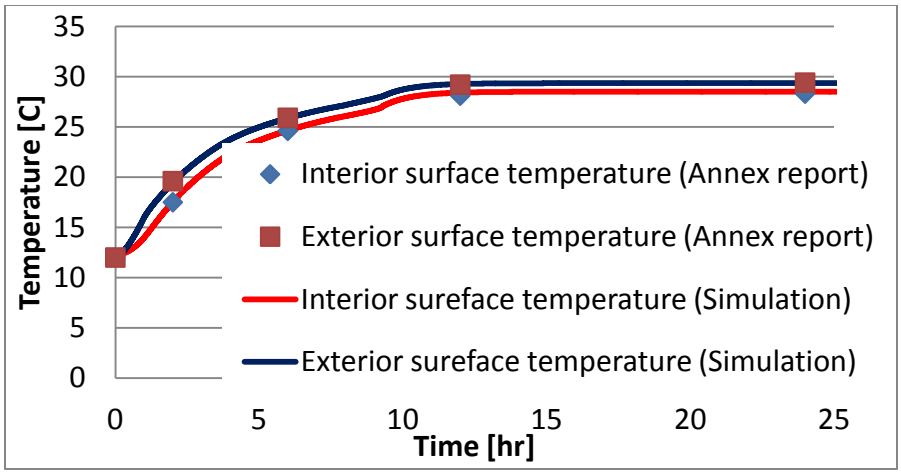

Figure 3.1 Validation of the PCM model with Case 2 in task C of Annex 23(IEA ANNEX 23, 2013)

Those figures illustrate the interior and exterior surface-temperatures of the wall section, confirming that there is a good agreement between the results. Furthermore, Figure 3.3 presents the liquid fraction along the wallboard for Case 2 as function of time, the phase transition phenomenon in PCM wallboard. Based on the magnitude of liquid fraction, liquid, mushy and solid zones can all be distinguished along the wallboard. In addition, the temperature distribution along the wall versus time was plotted in Figure 3.4.

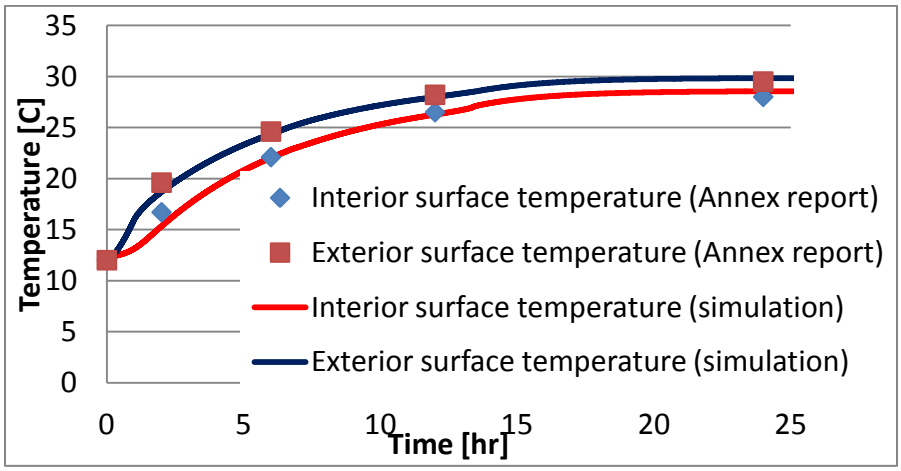

Figure 3.2 Validation of the PCM model with Case 4 in task C of Annex 23 (IEA ANNEX 23, 2013)

According to the simulation, the temperature of the wallboard in the steady state condition can be obtained. Table 3.3 shows the calculated steady state temperature of the wallboard in all nine cases and the comparison of the results from the report (IEA ANNEX 23, 2013).

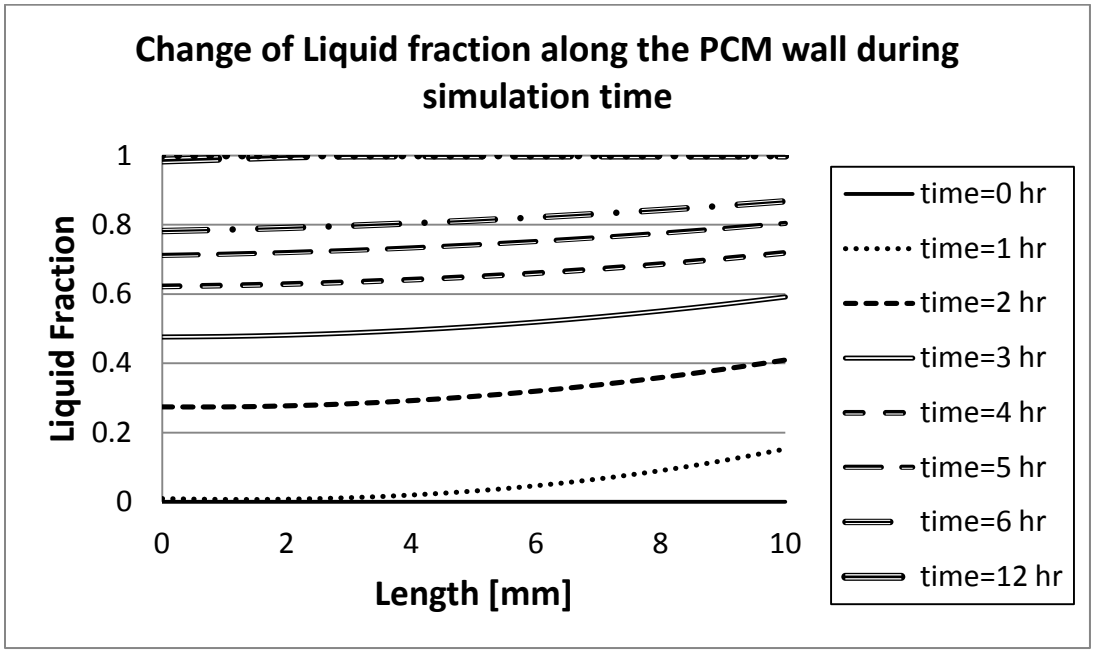

Figure 3.3 Change of liquid fraction along the PCM wallboard with time in Case 2

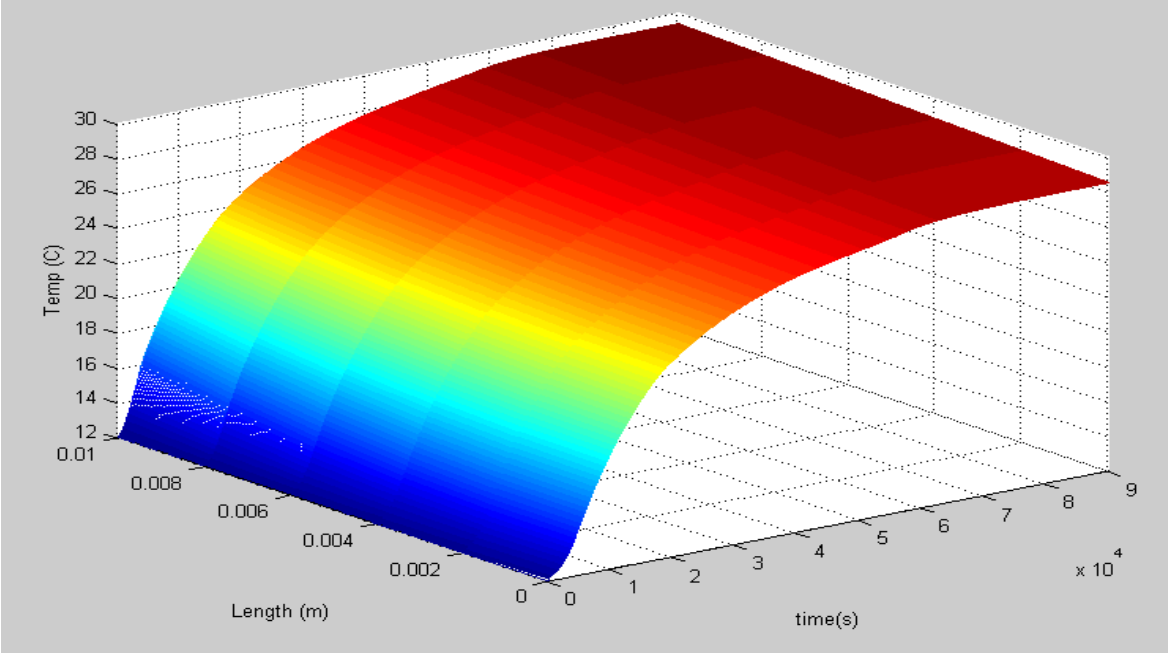

Figure 3.4 Temperature distribution inside the wallboard of Case 2

Table 3.3 Steady state temperature of the wall sections in 9 cases and the comparison with ANNEX report (IEA ANNEX 23, 2013)

Cases	Simulation Temperature (°C)			Temperature (ANNEX report) (°C)			Relative Error (%)		
	Exterior	Intersection	Interior	Exterior	Intersection	Interior	Exterior	Intersection	Interior
Case1	29.25	-	28.81	29.27	-	28.73	0.07	-	0.28
Case2	29.34	-	28.49	29.39	-	28.35	0.17	-	0.49
Case3	29.80	-	26.38	30.06	-	26.19	0.87	-	0.72
Case4	29.84	29.41	28.56	29.5	29.00	28.01	1.14	1.39	1.92
Case5	29.00	28.04	27.56	29.5	28.49	27.99	1.72	1.60	1.56
Case6	30.18	27.78	27.07	29.98	27.29	26.48	0.66	1.76	2.18
Case7	29.56	28.77	26.18	29.98	29.17	26.45	1.42	1.39	1.03
Case8	31.51	21.72	21.56	31.51	21.72	21.56	0.00	0.00	0.00
Case9	31.40	31.20	21.54	31.51	31.31	21.57	0.35	0.35	0.14

3.4.2.2 Pilot-scale cubical with PCM

In addition to a single wall simulation, the model was enhanced to simulate the thermal performance of a room with a PCM layer. The validation was conducted by replicating the result of an experiment with a pilot-scale cubical (0.5m*0.5m*0.5m) with

PCM layers (Kuznik and Virgone, 2009a). The cubical benchmark was exposed to two different outdoor conditions: the step change and the sinusoidal evolution of the outdoor temperature. The indoor temperature profiles of the cubicle with and without PCM in both the step and the sinusoidal changes of the outdoor temperature are presented in Figure 3.5 and Figure 3.6, respectively. As depicted in those figures, the model could predict the indoor temperature with high accuracy in both scenarios.

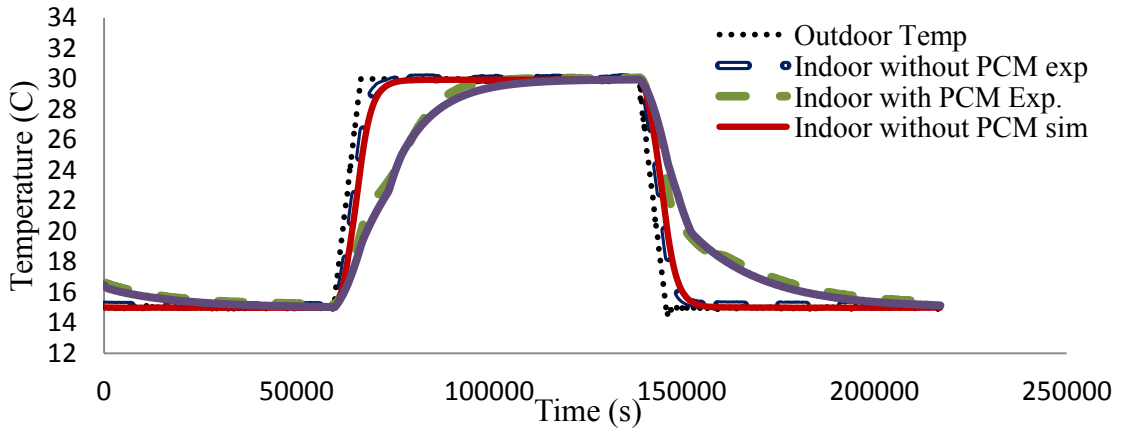

Figure 3.5 Indoor temperature profile of the benchmark cubicle with/out PCM (outdoor step change of temperature)

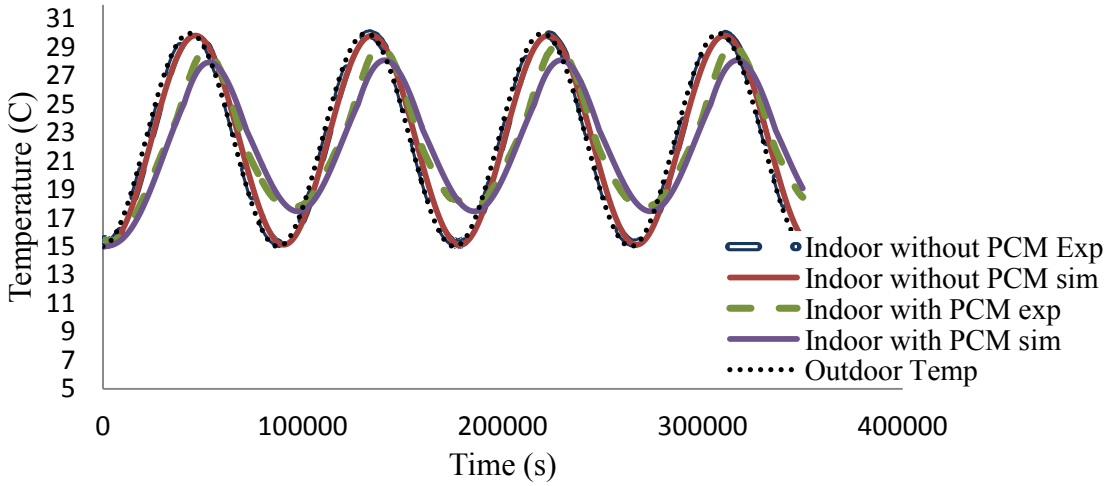

Figure 3.6 Indoor temperature profile of the benchmark cubicle with/out PCM (outdoor sinusoid change of temperature)

3.5 SUMMARY

To identify the best design parameters of a PCM wallboard, it is necessary to characterize the effect(s) of those parameters on the thermal performance of the PCM wallboard. To conduct such parametric studies two tasks were defined and accomplished. First, the thermal analysis of a PCM wallboard was mathematically modeled, and the governing equations were non-dimensionalized. The non-dimensionalized format of those equations identified the effective dimensionless numbers and their impacts on the thermal performance of the medium under phase transition. In the second task, a numerical model was developed and validated by replicating two studies from the literature. The first validation was carried out by simulating a single wall section; the second one was conducted by simulating a pilot-scale cubical furnished with PCM wallboards. Comparing the replicated results in the validations section and the results provided in the literatures demonstrates the accuracy and applicability of the developed model.

As required for the next step, the validated model is employed to conduct the parametric study to determine the impact of dimensionless numbers on the performance of a PCM wallboard. The aim is to identify the correlations between those numbers. The correlations are introduced as a framework to find the best design parameters of a PCM layer in a building envelope to effectively shift the space conditioning energy consumption to off-peak periods.

CHAPTER 4 FRAMEWORK DEVELOPMENT

4.1 INTRODUCTION

As mentioned in the previous chapter, the thermo-physical properties of a PCM wallboard and its thickness directly influence its thermal storage capacity (the heat transfer phenomenon inside the wallboard). Meanwhile, the film coefficient on the surface of the wallboard defines the resistance against the convection and radiation heat transfer between the inner surface of the wall and the indoor air.

Recalling the non-dimensionalizing procedure in the former chapter, the temperature distribution inside a PCM wallboard depends on the Biot number (*Bi*), Stefan number (*Ste*), Fourier number (*Fo*), and the relationship between its fusion temperature, melting range and the room air temperature. Each of these dimensionless numbers characterizes the heat transfer phenomenon: *Ste* defines the ratio of sensible heat storage to latent heat storage, and *Bi* of a material presents the ratio between its resistances against conduction and the resistance against heat transfer to the material from its boundary. In the case of a transient conduction, the system is characterized using *Fo*. Also, *Fo* of a material describes the ratio of the diffusive heat transport rate to the rate of thermal energy storage. Therefore, in the case of a PCM wallboard, the relationship between those dimensionless numbers characterizes the thermal performance of a wallboard and the correlations between those numbers builds a framework to specify the best design parameters of a PCM wallboard for any specific application. The purpose of this chapter is to explain the procedure required to develop this framework. The

procedure mainly consists of the parametric studies to illustrate the impact of the dimensionless numbers on the charging process of a PCM wallboard.

4.2 SIMULATION SCENARIO

Regarding the application of a PCM wallboard, the location of the layer inside a wall section may differ relative to the insulation (Zhang et al., 2007). In the case that the prevention of solar heat flow to the space is desired, the PCM layer is located between the insulation and outdoor area. However, in the case of load shifting and internally located energy sources, the PCM layer is mounted between the insulation and indoor space. Herein, the peak demand shifting is aimed. For the simulation of the thermal performance of a PCM wallboard, it is therefore assumed that the layer is mounted as the interior layer of a wall section. Thus, the room temperature serves as the boundary condition on one side and adiabatic boundary condition on the other side (prefect insulation or similar room air condition on the other side) of the PCM wallboard. This assumption is valid for internal walls which are utilized as partition or separators of two zones with the same thermal conditions and the external walls of a well-insulated building. Effective insulation with very low thermal conductivity creates almost no heat flux boundary condition for the interior layer which has the potential to be replaced by a PCM layer. Figure 4.1 illustrates the schematic diagram of a mounted PCM layer in an external wall section. Also considering the micro scale size of the encapsulated PCM, Figure 4.2, the assumptions to have constant conductivity and no volume expansion are valid. Figure 4.2 presents the schematic diagram a wallboard with microencapsulated PCM.

Another assumption was made regarding the room air temperature in the first stage of the simulations. The room air temperature is assumed to be equal to the set point temperature. Therefore, the sudden increase or decrease of the set-point temperature results in the consecutive change of the room air temperature. This assumption will be relaxed in the further stage of the framework development, and the effect of the room air temperature time lag will be investigated and integrated in the design framework development.

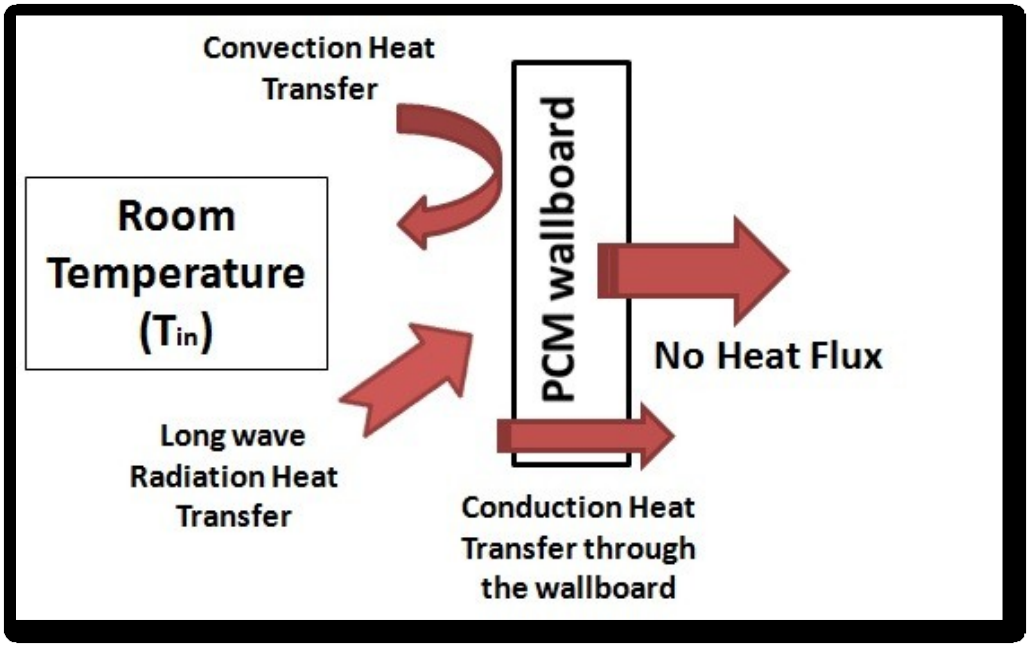

Figure 4.1 Schematic diagram of a PCM wallboard in the simulation scenario

In order to charge a PCM wallboard, the set-point temperature is increased from the lower bound of the thermal comfort to its upper bound during off-peak hours. Thus, the wall which is conditioned in the room temperature faces a temperature solicitation on its boundary. The required time for charging the PCM depends on the design parameters of the wallboard. These design parameters constitute the film coefficient, the wallboard's

thickness, its thermal conductivity, heat capacity and latent heat, which can be summarized as the *Ste* and *Bi* of the PCM layer. Moreover, the *Fo* provides a measure of charging/discharging time. Characterizing the effects of dimensionless parameters on the change of *Fo* quantifies the time required to fully charge a PCM wallboard.

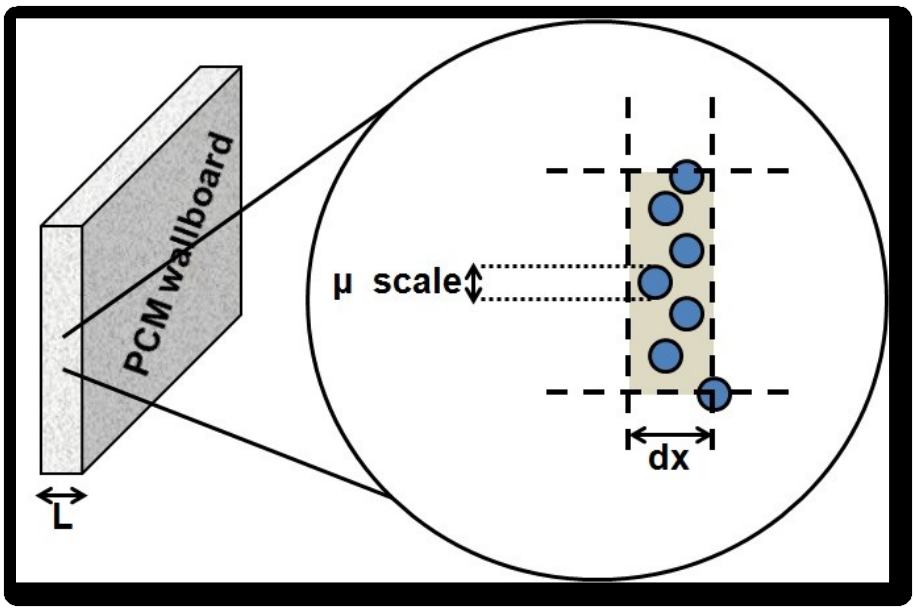

Figure 4.2 Schematic diagram of a micro-encapsulated PCM wallboard

4.3 EFFECTS OF STEFAN AND BIOT NUMBERS

To investigate the effect of *Ste* on the performance of a PCM layer, a number of simulations were conducted with different *Ste,* while the *Bi* was kept constant at 0.4. It was assumed that both the wall and the room initial temperature were 20°C, and the phase transition occurred between 17-23°C. The set-point temperature and consequently the room temperature were suddenly increased to 25°C to evaluate the time required to charge the PCM wallboard. Ten different cases with various *Ste* were simulated. To

generate different *Ste*, both heat capacity and latent heat were altered. Also, various magnitudes of the film coefficient, thickness and conductivity were selected, while the magnitude of *Bi* was kept constant at 0.4. In addition, two extra cases were generated with Ste^{-1}=50 and *Bi*=0.4 while the magnitude of the density was changed. The information of the simulated cases is tabulated in Table 4.1. Moreover, the inner surface temperature profile of the PCM wallboard is presented in Figure 4.3

Table 4.1 The parameters of the simulation cases for various *Ste* and similar *Bi*=0.4

Case	Thickness (*l*) [m]	Film Coef. (*h*)[$Wm^{-2}K^{-1}$]	Conductivity (*k*)[$W\ m^{-1}K^{-1}$]	Density (ρ)[$kg\ m^{-3}$]	Heat Capacity (*C*) [$J\ kg^{-1}K^{-1}$]	Latent (*L*) [$J\ kg^{-1}$]	Ste^{-1}	*Bi*
Case 1	0.010	10	0.250	1100	2500	140000	56.00	0.4
Case 2	0.010	8	0.200	1100	2500	100000	40.73	0.4
Case 3	0.015	12	0.450	1100	2500	80000	32.00	0.4
Case 4	0.008	15	0.300	1100	2500	120000	48.00	0.4
Case 5	0.010	5	0.125	1100	2500	70000	28.00	0.4
Case 6	0.010	10	0.250	1100	2000	70000	35.00	0.4
Case 7	0.010	8	0.200	1100	1500	70000	46.67	0.4
Case 8	0.015	12	0.450	1100	1000	70000	70.00	0.4
Case 9	0.008	15	0.300	1100	2000	100000	50.00	0.4
Case 10	0.010	5	0.125	1100	1000	50000	50.00	0.4
Case 11	0.010	10	0.250	700	2000	100000	50.00	0.4
Case 12	0.008	20	0.400	1400	1500	75000	50.00	0.4

Figure 4.3 shows that the temperature profile has two separate trends. At first the wall has both latent and sensible heat storage. When the PCM is completely liquefied, there is only sensible heat storage which alters the trend of the temperature profile. Comparing both states of storage, the change of θ_{pc} occurs in a larger *Fo* when both sensible and latent heat storage coexist.

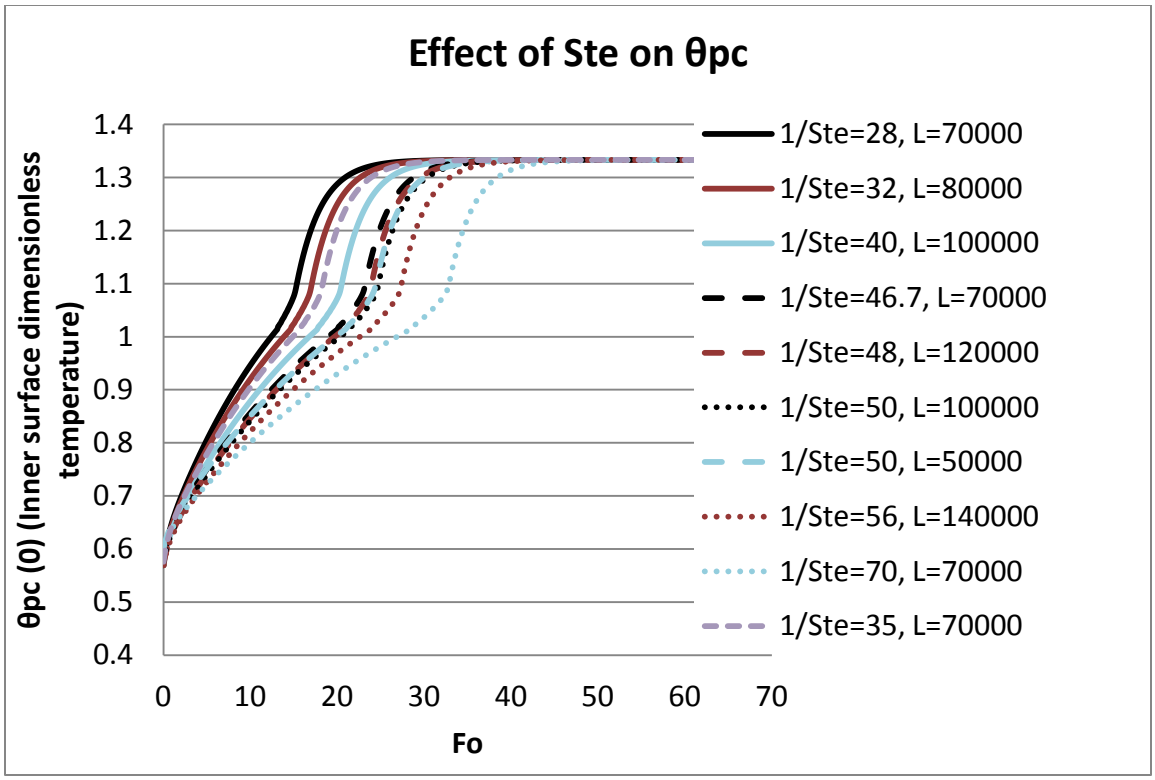

Figure 4.3 The change of inner surface temperature θ_{pc} VS *Fo* for different *Ste*

Three specific *Fo* were calculated for each case based on the wall thermal situation: 1) when half of the PCM is fully liquefied (Fo_{hl}), 2) when the entire PCM is fully liquefied (Fo_{fl}), and 3) when the wall reaches the steady state condition (Fo_{ss}) (no more change in temperature at 25°C). These measured *Fo* are presented in Table 4.2 for each simulated case, and their change is presented as a function of Ste^{-1} in Figure 4.4.

Table 4.2 Measured *Fo* for cases with various *Ste* and similar *Bi*=0.4

Case	Ste^{-1}	*Bi*	Fo_{hl} (Half of the PCM completely liquefied)	Fo_{fl} (PCM completely liquefied)	Fo_{ss} (Steady state condition)
Case 1	56.00	0.4	26.00	27.09	59.09
Case 2	40.73	0.4	19.42	20.22	52.22
Case 3	32.00	0.4	16.07	16.73	48.73
Case 4	48.00	0.4	22.50	23.35	55.40
Case 5	28.00	0.4	14.45	15.04	47.04

Case 6	35.00	0.4	17.27	17.95	50.00
Case 7	46.67	0.4	22.06	22.91	55.03
Case 8	70.00	0.4	31.45	32.73	64.73
Case 9	50.00	0.4	23.01	24.08	56.25
Case 10	50.00	0.4	23.41	24.43	56.48
Case 11	50.00	0.4	23.21	24.29	56.25
Case 12	50.00	0.4	22.92	23.81	55.95

As illustrated in Figure 4.4, there is a linear relationship between *Fo* and *Ste* of the PCM wallboard with an almost similar slope of 0.42. The similarity of these slopes implies that the storage capacity enhances linearly by reducing *Ste*. Moreover, as presented in Table 4.2, the simulation cases 9, 10, 11, and 12 have Ste^{-1}=50, while their thickness and thermo-physical properties are different. In those cases, however, all those measured *Fo* were almost the same. Therefore, one can conclude that neither the change of the thickness nor the change of the thermo-physical properties of the medium has an effect on *Fo* when *Ste* and *Bi* are kept constant.

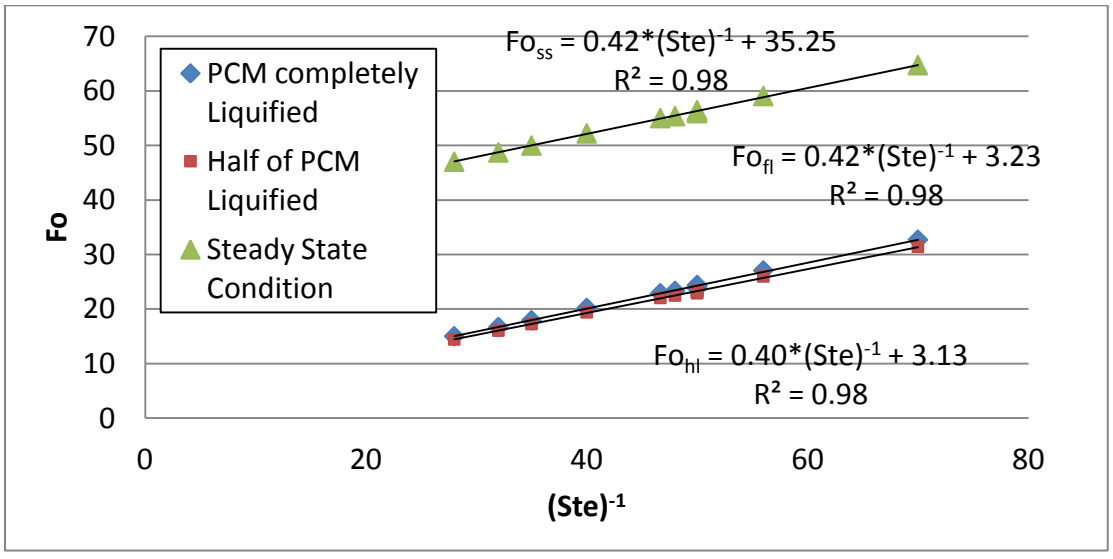

Figure 4.4 The change of *Fo* as a function of $(Ste)^{-1}$ for *Bi*=0.4

To investigate the correlation of *Fo* versus *Ste*, a study was conducted for different *Bi* and *Ste*. The PCM parameters in these simulation cases are presented in Table 4.3; the measured *Fo* in these simulated cases are tabulated in Table 4.4. In these simulation cases, dissimilar physical properties for equal dimensionless numbers were selected. Therefore, for cases with similar dimensionless numbers, the independence of *Fo* to the physical properties was investigated.

Table 4.3 The parameters of the simulation cases for various *Ste* and *Bi*

Case	Thickness (l) [m]	Film Coef. (h) [$Wm^{-2}K^{-1}$]	Conductivity (k)[$Wm^{-1}K^{-1}$]	Density (ρ)[$kg\ m^{-3}$]	Heat Capacity (C) [$J\ kg^{-1}K^{-1}$]	Latent (L) [$J\ Kg^{-1}$]	Ste^{-1}	Bi
Case 13	0.0100	10	0.50	1100	2500	75000	30	0.2
Case 14	0.0175	8	0.70	1400	1000	50000	50	0.2
Case 15	0.0100	10	0.50	1400	1200	72000	60	0.2
Case 16	0.0060	10	0.30	1100	1500	105000	70	0.2
Case 17	0.0165	10	0.55	700	2500	75000	30	0.3
Case 18	0.0100	12	0.40	700	1000	50000	50	0.3
Case 19	0.0050	15	0.25	1400	1200	72000	60	0.3
Case 20	0.0240	5	0.40	900	1500	105000	70	0.3
Case 21	0.0320	5	0.40	1400	2000	60000	30	0.4
Case 11	0.0100	10	0.25	700	2000	100000	50	0.4
Case 22	0.0080	15	0.30	1400	1200	72000	60	0.4
Case 8	0.0150	12	0.45	1100	1000	70000	70	0.4
Case 23	0.0250	8	0.40	1100	2500	75000	30	0.5
Case 24	0.0150	15	0.45	1400	1000	50000	50	0.5
Case 25	0.0300	5	0.30	900	2000	120000	60	0.5
Case 26	0.0100	10	0.20	700	1500	105000	70	0.5
Case 27	0.0117	15	0.25	700	2700	81000	30	0.7
Case 28	0.0245	10	0.35	1100	900	45000	50	0.7
Case 29	0.0175	12	0.30	700	2000	120000	60	0.7
Case 30	0.0175	10	0.25	1100	1700	119000	70	0.7

Table 4.4 Measured *Fo* for simulation cases with various *Ste* and *Bi*

Case	Ste^{-1}	*Bi*	Fo_{fl}	Fo_{ss}
Case 13	30	0.2	29.45	89.64
Case 14	50	0.2	45.55	105.80
Case 15	60	0.2	53.27	113.39
Case 16	70	0.2	60.10	120.20
Case 17	30	0.3	20.32	61.88
Case 18	50	0.3	30.28	74.24
Case 19	60	0.3	35.12	80.12
Case 20	70	0.3	42.85	85.21
Case 21	30	0.4	15.92	47.92
Case 11	50	0.4	24.29	56.25
Case 22	60	0.4	28.18	61.10
Case 8	70	0.4	32.73	64.73
Case 23	30	0.5	13.17	38.51
Case 24	50	0.5	20.00	46.43
Case 25	60	0.5	23.96	49.53
Case 26	70	0.5	26.86	53.33
Case 27	30	0.7	9.95	29.86
Case 28	50	0.7	15.43	35.40
Case 29	60	0.7	18.12	38.06
Case 30	70	0.7	20.91	40.82

Figure 4.5 and Figure 4.6 illustrate variations of Fo_{fl} and Fo_{ss} as a function of *Ste* for different *Bi*, respectively. These figures imply that the change of *Fo* as a function of $(Ste)^{-1}$ is linear for a given *Bi*. Moreover, the slope of the graphs is the same for both Fo_{fl} and Fo_{ss} in any given *Bi*. It also shows that the magnitude of the slope varies as a function of *Bi*, and *Fo* is also a function of *Bi*.

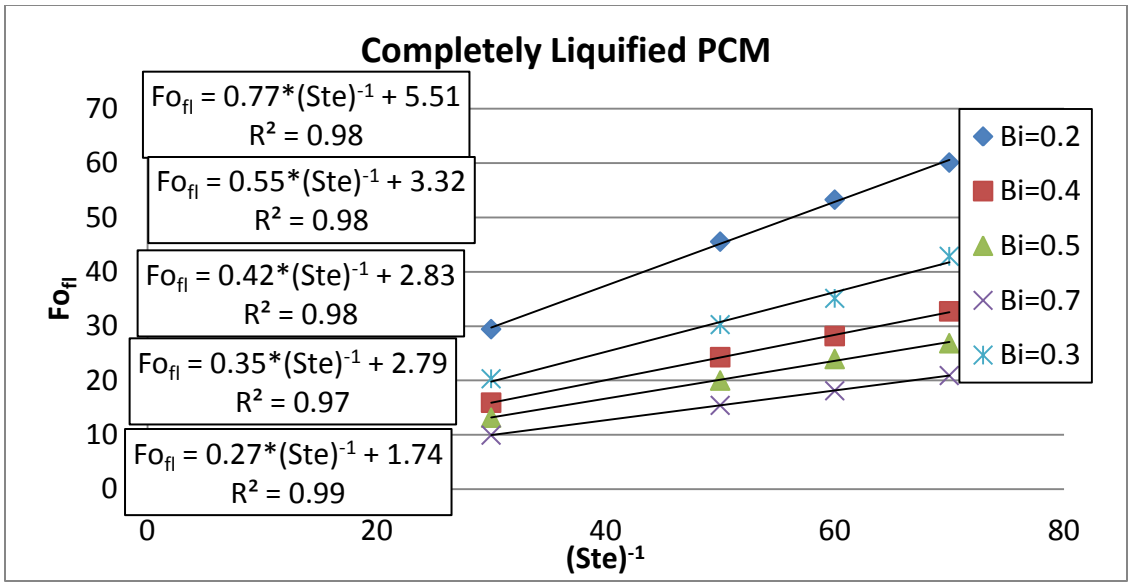

Figure 4.5 Fo_{fl} as a function of $(Ste)^{-1}$ in different Bi

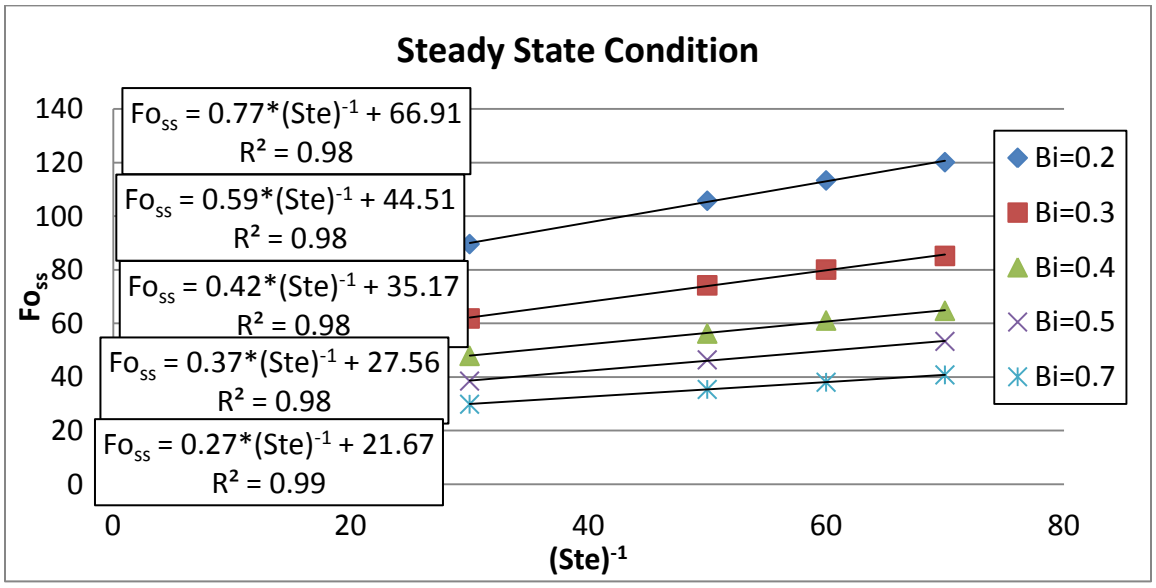

Figure 4.6 Fo_{ss} as a function of $(Ste)^{-1}$ in different Bi

Figure 4.7 and Figure 4.8 present the change of Fo_{fl} and Fo_{ss} as a function of Bi for different Ste, respectively. Here, unlike the correlation for the Ste, the logarithmic magnitude of Fo changes linearly with the logarithmic value of Bi: Increasing Bi reduces

Fo. Lower *Fo* is expected for higher magnitude of *Bi*. The wallboard with larger *Bi* has stronger resistance against conduction heat transfer. Therefore, *Fo* as the ratio of heat conduction rate to the sensible thermal storage is reduced by increasing the resistance against conduction heat transfer.

Figure 4.7 illustrates that the correlation for different $(Ste)^{-1}$ has almost the similar exponent (0.86). The same equality was observed in Figure 4.8 for the steady state condition (exponent for all $(Ste)^{-1}$ is around 0.88).

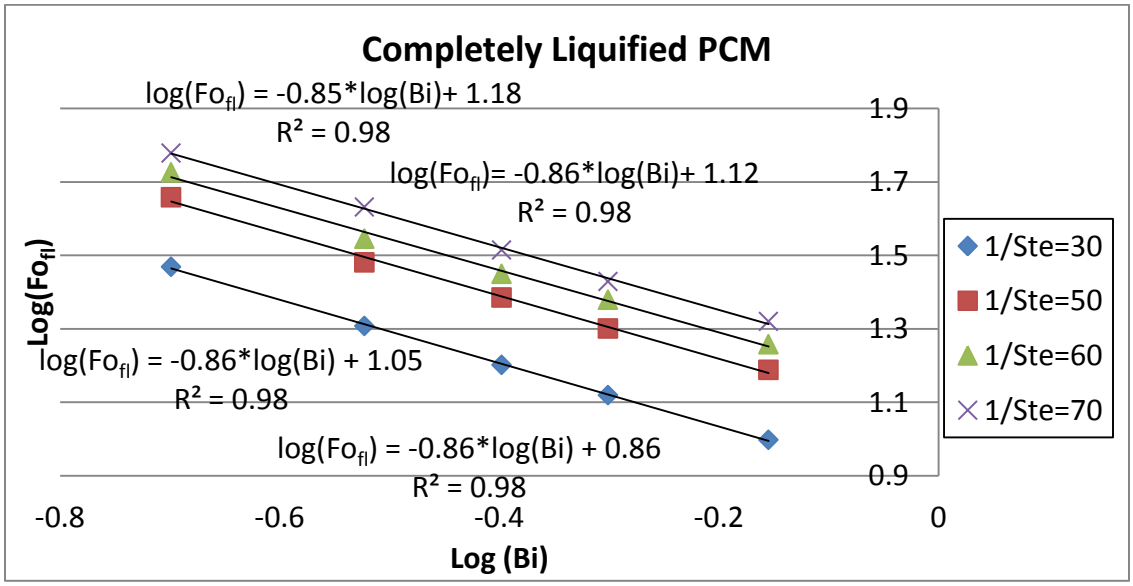

Figure 4.7 Fo_{fl} as a function of *Bi* in different *Ste*

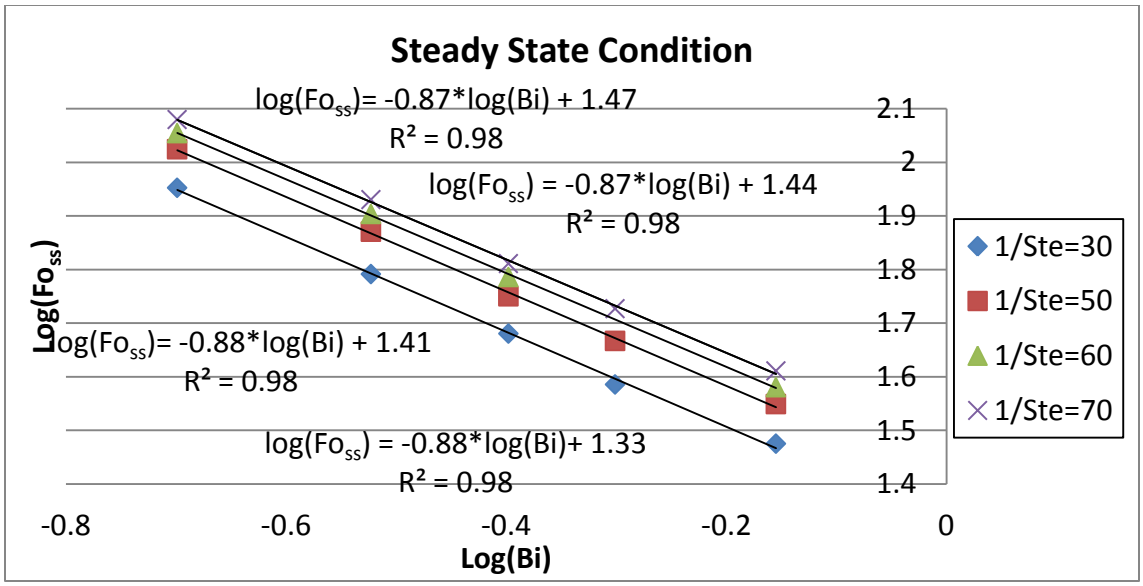

Figure 4.8 Fo_{ss} as a function of *Bi* in different *Ste*

The correlations shown in Figure 4.5 and Figure 4.7 can be used to estimate the time required to fully charge a PCM wallboard. Depending on the applications, the PCM wallboard as the thermal storage needs to be conditioned to a certain temperature in a given period of time. In other words, these correlations can be used as a design framework to size a PCM wallboard to store the required thermal energy in a pre-determined time period.

While Fo_{fl} is generally utilized as the design objective, both Fo_{fl} and Fo_{ss} can be employed to validate the correlations presented so far by comparing with the Heisler chart for a plane wall (Cengel and Ghajar, 2011) and the approximate analytical solution of the transient heat transfer in a plane wall with no phase transition. Presented in almost all heat transfer textbooks i.e. Heat and Mass Transfer, Fundamentals and Applications by Cengel and Ghajar (2011), the temperature distribution inside a plane wall of thickness 2a with one-term approximation is expressed as:

$$\theta = \frac{T(x,t)-T_\infty}{T_i-T_\infty} = A_1 \exp(-\lambda_1^2\, Fo\,)\, COS(\frac{\lambda_1\, x}{a}) \quad (4\text{-}1)$$

The wall is initially at a uniform temperature of T_i subjected to convection from both sides to an environment at temperature T_∞. The two coefficients (A_1 and λ_1) in equation (4-1) are a function of *Bi* of the wallboard. Like the PCM wallboard in this study, the wall has Robin boundary condition in one side. Also, it has no heat transfer in the middle of the wall like the outer side of the PCM wallboard. However, the wall does not present a phase transition in its operational temperature resembling a PCM wallboard with $(Ste)^{-1}$=0. Here, when the transient system gets to the steady state situation, *T(x,t)* will not change any more, and the magnitude of θ becomes close to zero. Knowing the coefficients (A_1 and λ_1) in different *Bi*, the time and the Fo_{ss} at which the state of the wall becomes steady can be calculated using equation (4-1). These Fo_{ss} were compared with the y-intercepts of the fitted curves of different *Bi* in Figure 4.6. Moreover, the y-intercepts of Figure 4.5 show the *Fo* where the temperature at the outer surface of the wallboard increased to 23°C. It is similar to the situation in which the middle of plane wall temperature is at 23°C and θ in the middle of wall is equal to 0.4 considering T_i and T_∞ at 20°C and 25°C, respectively. As presented in Table 4.5, the is no significant difference between the measured *Fo* in both methods.

Table 4.5 Comparison of the analytical method and the framework for Ste^{-1}=0

Bi	***Fo* @ *x*=0 and θ=0.4 (Equation 4-1)**	**Fo_{fl} @ $(Ste)^{-1}$=0 (Figure 4.5)**	**Fo_{ss} @ *x*=0 and $(Ste)^{-1}$=0 (Equation 4-1)**	**Fo_{ss} @ $(Ste)^{-1}$=0 (Figure 4.6)**
0.2	5.06	5.51	65.33	66.91
0.3	3.53	3.32	44.99	44.51
0.4	2.76	2.83	34.85	35.17
0.5	2.31	2.79	28.76	27.56
0.7	1.78	1.74	21.82	21.67

In addition, *Fo* at $\theta \approx 0$ and $\theta = 0.4$ were measured for the other *Bi* using equation (4-1)[1]. The change of the logarithmic magnitude of *Fo* is presented as a function of logarithmic value of *Bi* in Figure 4.9.

Like the other fitted curves for various magnitude of $(Ste)^{-1}$ in Figure 4.7 and Figure 4.8, the slope is 0.86 and 0.88, respectively. Indeed, the comparison with $Ste^{-1}=0$ presents the analytical interpretation of the correlations derived from the framework. In addition, the framework developed in this study is an expansion of Heisler chart for studying the transient heat transfer for materials during their phase transition.

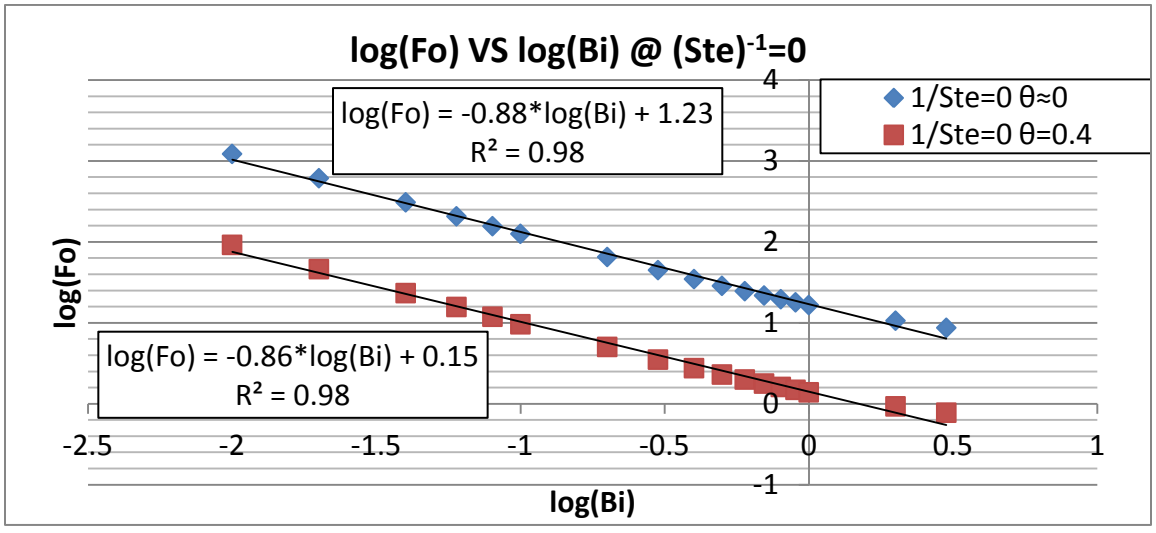

Figure 4.9 Fo_{ss} as a function of *Bi* in $(Ste)^{-1}=0$

To evaluate the accuracy of the developed design framework, ten design scenarios were selected in which the Fo_{fl} was calculated using the correlations developed in this study. The results of those testing scenarios were then compared with the Fo_{fl} calculated

[1] The magnitudes of the coefficients of equation (4-1) were extracted from Cengel Y.A., Ghajar A.J. (2011) Heat and mass transfer; Fundamentals and applications. The McGraw-Hill Companies, Inc., New York, NY 4th edition.

using numerical simulation. The thickness and the thermo-physical properties of the PCM wallboards in those testing scenarios were selected randomly from the following ranges: thickness (0.005-0.05 m), heat capacity (500-3000 J $kg^{-1}K^{-1}$), conductivity (0.1-1.2 W $m^{-1}K^{-1}$), latent heat (25000-400000 J kg^{-1}), density (700-1400 $kg.m^{-3}$) and film coefficient (5-20 $W.m^{-2}.K^{-1}$).The aforementioned ranges were selected based on the available materials in the literatures. The specifications of the PCM wallboards in the testing scenarios are presented in Table 4.6. Figure 4.10 shows the Fo_{fl} for a wide range of *Bi* and *Ste*. This figure makes it possible to calculate the time required to fully melt a PCM wallboard with a melting range of [17-23°C], when the room set-point temperature is altered from 20°C to 25°C.

For the testing scenarios, the Fo_{fl} was calculated using both the simulation results and the graph in Figure 4.10. For comparison, the simulation results are presented as the circular markers in Figure 4.10. Both calculated Fo_{fl} in testing cases either by simulation or the graph, and the relative error between both calculations methods is presented in Table 4.7. The mean average error for the testing scenarios was less than 3%.

Table 4.6 The parameters of PCM in the testing cases

Testing Case	**Thickness (l) [m]**	**Film Coef. (h) [$Wm^{-2}K^{-1}$]**	**Conductivity (k)[$W m^{-1}K^{-1}$]**	**Density (ρ)[$kg\ m^{-3}$]**	**Heat Capacity (C) [$J\ kg^{-1}K^{-1}$]**	**Latent (L) [$J\ kg^{-1}$]**	***Ste*$^{-1}$**	***Bi***
T-Case 1	0.017	18	0.35	1320	2070	195000	94	0.86
T-Case 2	0.042	9	0.43	700	1640	93000	57	0.88
T-Case 3	0.031	16	0.93	1220	1240	144000	116	0.53
T-Case 4	0.007	11	0.71	990	1360	84000	62	0.11
T-Case 5	0.008	13	1.10	1100	2790	126000	45	0.09
T-Case 6	0.018	12	0.82	990	1940	370000	191	0.26
T-Case 7	0.016	8	0.58	840	2610	355000	136	0.22
T-Case 8	0.011	15	0.50	1300	2940	66000	22	0.33
T-Case 9	0.018	14	0.52	1150	620	117000	189	0.49

T-Case 10	0.035	10	0.80	980	860	158000	184	0.44

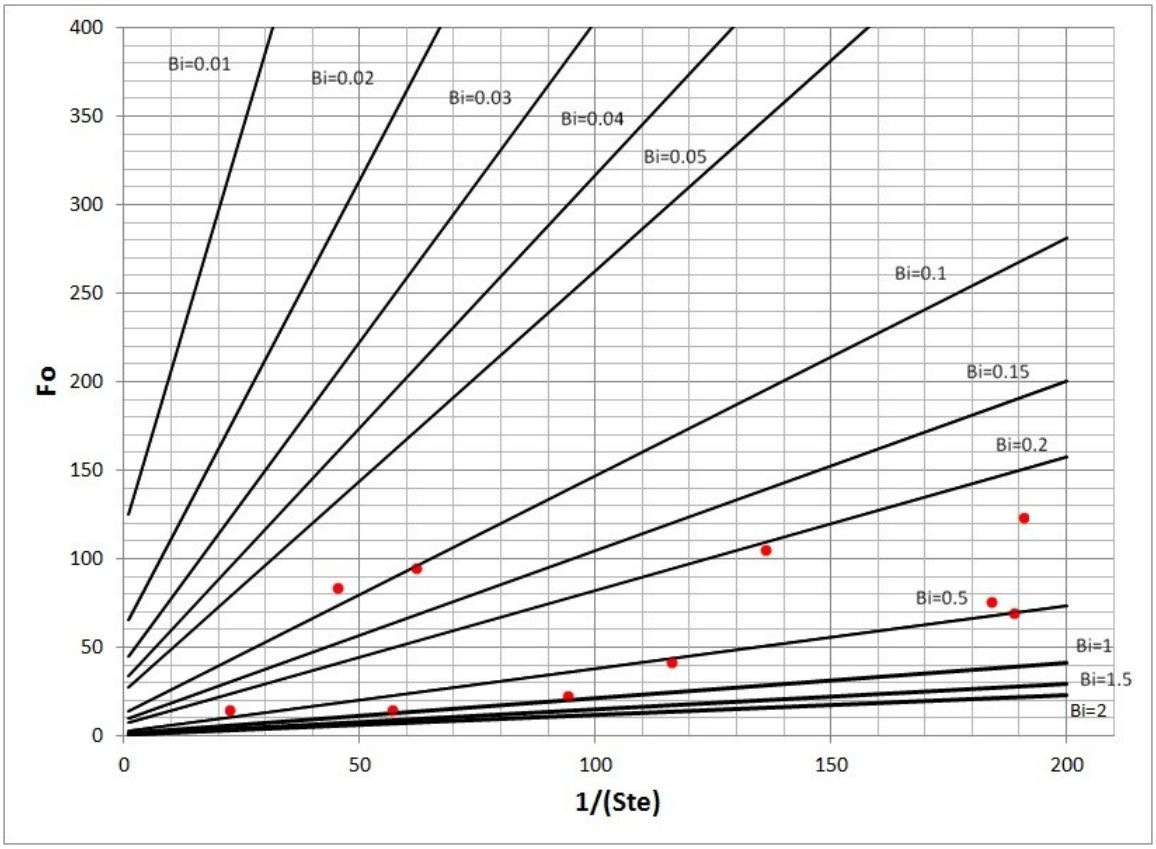

Figure 4.10 Fo_{fl} of wallboard as function of Bi and $(Ste)^{-1}$

Table 4.7 Fo_{fl} calculated in testing scenarios either with simulation or the graph

Testing Case	Ste^{-1}	Bi	$^{1}Fo_{fl}$	$^{2}Fo_{fl}$	Error [%]
T-Case 1	94	0.86	23.14	22.81	1.42
T-Case 2	57	0.88	14.59	14.11	3.26
T-Case 3	116	0.53	41.52	41.82	0.73
T-Case 4	62	0.11	94.70	88.75	6.28
T-Case 5	45	0.09	84.00	80.20	4.52
T-Case 6	191	0.26	123.21	121.58	1.32
T-Case 7	136	0.22	105.30	99.75	5.27
T-Case 8	22	0.33	14.81	15.16	2.34

T-Case 9	189	0.49	69.33	71.14	2.62
T-Case 10	184	0.44	75.86	75.45	0.54

(1) PCM completely liquefied (simulation)
(2) PCM completely liquefied (Figure 4.10)

4.4 Effect of Fusion Temperature and Melting Range

Beside *Bi* and *Ste*, the solidification temperature, the melting temperature, the relation between the operational temperatures and the temperature range in which the material faces phase transition impact the performance of a PCM wallboard. Therefore, knowledge on the effects of the PCM solidification and melting temperature is required for designing an appropriate PCM wallboard. For this purpose, parametric studies were conducted to characterize the effects of two dimensionless temperature ratios; Ψ and Ψ_{pc} on the Fo_{fl} of PCM wallboard. These two dimensionless ratios express the phase transition temperature range and the phase status of PCM when the charging process is initiated. Thus, having knowledge of the effect of those dimensionless numbers on the time required to fully charge the thermal storage is essential. As the operational temperature of the building was assumed to be consistent for all the cases (20°C -25°C), the effect of Ψ_{op} has not been investigated in this study.

4.4.1 Effect of Ψ:

In the previous section the effects of *Bi* and *Ste* on the Fo_{fl} were studied. Resulting from those parametric studies, the variation of Fo_{fl} was characterized as a function of *Bi* and *Ste* for any specific fusion temperature and melting range. To expand the results for different melting ranges, a number of simulations were conducted with constant *Bi*, *Ste*

and Ψ_{pc} for a PCM wallboard, while the Ψ varied. Similar to the previous section, the Fo_{fl} was calculated, and the effect of Ψ was characterized. Ψ represents the range and the magnitude of the temperature in which the PCM undergoes phase transition. To have a constant Ψ_{pc}, the simulation cases were designed in a way to yield a similar mean temperature in their melting range.

To study the effect of Ψ, nine simulation cases were designed with different *Bi* and *Ste*. Each of them was modeled with three different melting ranges, while the mean temperature of their melting range (fusion temperature) was kept constant at 20°C. Therefore, 27 simulations were carried out to investigate the impact of Ψ on the time required to completely liquefy a PCM wallboard with a similar *Bi*, *Ste* and Ψ_{pc}. The specifications of those 27 simulated cases are presented in Table 4.8. Like the former section, all the simulations were conducted for a room temperature changed from 20°C to 25°C.

Table 4.8 The parameters of the simulations cases for various Ψ

Case	l [m]	h [$Wm^{-2}K^{-1}$]	k [$Wm^{-1}K^{-1}$]	ρ[$kg\ m^{-3}$]	C [$J\ kg^{-1}K^{-1}$]	L [$J\ kg^{-1}$]	T_s [°C]	T_m [°C]
Case 13	0.0100	10	0.50	1100	2500	75000	17	23
Case 14	0.0175	8	0.70	1400	1000	50000	17	23
Case 16	0.0060	10	0.30	1100	1500	105000	17	23
Case 21	0.0320	5	0.40	1400	2000	60000	17	23
Case 11	0.0100	10	0.25	700	2000	100000	17	23
Case 8	0.0150	12	0.45	1100	1000	70000	17	23
Case 27	0.0117	15	0.25	700	2700	81000	17	23
Case 28	0.0245	10	0.35	1100	900	45000	17	23
Case 30	0.0175	10	0.25	1100	1700	119000	17	23
Case 31	0.0100	10	0.50	1100	2500	75000	18	22
Case 32	0.0175	8	0.70	1400	1000	50000	18	22
Case 33	0.0060	10	0.30	1100	1500	105000	18	22
Case 34	0.0320	5	0.40	1400	2000	60000	18	22

Case 35	0.0100	10	0.25	700	2000	100000	18	22
Case 36	0.0150	12	0.45	1100	1000	70000	18	22
Case 37	0.0117	15	0.25	700	2700	81000	18	22
Case 38	0.0245	10	0.35	1100	900	45000	18	22
Case 39	0.0175	10	0.25	1100	1700	119000	18	22
Case 40	0.0100	10	0.50	1100	2500	75000	19	21
Case 41	0.0175	8	0.70	1400	1000	50000	19	21
Case 42	0.0060	10	0.30	1100	1500	105000	19	21
Case 43	0.0320	5	0.40	1400	2000	60000	19	21
Case 44	0.0100	10	0.25	700	2000	100000	19	21
Case 45	0.0150	12	0.45	1100	1000	70000	19	21
Case 46	0.0117	15	0.25	700	2700	81000	19	21
Case 47	0.0245	10	0.35	1100	900	45000	19	21
Case 48	0.0175	10	0.25	1100	1700	119000	19	21

l: Thickness, h: Film Coefficient, k: Thermal Conductivity, ρ: Density, C: Specific Heat Capacity, L: Latent Heat, T_s: Solidification Temperature, T_m: Melting Temperature

The dimensionless numbers and the calculated Fo_{fl} of PCM wallboards in those simulations cases are tabulated in Table 4.9.

Table 4.9 Measured Fo_{fl} for simulation cases with different Bi, Ste, and Ψ

Case	Ste^{-1}	Bi	Ψ_{pc}	Ψ	Fo_{fl}
Case 13	30	0.2	-0.5	0.17	29.45
Case 14	50	0.2	-0.5	0.17	45.55
Case 16	70	0.2	-0.5	0.17	60.10
Case 21	30	0.4	-0.5	0.17	15.92
Case 11	50	0.4	-0.5	0.17	24.29
Case 8	70	0.4	-0.5	0.17	32.73
Case 27	30	0.7	-0.5	0.17	9.95
Case 28	50	0.7	-0.5	0.17	15.43
Case 30	70	0.7	-0.5	0.17	20.91
Case 31	30	0.2	-0.5	0.25	23.09
Case 32	50	0.2	-0.5	0.25	36.57
Case 33	70	0.2	-0.5	0.25	47.47
Case 34	30	0.4	-0.5	0.25	12.65
Case 35	50	0.4	-0.5	0.25	19.28
Case 36	70	0.4	-0.5	0.25	26.18
Case 37	30	0.7	-0.5	0.25	7.83
Case 38	50	0.7	-0.5	0.25	11.94

Case 39	70	0.7	-0.5	0.25	17.02
Case 40	30	0.2	-0.5	0.50	18.54
Case 41	50	0.2	-0.5	0.50	29.88
Case 42	70	0.2	-0.5	0.50	35.86
Case 43	30	0.4	-0.5	0.50	10.49
Case 44	50	0.4	-0.5	0.50	15.36
Case 45	70	0.4	-0.5	0.50	20.73
Case 46	30	0.7	-0.5	0.50	6.28
Case 47	50	0.7	-0.5	0.50	10.31
Case 48	70	0.7	-0.5	0.50	14.36

As presented in Table 4.9, these cases consist of three different values *Bi*, *Ste* and Ψ. Three different Ψ express three different melting ranges. To confirm the outcome of the former section on the effect of *Bi* and *Ste*, the change of Fo_{fl} as a function of *Bi* and *Ste* in other melting ranges was investigated and illustrated in the following figures.

Figure 4.11 and Figure 4.12 show the changes of Fo_{fl} as a function of Ste^{-1} for Ψ=0.25 and Ψ=0.5, respectively. Also, the change of Fo_{fl} as a function of *Bi* in those Ψ is presented in Figure 4.13 and Figure 4.14.

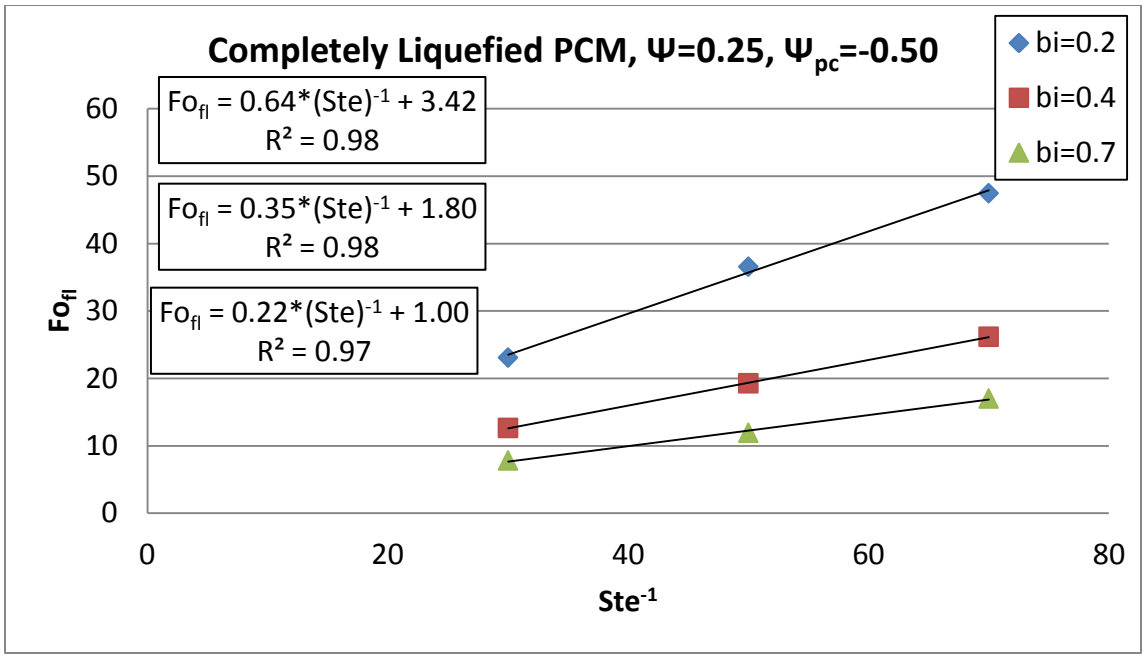

Figure 4.11 Fo_{fl} as a function of $(Ste)^{-1}$ in different Bi, Ψ=0.25 and Ψ_{pc}= -0.50

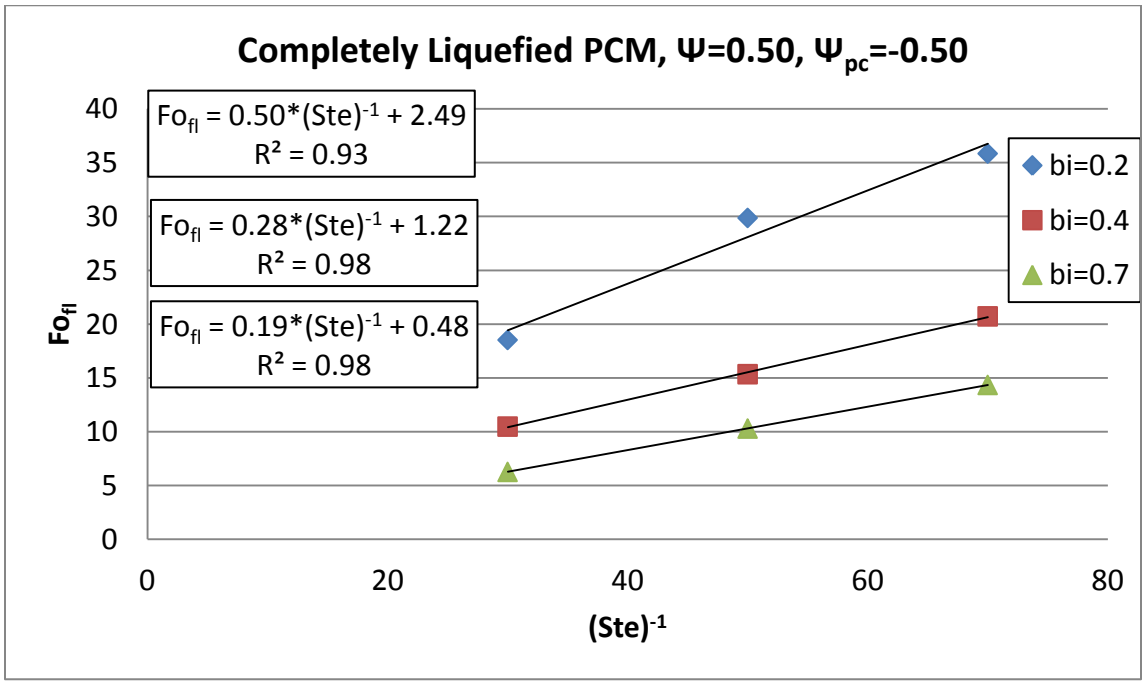

Figure 4.12 Fo_{fl} as a function of $(Ste)^{-1}$ in different Bi, Ψ=0.50 and Ψ_{pc}= -0.50

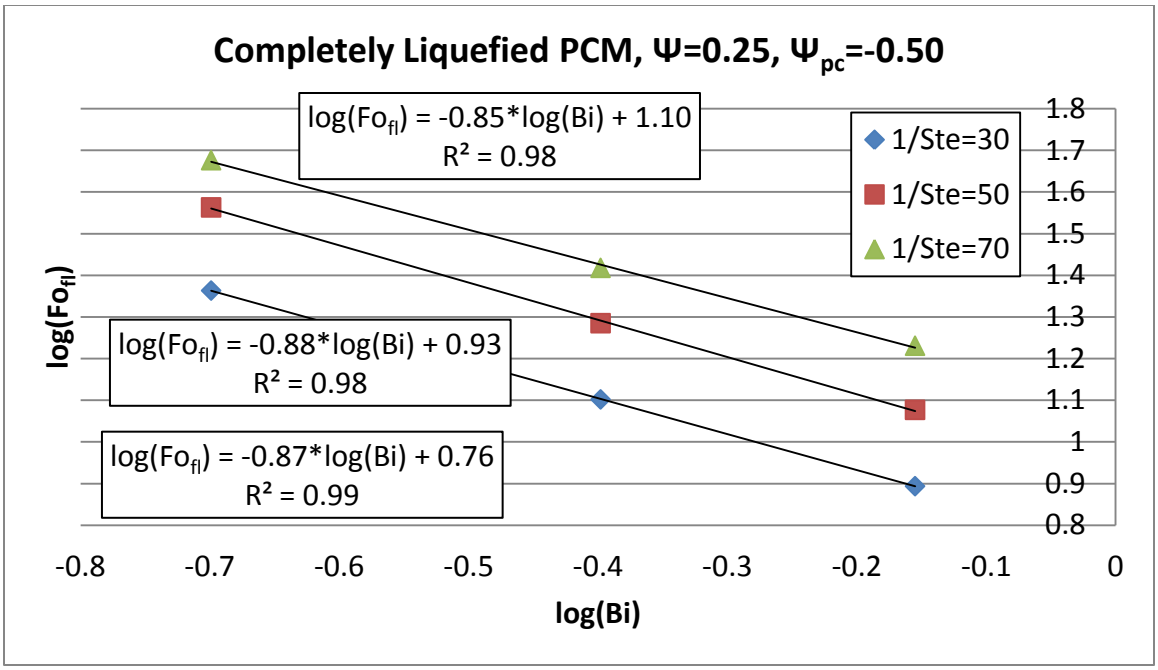

Figure 4.13 Fo_{fl} as a function of *Bi* in different *Ste*, Ψ=0.25 and Ψ_{pc}= -0.50

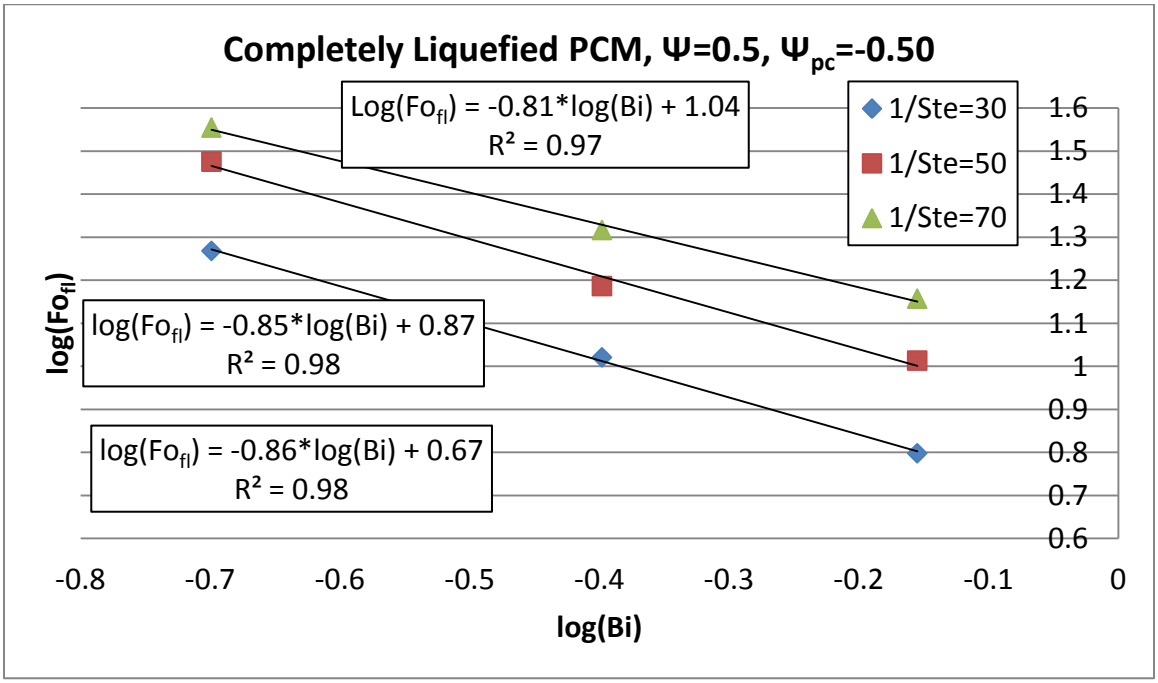

Figure 4.14 Fo_{fl} as a function of *Bi* in different *Ste*, Ψ=0.50 and Ψ_{pc}= -0.50

Confirming the outcome of the parametric study in the previous section, *Fo* is changing linearly as a function of *Ste*. log (*Fo*) is also changing linearly as a function of log (*Bi*) for different Ψ. In addition, the change of log (*Fo*) as a result of the change in log (*Bi*) occurs with a similar slope in different *Ste* and Ψ. Similar to the cases with Ψ=0.17, the y-intercepts of the trend-lines in Figure 4.11 and Figure 4.12 were compared with the analytically calculated *Fo* for the cases with $(\text{Ste})^{-1}=0$ utilizing equation (4-1). As presented in Table 4.10, there is no significant difference between the measured *Fo* of both methods, validating the outcome of the curve fitting with the analytical solution for the cases with $(Ste)^{-1}=0$.

The effect of Ψ on Fo_{fl} is illustrated in each single set of (*Bi*, *Ste*) in Figure 4.15. The figure shows the change of log (Fo_{fl}) as a function of log (Ψ) in constant Ψ_{pc}. Regarding the curve fitting of the data in Figure 4.15, the change of log (Fo_{fl}) is linear as a result of a change of log (Ψ) with a similar slope of almost -0.40 in various sets of *Bi* and *Ste*. Employing this relationship between Fo_{fl} and Ψ, any chart such as the one presented in Figure 4.10, can be mapped in another melting range of the same PCM wallboard.

Table 4.10 Comparison of the analytical method and the framework for $Ste^{-1}=0$ @ Ψ=0.25 and Ψ=0.50

Bi	***Fo* @ x=0 and θ=0.6 (Equation 4-1)**	***Fo_{fl}* @ $(Ste)^{-1}=0$ (Figure 4.11)**	***Fo* @ x=0 and θ=0.8 (Equation 4-1)**	***Fo_{fl}* @ $(Ste)^{-1}=0$ (Figure 4.12)**
0.2	2.89	3.42	1.35	2.49
0.4	1.61	1.80	0.79	1.22
0.7	1.06	1.00	0.55	0.48

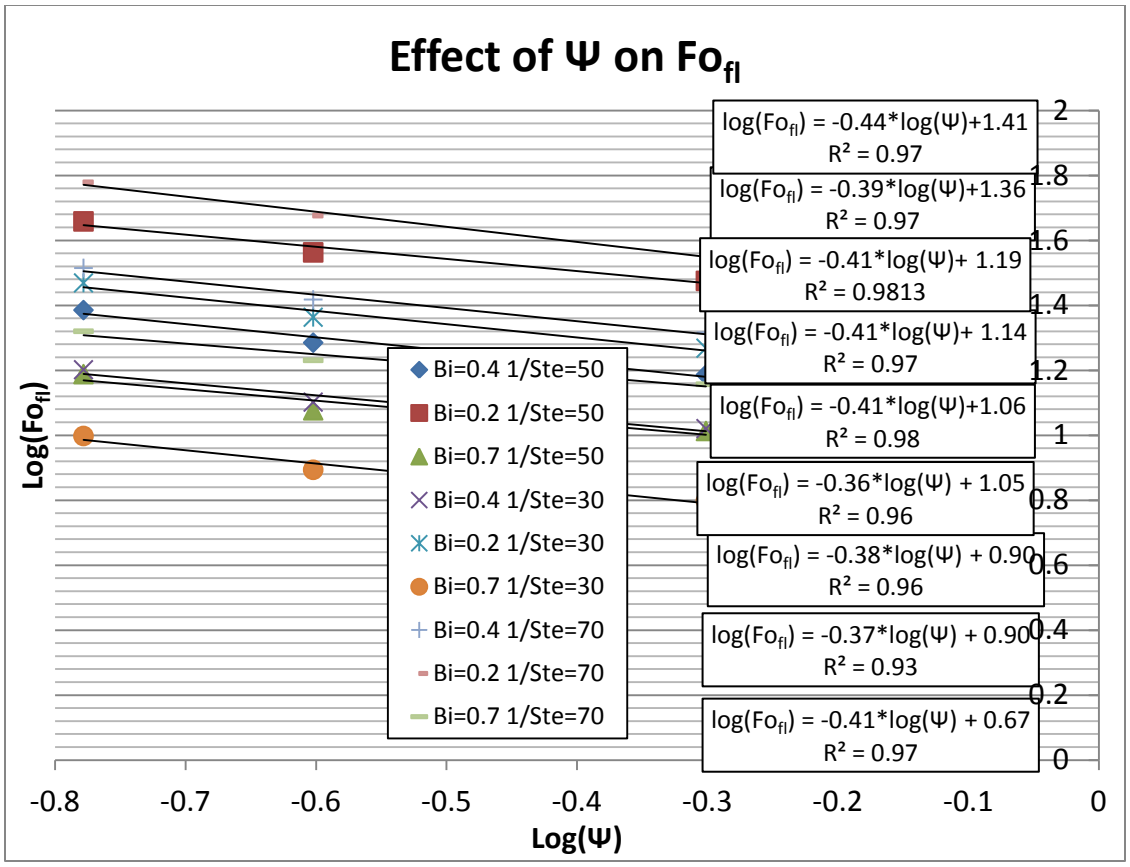

Figure 4.15 Effect of Ψ (melting range) on the Fo_{fl} in different *Bi* and *Ste* with similar Ψ_{pc}

4.4.2 Effect of Ψ_{pc}

The last effective dimensionless parameter is Ψ_{pc} which can be different for diverse PCM wallboards. Based on the definition that was given in this study, Ψ_{pc} consists of the melting range of the PCM wallboard in its denominator. Moreover, it has the difference between the solidification temperature and the lower bond of thermal comfort temperature as the lowest limit of the operational temperature in its numerator. Thus, the numerator of this ratio presents the phase status of the PCM wallboard when the charging procedure is initiated. In addition, different PCM wallboards with similar

melting range may have dissimilar Ψ_{pc} when their solidification temperature (T_s) is different. In other words, the link between the fusion temperature, the melting range of a PCM wallboard and the operational temperature of a room are expressed by Ψ_{pc}.

The magnitude of Ψ_{pc} may have three states depending on the solidification temperature of a PCM wallboard: either positive, negative or zero. The sign of the magnitude of Ψ_{pc} implies the state of PCM at the time when the charging process is initiated: Positive magnitude indicates that PCM is at the solid phase, while the negative magnitude indicates it is at the mushy/liquid phase. Consecutively, zero Ψ_{pc} points out that phase transition of the PCM wallboard is going to start by the charging procedure.

Like the procedure applied for the melting range, the effect of Ψ_{pc} on the Fo_{fl} is investigated to characterize the impact of fusion temperature on the performance of the PCM wallboard as a thermal storage. For this purpose 36 simulation cases were designed with nine different sets of (*Bi*, *Ste*), similar Ψ, and four different Ψ_{pc}. The four different sets of solidification and melting temperatures were selected to have four different Ψ_{pc}, while the melting range of those sets was kept similar. The specifications of those 36 simulated cases are presented in Table 4.11. As in the previous sections, all the simulations were conducted for a room where the temperature was changed from 20°C to 25°C.

Table 4.11 The parameters of the simulations cases for various Ψ_{pc}

Case	l [m]	h [$Wm^2 K^{-1}$]	k [$Wm^{-1}K^{-1}$]	ρ[Kgm^{-3}]	C [$J\ Kg^{-1}\ K^{-1}$]	L [$J\ Kg^{-1}$]	T_s [°C]	T_m [°C]
Case 49	0.0100	10	0.50	1100	2500	75000	20	23
Case 50	0.0175	8	0.70	1400	1000	50000	20	23
Case 51	0.0060	10	0.30	1100	1500	105000	20	23
Case 52	0.0320	5	0.40	1400	2000	60000	20	23
Case 53	0.0100	10	0.25	700	2000	100000	20	23
Case 54	0.0150	12	0.45	1100	1000	70000	20	23
Case 55	0.0117	15	0.25	700	2700	81000	20	23
Case 56	0.0245	10	0.35	1100	900	45000	20	23
Case 57	0.0175	10	0.25	1100	1700	119000	20	23
Case 58	0.0100	10	0.50	1100	2500	75000	21	24
Case 59	0.0175	8	0.70	1400	1000	50000	21	24
Case 60	0.0060	10	0.30	1100	1500	105000	21	24
Case 61	0.0320	5	0.40	1400	2000	60000	21	24
Case 62	0.0100	10	0.25	700	2000	100000	21	24
Case 63	0.0150	12	0.45	1100	1000	70000	21	24
Case 64	0.0117	15	0.25	700	2700	81000	21	24
Case 65	0.0245	10	0.35	1100	900	45000	21	24
Case 66	0.0175	10	0.25	1100	1700	119000	21	24
Case 67	0.0100	10	0.50	1100	2500	75000	19	22
Case 68	0.0175	8	0.70	1400	1000	50000	19	22
Case 69	0.0060	10	0.30	1100	1500	105000	19	22
Case 70	0.0320	5	0.40	1400	2000	60000	19	22
Case 71	0.0100	10	0.25	700	2000	100000	19	22
Case 72	0.0150	12	0.45	1100	1000	70000	19	22
Case 73	0.0117	15	0.25	700	2700	81000	19	22
Case 74	0.0245	10	0.35	1100	900	45000	19	22
Case 75	0.0175	10	0.25	1100	1700	119000	19	22
Case 76	0.0100	10	0.50	1100	2500	75000	18	21
Case 77	0.0175	8	0.70	1400	1000	50000	18	21
Case 78	0.0060	10	0.30	1100	1500	105000	18	21
Case 79	0.0320	5	0.40	1400	2000	60000	18	21
Case 80	0.0100	10	0.25	700	2000	100000	18	21
Case 81	0.0150	12	0.45	1100	1000	70000	18	21
Case 82	0.0117	15	0.25	700	2700	81000	18	21
Case 83	0.0245	10	0.35	1100	900	45000	18	21
Case 84	0.0175	10	0.25	1100	1700	119000	18	21

l: Thickness, h: Film Coefficient, k: Thermal Conductivity, ρ: Density, C: Specific Heat Capacity, L: Latent Heat, T_s: Solidification Temperature, T_m: Melting Temperature

The dimensionless numbers and the calculated Fo_{fl} in those simulations cases are tabulated in Table 4.12.

Table 4.12 Measured Fo_{fl} for simulation cases with different *Bi*, *Ste*, and Ψ_{pc}

Case	Ste^{-1}	Bi	Ψ	Ψ_{pc}	Fo_{fl}
Case 49	30	0.2	0.33	0.00	53.64
Case 50	50	0.2	0.33	0.00	85.88
Case 51	70	0.2	0.33	0.00	114.65
Case 52	30	0.4	0.33	0.00	28.14
Case 53	50	0.4	0.33	0.00	45.36
Case 54	70	0.4	0.33	0.00	62.18
Case 55	30	0.7	0.33	0.00	17.97
Case 56	50	0.7	0.33	0.00	28.92
Case 57	70	0.7	0.33	0.00	39.81
Case 58	30	0.2	0.33	0.33	82.73
Case 59	50	0.2	0.33	0.33	131.92
Case 60	70	0.2	0.33	0.33	177.27
Case 61	30	0.4	0.33	0.33	43.20
Case 62	50	0.4	0.33	0.33	70.36
Case 63	70	0.4	0.33	0.33	96.54
Case 64	30	0.7	0.33	0.33	27.73
Case 65	50	0.7	0.33	0.33	44.29
Case 66	70	0.7	0.33	0.33	60.85
Case 67	30	0.2	0.33	-0.33	29.82
Case 68	50	0.2	0.33	-0.33	47.67
Case 69	70	0.2	0.33	-0.33	62.18
Case 70	30	0.4	0.33	-0.33	16.31
Case 71	50	0.4	0.33	-0.33	25.00
Case 72	70	0.4	0.33	-0.33	34.18
Case 73	30	0.7	0.33	-0.33	10.05
Case 74	50	0.7	0.33	-0.33	16.20
Case 75	70	0.7	0.33	-0.33	22.31
Case 76	30	0.2	0.33	-0.67	12.91
Case 77	50	0.2	0.33	-0.67	20.41
Case 78	70	0.2	0.33	-0.67	24.75
Case 79	30	0.4	0.33	-0.67	7.30
Case 80	50	0.4	0.33	-0.67	10.54
Case 81	70	0.4	0.33	-0.67	14.36

Case 82	30	0.7	0.33	-0.67	4.44
Case 83	50	0.7	0.33	-0.67	7.31
Case 84	70	0.7	0.33	-0.67	9.82

As presented in Table 4.12, these cases consist of three different *Bi*, and *Ste* and four different Ψ_{pc}. To confirm the outcome of the section about the effect of *Bi* and *Ste*, the change of *Fo* as a function of *Bi* and *Ste* in other Ψ and Ψ_{pc} were investigated and illustrated in Figure 4.16 to Figure 4.19. These figures show the change of Fo_{fl} as a function of Ste^{-1} for Ψ= 0.33 and Ψ_{pc} = 0, Ψ_{pc} = 0.33, Ψ_{pc} = -0.33, and Ψ_{pc} = -0.67, respectively. Also, the change of Fo_{fl} as a function of *Bi* for those Ψ and Ψ_{pc} are presented in Figure 4.20 to Figure 4.23.

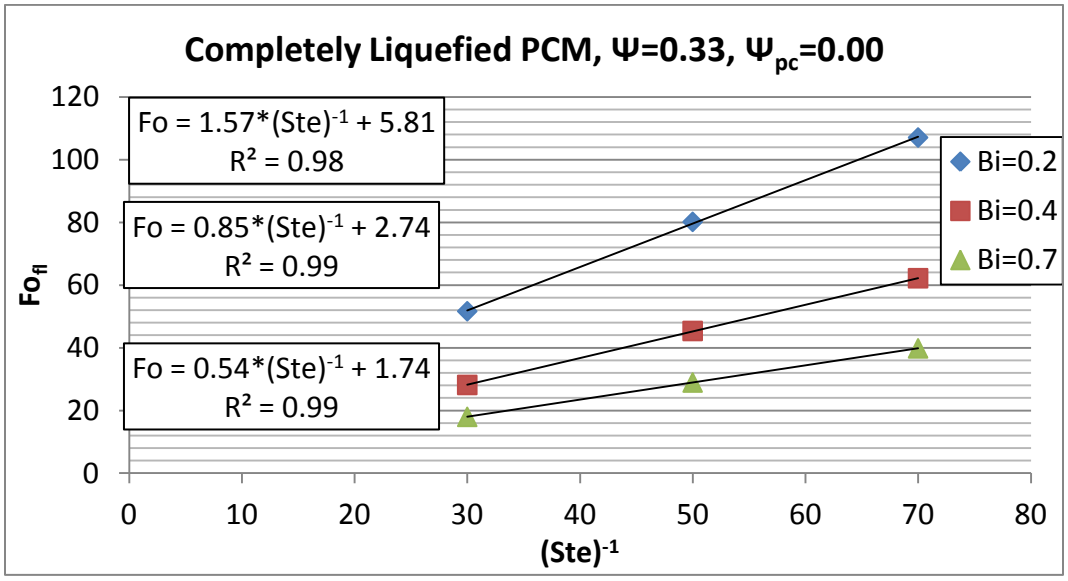

Figure 4.16 PCM completely liquefied Fo_{fl} as a function of $(Ste)^{-1}$ in different *Bi*, Ψ=0.33 and Ψ_{pc}=0

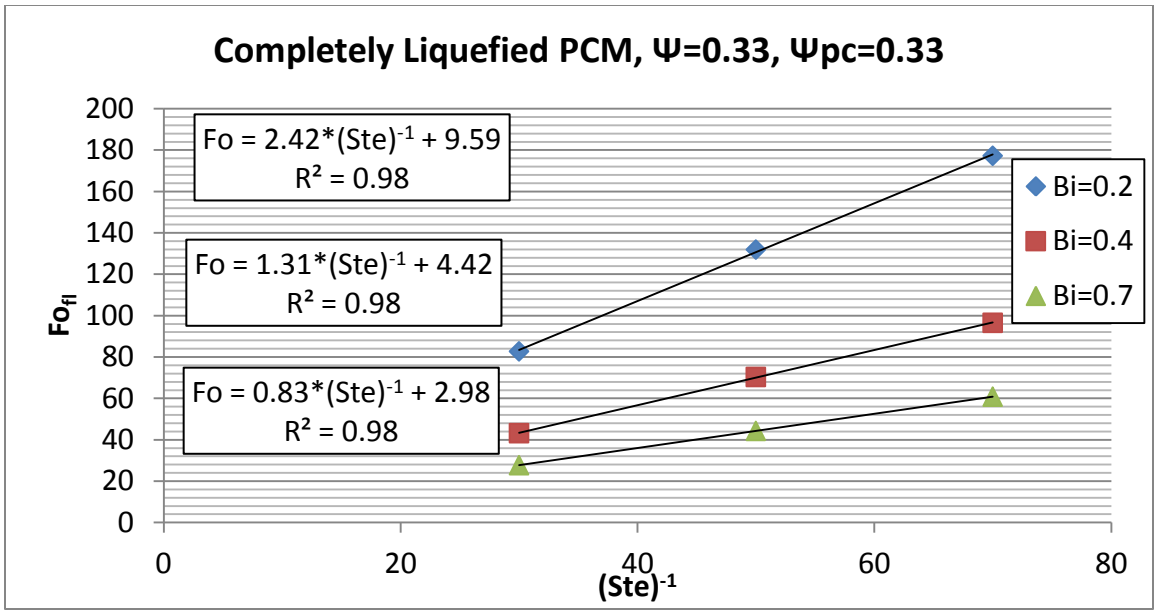

Figure 4.17 PCM completely liquefied Fo_{fl} as a function of $(Ste)^{-1}$ in different Bi, Ψ=0.33 and Ψ_{pc}=0.33

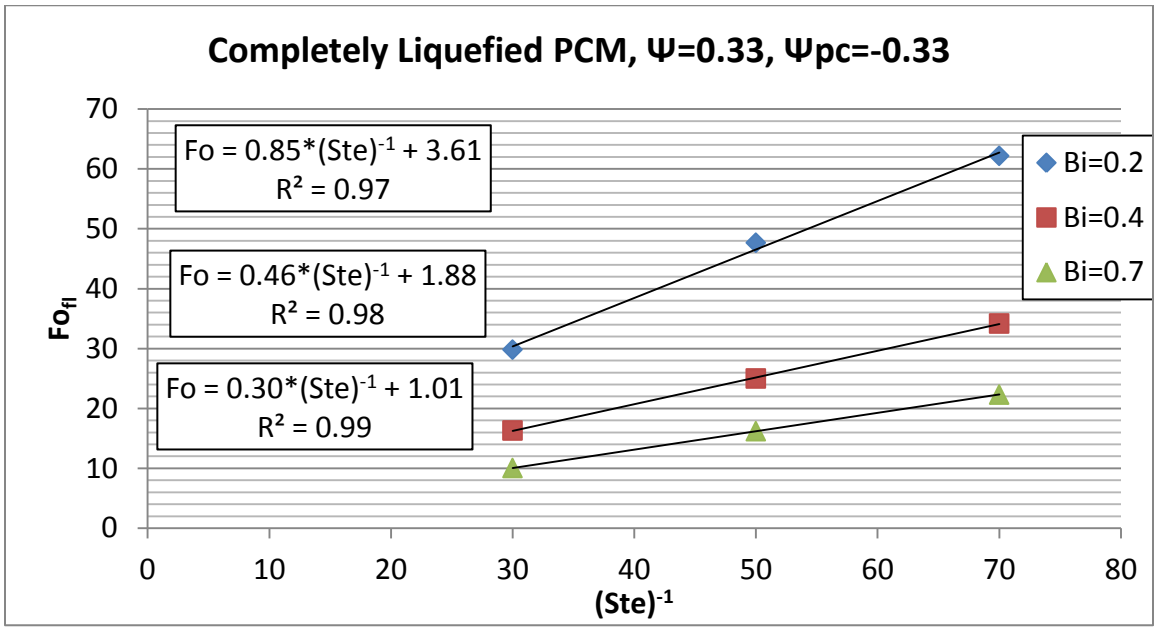

Figure 4.18 PCM completely liquefied Fo_{fl} as a function of $(Ste)^{-1}$ in different Bi, Ψ=0.33 and Ψ_{pc}= -0.33

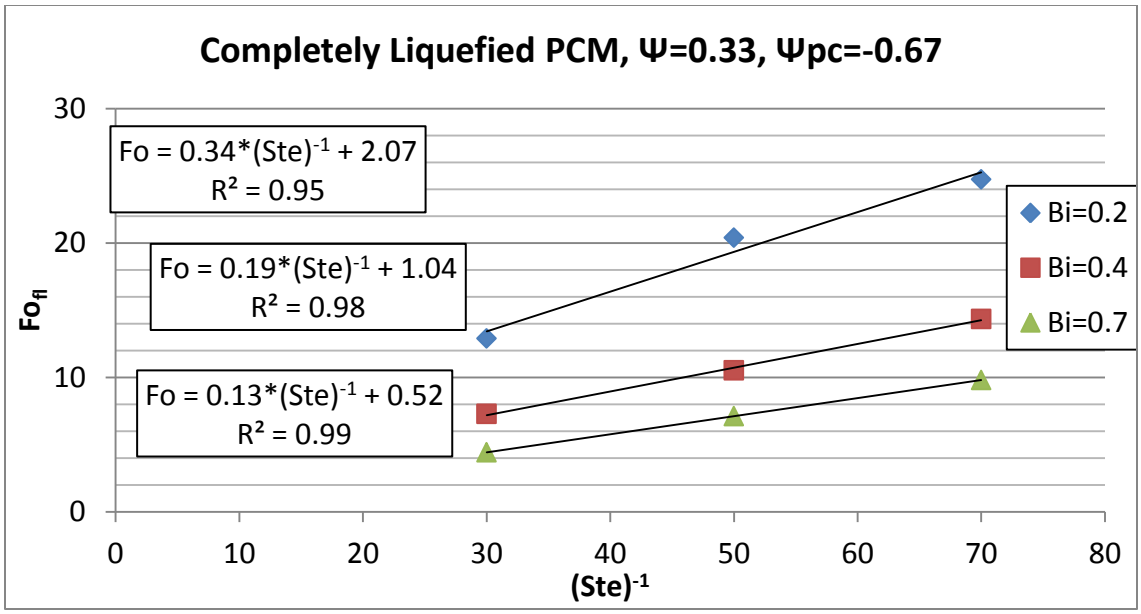

Figure 4.19 PCM completely liquefied Fo_{fl} as a function of $(Ste)^{-1}$ in different Bi, Ψ=0.33 and Ψ_{pc}= -0.67

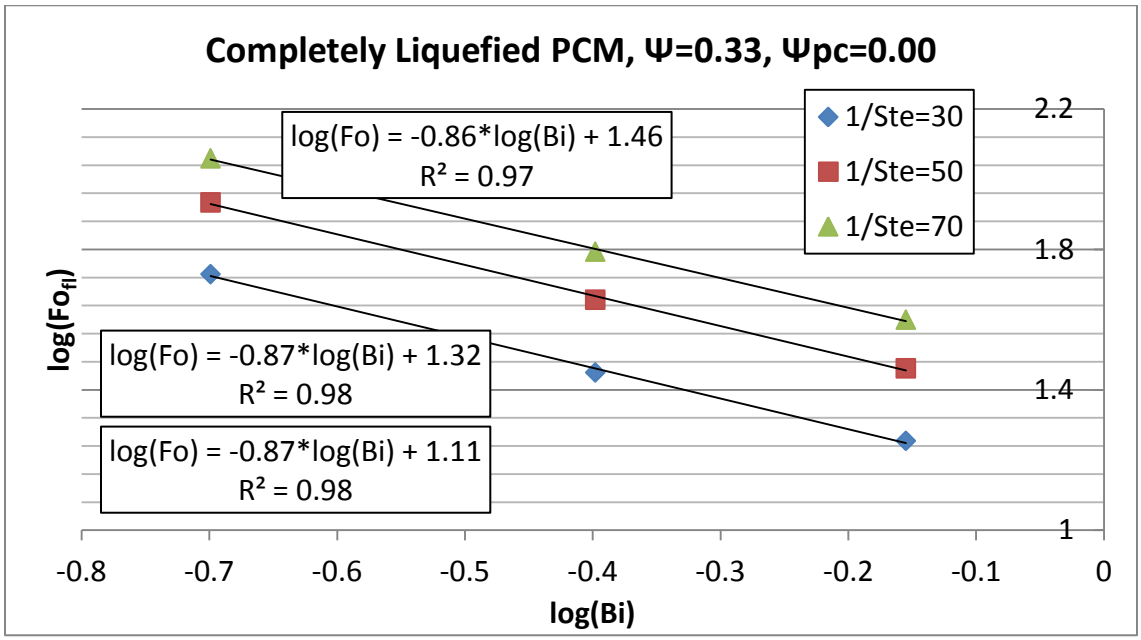

Figure 4.20 PCM completely liquefied Fo_{fl} as a function of Bi in different Ste, Ψ=0.33 and Ψ_{pc}= 0

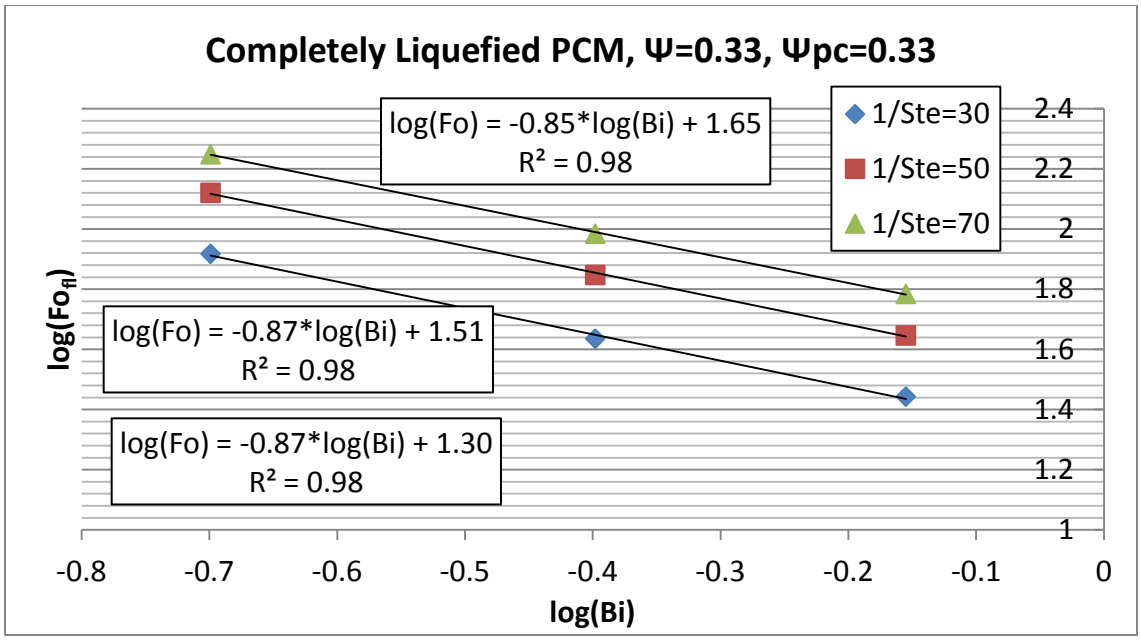

Figure 4.21 PCM completely liquefied Fo_{fl} as a function of Bi in different Ste, Ψ=0.33 and Ψ_{pc}= 0.33

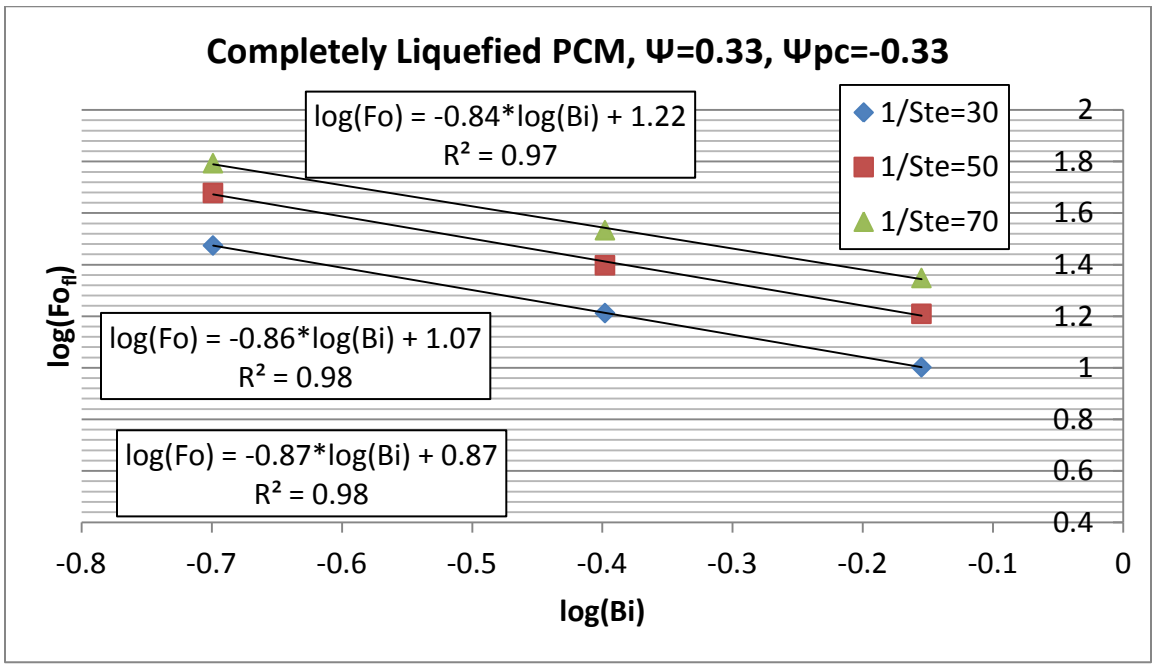

Figure 4.22 PCM completely liquefied Fo_{fl} as a function of Bi in different Ste, Ψ=0.33 and Ψ_{pc}= -0.33

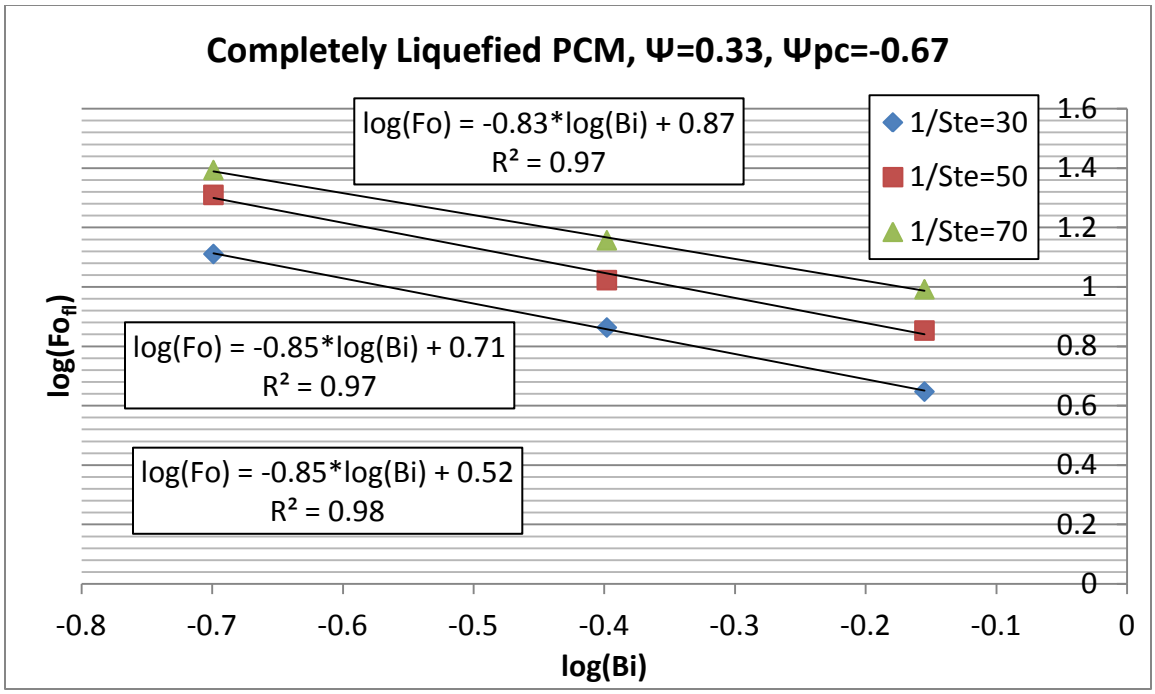

Figure 4.23 PCM completely liquefied Fo_{fl} as a function of *Bi* in different *Ste*, Ψ=0.33 and Ψ_{pc}= -0.67

The fitted curves presented in Figure 4.16-23 confirm that *Fo* changes linearly as a function of *Ste,* and it is independent of the melting ranges and fusion temperatures. Moreover, log (*Fo*) also changes linearly as a function of log (*Bi*) for different Ψ and Ψ_{pc}. In addition, the change of log (*Fo*) as a result of the change in log (*Bi*) occurs with a similar slope for different *Ste*, Ψ and Ψ_{pc} (independent of the melting range and fusion temperature).

Similar to the cases with Ψ_{pc}=-0.5, the y-intercepts of the trend-lines in Figure 4.16 to Figure 4.19 were compared with the analytically calculated *Fo* of the cases with $(Ste)^{-1}$=0 utilizing the equation (4-1). Based on their T_m, the y-intercepts of the trend-lines in Figure 4.16 need to be similar to the ones in Figure 4.5. Although the cases in those figures have different fusion temperatures and melting ranges, they become

completely melted when the temperature across the wallboard exceeds 23°C. The materials with $(Ste)^{-1}=0$ have the same temperature profile after the same time period; it is independent of their melting range and fusion temperature. Considering this argument, the y-intercepts of the trend-lines in Figure 4.18 and Figure 4.19 need to be close to the ones in Figure 4.11 and Figure 4.12, respectively. Moreover, for the cases in Figure 4.17 with T_m=24°C, the y-intercepts are compared with *Fo* calculated by equation (4-1) at x=0 and θ=0.2. The comparison is presented in Table 4.13. The trivial difference between the measured *Fo* of both methods validated the outcome of curve fitting with analytical solution for the cases with $(Ste)^{-1}=0$.

Table 4.13 Comparison of the analytical method and the framework for $Ste^{-1}=0$ @ $\Psi_{pc}=0.33$

Bi	***Fo* @ x=0 and θ=0.2 (Equation 4-1)**	***Fo*$_{fl}$ @ $(Ste)^{-1}=0$ (Figure 4.17)**
0.2	8.76	9.59
0.4	4.73	4.42
0.7	3.01	2.98

The effect of Ψ_{pc} on *Fo* is illustrated in each single set of (*Bi*, *Ste*) in Figure 4.24. This figure shows the change of *Fo* when PCM is completely liquefied as a function of Ψ_{pc} in constant Ψ. Regarding the curve fitting of data , the change of *Fo* is linear for any set of (*Bi*, *Ste*). To map the result from one available Ψ_{pc} to another, the correlation between the slope of the fitted curves, *Bi* and *Ste* needs to be studied. For the simulated sets of *Ste* and *Bi*, the magnitudes of the slopes of the fitted curves are tabulated in Table 4.14.

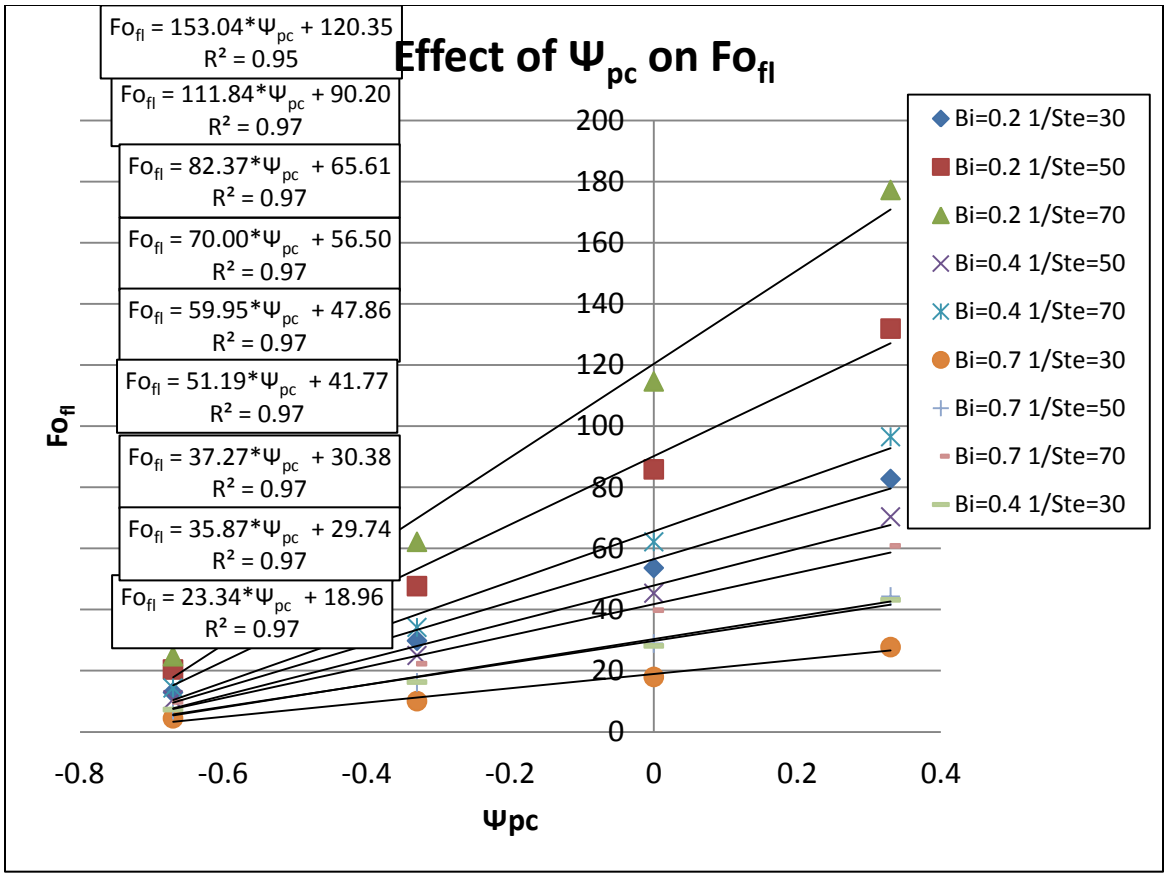

Figure 4.24 Effect of Ψ_{pc} on *Fo* in different *Bi* and *Ste* with similar Ψ

Table 4.14 S_L of linear fitted curve in the simulated set of (*Bi*, *Ste*)

Set	Ste^{-1}	*Bi*	Slope (S_L)
Set 1	30	0.2	70.00
Set 2	50	0.2	111.84
Set 3	70	0.2	153.04
Set 4	30	0.4	35.87
Set 5	50	0.4	59.95
Set 6	70	0.4	82.37
Set 7	30	0.7	23.34
Set 8	50	0.7	37.27
Set 9	70	0.7	51.19

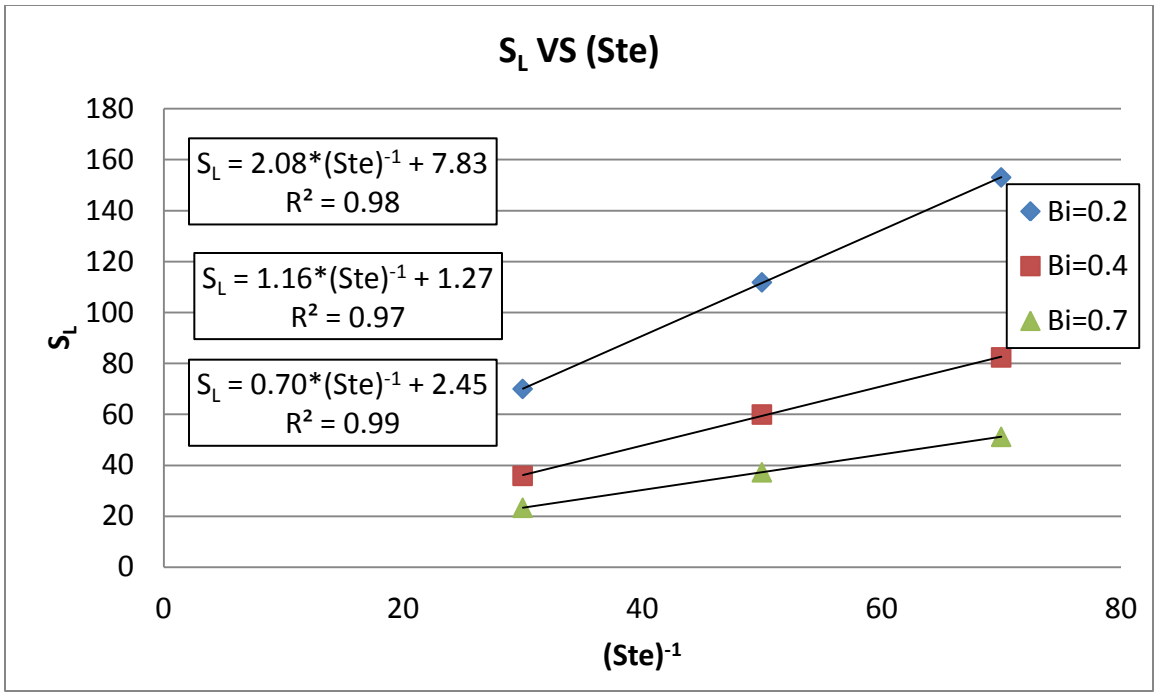

Figure 4.25 S_L as a function of $(Ste)^{-1}$ in different Bi

The way that those slopes change as a function of Bi and Ste quantifies the correlation to map Fo_{fl} from one Ψ_{pc} to another.

Figure 4.25 and Figure 4.26 illustrate the correlations between S_L, Ste and Bi, respectively. Like Fo, S_L increases linearly as a function of $(Ste)^{-1}$, and log (S_L) decreases linearly by increasing log (Bi). Moreover, like the graph developed for Fo for different Ste and Bi (Figure 4.10), the correlations obtained in Figure 4.25 and Figure 4.26 are utilized to build up a graph to calculate S_L for any set of (Bi, Ste).

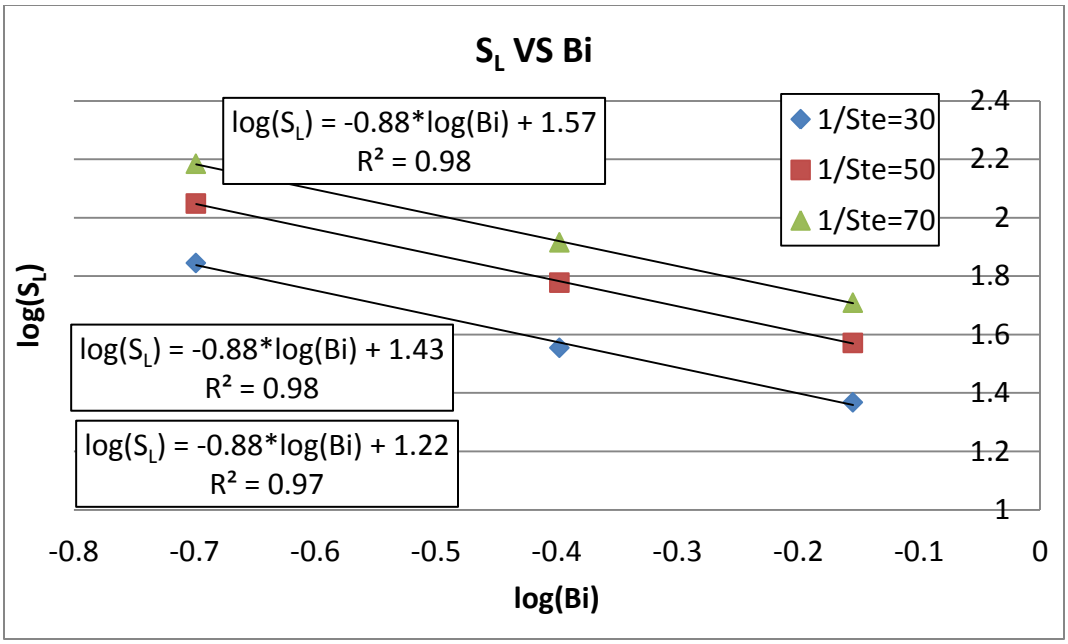

Figure 4.26 S_L as a function of *Bi* in different $(Ste)^{-1}$

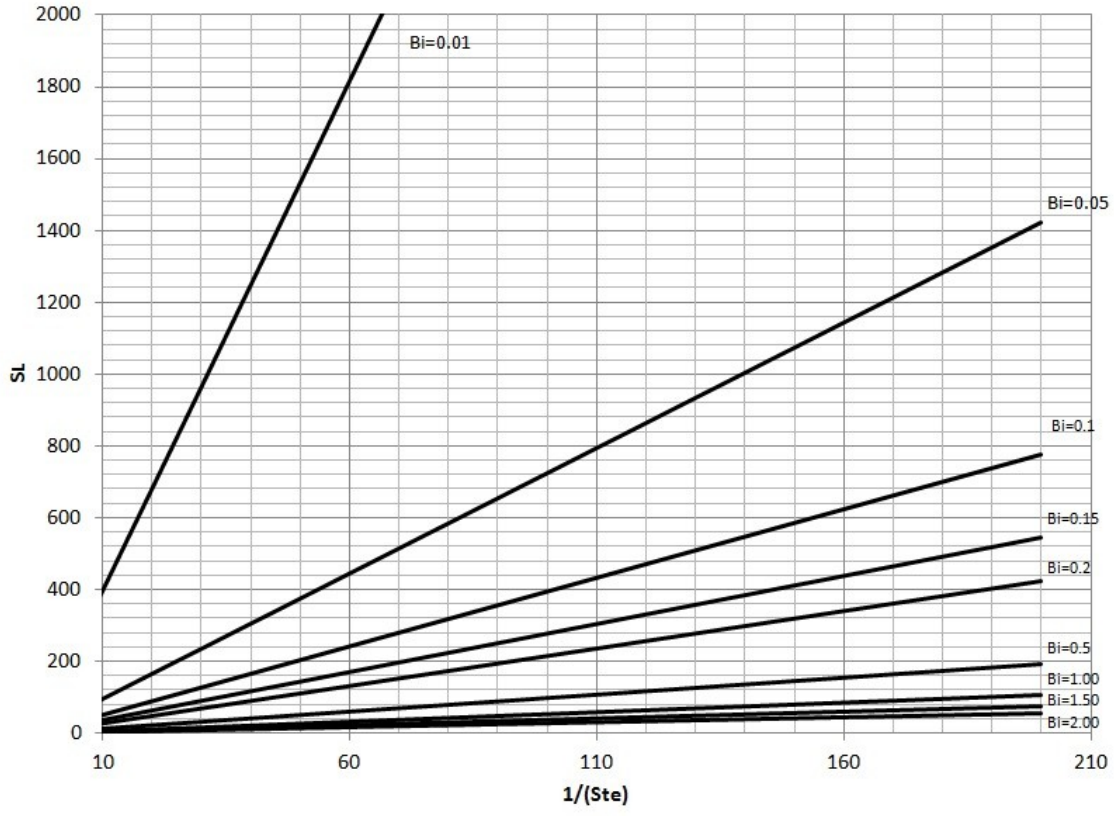

Figure 4.27 S_L calculator for different *Bi* and *Ste*

Considering the chart in Figure 4.10 as the base graph of the design framework, the slopes calculated from the impact of Ψ and Ψ_{pc} are applied to map the base graph from one fusion temperature and melting range to other magnitudes. To check the accuracy of the extrapolation regarding the change of Ψ and Ψ_{pc}, the testing cases designed and utilized in section 4.3 (Table 4.6) are employed for different T_s and T_m in order to compare the Fo_{fl} of the PCM wallboard acquired by simulation with the one calculated with the extrapolation from the base graph. Both calculated Fo_{fl} in these testing cases either by simulation or from the framework. The relative error is also presented in Table 4.15. The mean average error for the testing scenarios was less than 5%.

Table 4.15 Fo_{fl} calculated in testing scenarios with both simulation and the framework (effect of Ψ and Ψ_{pc})

Testing Case	T_s [°C]	T_m [°C]	Ψ	Ψ_{pc}	$^{1}Fo_{fl}$	$^{2}Fo_{fl}$	$^{3}Fo_{fl}$	Error [%]
T-Case 1	18	23	0.20	-0.40	22.81	26.85	27.44	2.14
T-Case 2	19	23	0.25	-0.25	14.11	20.57	21.08	2.42
T-Case 3	20	23	0.33	0.00	41.82	84.50	80.47	5.01
T-Case 4	19	22	0.33	-0.33	88.75	106.29	99.01	7.35
T-Case 5	18	21	0.33	-0.66	80.20	229.29	217.29	5.52
T-Case 6	20	22	0.50	0.00	121.58	238.00	227.43	4.65
T-Case 7	18	23	0.20	-0.40	99.75	119.25	125.35	4.87
T-Case 8	19	23	0.25	-0.25	15.16	21.20	20.54	3.23
T-Case 9	20	23	0.33	0.00	71.14	144.97	135.73	6.81
T-Case 10	20	22	0.50	0.00	75.45	146.02	136.52	6.96

(1) The base Fo_{fl} (Figure 4.10)
(2) Fo_{fl} after the effect of Ψ and Ψ_{pc} (From the design framework)
(3) Fo_{fl} calculated by simulation

4.5 Effect of Room Temperature Time Lag

To have the shift of space heating from peak to off peak periods, PCM wallboards in the enclosed space need to be charged during night time by increasing the room temperature to the highest bound of thermal comfort. As explained at the beginning of this chapter, to heat up a mounted PCM wallboard in the simulation scenarios, the room set point temperature was increased from 20°C to 25°C during the night time and kept at 25°C until the onset of peak hours. At first the assumption was made to have a sudden change of room air temperature as a result of a change in set-point temperature with no delay time in room temperature. The assumption of step change in room temperature is relaxed in this section. Although the set-point is fixed at 25°C, the room temperature is raised to 25°C with a time lag resulted from the room thermal mass (including the furniture inside the space). This time lag also affects the charging of the PCM wallboard. This section highlights the effect of room temperature time lag (Γ_{RTL}) on the time period required to fully charge a PCM wallboard.

To simulate the room temperature change, it is assumed that it rises linearly in a pre-determined time period. Therefore, starting from 20°C, the temperature rises up to 25°C during the pre-determined time lag period. The range of time lag was assumed to be from zero to six hours. While the zero hour Γ_{RTL} corresponds to immediate room temperature change from 20°C to 25°C, the other Γ_{RTL} magnitudes correspond to the period in which the room temperature changes linearly from 20°C to 25°C.

A number of simulations were conducted to calculate the time required for the PCM wallboard to become fully liquefied. To determine the change of the time required

to fully melt the PCM wallboard with Γ_{RTL}, 11 simulations were performed with 11 different Γ_{RTL} magnitudes for a PCM wallboard with corresponding *Bi* and *Ste*. The simulations were carried out for a PCM wallboard with *Bi*=0.4 and Ste^{-1}=56. Table 4.16 shows the specifications of the simulated cases in addition to the Fo_{fl} and the time required to have the PCM wallboard fully melted. The change of the time required to fully melt the PCM wallboard is presented as a function of Γ_{RTL} in Figure 4.28. The graph shows that the liquefaction time changes linearly with Γ_{RTL}.

Table 4.16 Simulated cases for Bi=0.4 and Ste^{-1}=56 with various room temperature time lag

Time Lag Case	Ste^{-1}	*Bi*	Γ_{RTL} [hr]	Fo_{fl}	Time [hr]
TL-Case 1	56	0.4	0	27.09	8.28
TL-Case 2	56	0.4	0.5	28.18	8.61
TL-Case 3	56	0.4	1	29.09	8.89
TL-Case 4	56	0.4	1.5	29.91	9.14
TL-Case 5	56	0.4	2	30.73	9.39
TL-Case 6	56	0.4	2.5	31.54	9.64
TL-Case 7	56	0.4	3	32.45	9.92
TL-Case 8	56	0.4	3.5	33.27	10.17
TL-Case 9	56	0.4	4	34.18	10.44
TL-Case 10	56	0.4	5	35.91	10.97
TL-Case 11	56	0.4	6	37.82	11.56

To investigate the influence of *Ste* and *Bi* on the rate of change of the liquefaction time, a number of simulations were carried out with PCM wallboards with a range of *Ste* and *Bi*. Three *Bi* (0.2, 0.4, and 0.7) and three $(Ste)^{-1}$ (30, 50, and 70) were selected. The time required for the PCM wallboard to become fully melted was calculated in three Γ_{RTL} (0, 2, and 4 hours).

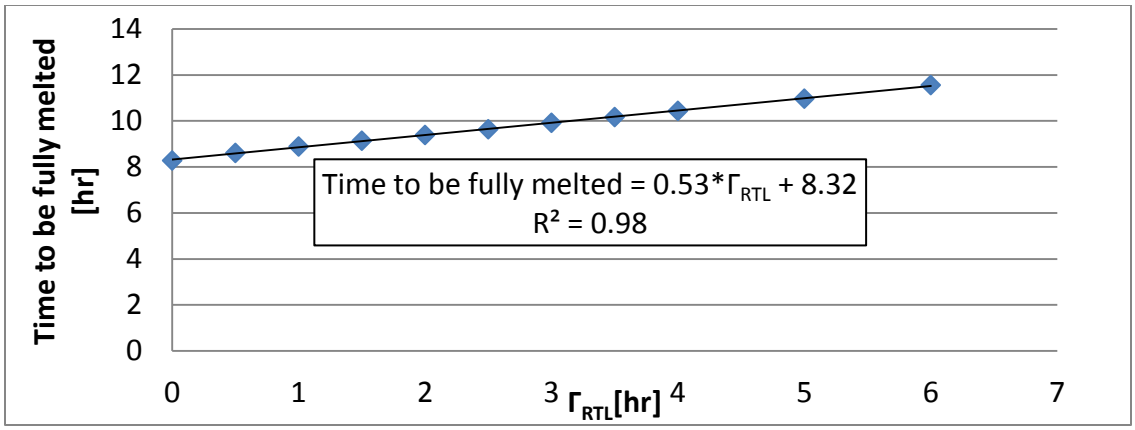

Figure 4.28 Change of time required to fully liquefied a PCM wallboard as a function of room temperature time lag

Table 4.17 presents the calculated time for liquefaction for different *Bi*, *Ste* and Γ_{RTL}. Expecting to have linear changes of liquefaction time as seen in Figure 4.28, their rates of change for different *Bi* and *Ste* were calculated using curve fitting as presented in Figure 4.29.

As presented in Figure 4.29, the fitted curves have the slope around 0.55 for the simulated *Bi* and *Ste*. While the required time for $\Gamma_{RTL}=0$ can be calculated using the correlations like the one in Figure 4.10, the result can be corrected for the real Γ_{RTL} by extrapolation using the linear equation with the slope of 0.55.

To check the accuracy of this extrapolation, the testing cases designed and utilized in section 4.3 (Table 4.6) were employed with $\Gamma_{RTL}\neq 0$ to compare the liquefaction time of the PCM wallboard acquired by the simulation with the one calculated using the correlation. Those cases once were simulated with $\Gamma_{RTL}=0$ in section 4.3 and with random Γ_{RTL} in this section. Table 4.18 presents the cases with the required time of complete

liquefaction calculated by the simulation and correlation. The mean average relative error of these results was around 1%.

Table 4.17 Simulation cases for studying the effect of *Ste*, *Bi* and Γ_{RTL} on the liquefaction time

Time Lag Case	Ste^{-1}	Bi	Γ_{RTL} [hr]	Fo_{fl}	Time [hr]
TL-Case 12	30	0.2	0	29.45	4.5
TL-Case 13	30	0.2	2	36.54	5.58
TL-Case 14	30	0.2	4	43.64	6.67
TL-Case 15	30	0.4	0	15.91	11.67
TL-Case 16	30	0.4	2	17.35	12.72
TL-Case 17	30	0.4	4	18.75	13.75
TL-Case 18	30	0.7	0	10.03	6.08
TL-Case 19	30	0.7	2	11.82	7.17
TL-Case 20	30	0.7	4	13.56	8.22
TL-Case 21	50	0.2	0	45.13	3.86
TL-Case 22	50	0.2	2	58.44	5
TL-Case 23	50	0.2	4	71.1	6.08
TL-Case 24	50	0.4	0	24.43	5.97
TL-Case 25	50	0.4	2	28.98	7.08
TL-Case 26	50	0.4	4	33.3	8.14
TL-Case 27	50	0.7	0	15.43	7.28
TL-Case 28	50	0.7	2	17.79	8.39
TL-Case 29	50	0.7	4	20.02	9.44
TL-Case 30	70	0.2	0	60.1	3.3
TL-Case 31	70	0.2	2	81.82	4.5
TL-Case 32	70	0.2	4	102.02	5.61
TL-Case 33	70	0.4	0	32.5	3.97
TL-Case 34	70	0.4	2	42.04	5.14
TL-Case 35	70	0.4	4	51.14	6.25
TL-Case 36	70	0.7	0	20.91	13.3
TL-Case 37	70	0.7	2	22.7	14.44
TL-Case 38	70	0.7	4	24.32	15.47

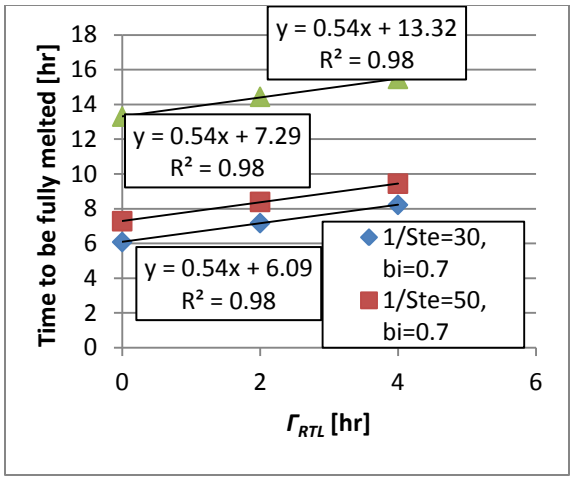

(a)

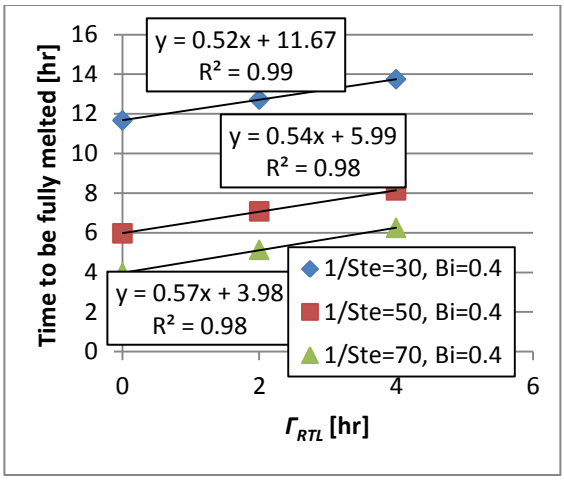

(b)

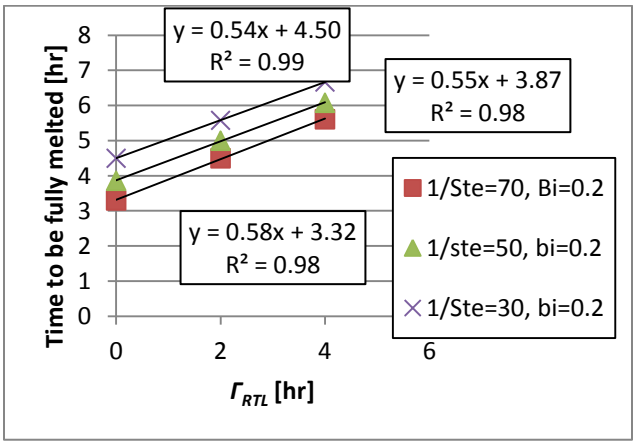

(c)

Figure 4.29 Change of fully melting time versus Γ_{RTL} for three *Ste* a) *Bi*=0.7 b)*Bi*=0.4 c)*Bi*=0.2

Table 4.18 The testing cases for Γ_{RTL}

Testing Case	$(Ste)^{-1}$	Bi	Γ_{RTL} [hr]	Fo_{fl} @ $\Gamma_{RTL}=0$	Time @ $\Gamma_{RTL}=0$	(1)Time @ $\Gamma_{RTL}\neq0$	(2)Time @ $\Gamma_{RTL}\neq0$	Error [%]
T-Case 1	94	0.86	1.5	23.14	14.50	15.44	15.32	0.75
T-Case 2	57	0.88	2.5	14.59	19.08	20.44	20.46	0.07
T-Case 3	116	0.53	6.0	41.52	18.03	21.36	21.33	0.14
T-Case 4	62	0.11	4.0	94.70	2.44	4.78	4.64	3.02
T-Case 5	45	0.09	0.5	84.00	4.17	4.50	4.44	1.24
T-Case 6	191	0.26	2.0	123.21	25.97	27.39	27.07	1.18
T-Case 7	136	0.22	3.5	105.30	28.30	30.33	30.22	0.35
T-Case 8	22	0.33	1.0	14.81	3.80	4.36	4.35	0.23
T-Case 9	189	0.49	3.0	69.33	8.56	10.53	10.21	3.13
T-Case 10	184	0.44	5.0	75.86	27.19	30.11	29.94	0.57

(1) Time when PCM completely liquefied (simulation)
(2) Time when PCM completely liquefied (correlation)

4.6 SUMMARY

In this chapter, a framework was developed to design a building envelope integrated with a PCM wallboard in order to shift the space conditioning from peak to off peak periods. Due to the fact that the focus is to charge and store thermal energy in the PCM wallboard during off-peak periods, the design framework mainly consists of the relationship between the design parameters and the time required to fully melt the PCM. The time required to charge the PCM wallboard is the key for an effective design of such a system: The wallboard must be fully charged during off-peak hours. Therefore, the length of the charging period is determined based on the application. Also, it is set as the time in which the room temperature set-point is increased from the lower bond to the higher bond of thermal comfort. Therefore, the PCM wallboard goes through phase transition and stores latent heat energy while the thermal comfort is satisfied.

Each PCM wallboard has its own thermo-physical specifications and changing the composition of the materials results in a change in all other thermo-physical properties. Moreover, based on the thermo-physical properties of a material, the size of the layer has to be altered to be charged in a pre-determined time period. Therefore, the design framework is needed to be general to consider the simultaneous change of all thermo-physical properties of all available materials in the market. Taking this into account, the dimensionless study was conducted and the effective dimensionless parameters were introduced. Moreover, the charging time of a PCM wallboard was characterized by Fo, and the effects of dimensionless parameters on the magnitude of Fo_{fl} were investigated. As the results, the change of Fo_{fl} was characterized based on the change of Bi, Ste, melting range, fusion temperature and $\Gamma_{RTL.}$ The study provided a number of graphs as a framework to correlate Fo_{fl} as a function of dimensionless parameters which can be utilized to size or improve a wallboard to be charged in a pre-determined time period. Indeed, the design framework consists of a number of steps to be taken to size a PCM wallboard which is summarized in Figure 4.30. The flowchart encompasses three stages: In the first one, the thermo-physical properties of the available PCM wallboard in the market are identified, and an arbitrary thickness is estimated for it. Then, in the second stage, the design framework is utilized to characterize the charging time of the PCM wallboard based on its properties. In the last stage, the charging times calculated in both stages are compared to identify the best size of the wallboard.

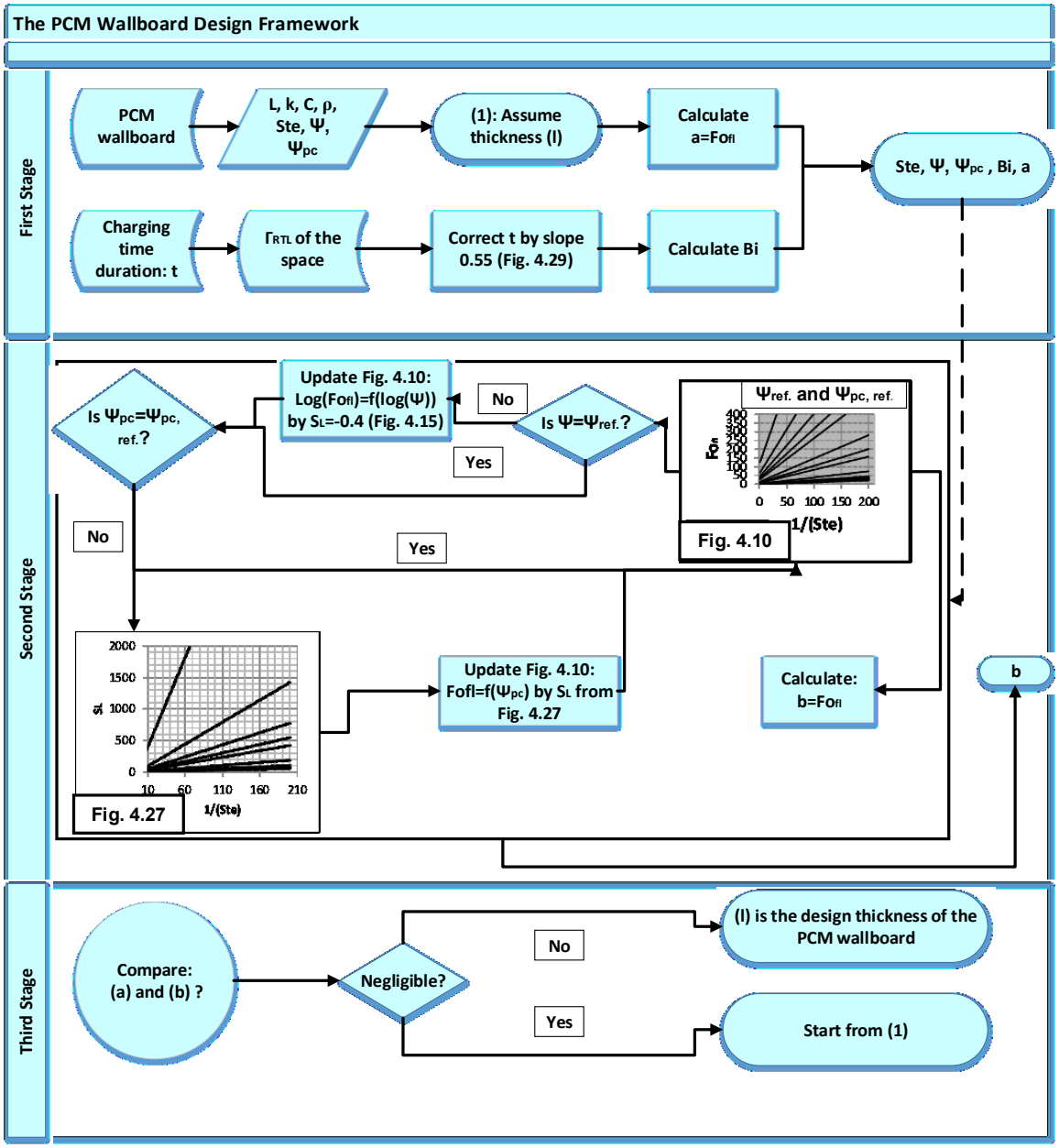

Figure 4.30 The flowchart of the PCM wallboard design framework

CHAPTER 5 APPLICATION OF DESIGN TOOL IN REAL BUILDING SIMULATION

5.1 INTRODUCTION

The dimensionless parameters influencing the performance of a PCM wallboard were identified and discussed in the previous chapter. In addition, the correlations between those effective parameters and Fo_{fl} were characterized in order to develop a framework to select and size a PCM wallboard which can be fully melted during a given time, i.e. off-peak hours. Regarding the thermo-physical properties of materials and the length of the off-peak period, the available PCM wallboards in the market need to be mounted in a specific thickness to be fully melted. Selecting the best choice of the available wallboards and identifying the best size are accomplished using the framework prepared and provided in the former chapter.

To evaluate the performance of the framework for a real application, an existing building was simulated with a mounted PCM wallboard using TRNSYS simulation software. Three PCM wallboards were selected from the literature, and each of them was sized separately for the simulated building on which the developed framework was employed. Moreover, both the charging and discharging procedure of the mediums were characterized regarding the temperature of the wallboard and the load demand shift.

5.2 TRNSYS SIMULATION CASE SPECIFICATION

5.2.1 Building description

The building selected as the real scenario for this study was a bungalow-style residential building with two conditioned floors modeled and validated by Aongya (2010). It is a two-story building with a floor area of 104 m^2 and approximate dimensions of 12.8 m* 8.1 m, the ground floor and the basement. It consists of three bedrooms and a bathroom on the ground floor and a finished basement space. The house, which dates back to 1960s, was recently partially renovated. It is located in a typical residential area in the city of Trois-Rivières, Quebec, Canada, and the front wall of the built space is oriented N46.5° W.

The thermal performance of this building was modeled using the TRNSYS simulation tool. TRNSYS is a simulation environment employed to simulate the transient thermal behavior of a multi-zone building and analyze its energy consumption. It consists of several programs including Simulation Studio, Simulation Engine (TRNDll), the building input data visual interface (TRNBuild), and its editor (TRNEdit). The TRNSYS Simulation Studio is the main interface in which a project can be created by drag and dropping different components and connecting them together. The adopted and connected components in the Simulation Studio set up the global simulation parameters. Type 56 is employed as one of the main components to create a multi-zone building with its defined envelopes and conditioned zones.

The simulated house was divided into 16 distinct zones. The plan of the house and the dimension of the zones are presented in Figure 5.1. The attic as the last zone is not presented in Figure 5.1. More details about the wall sections, fenestrations and the built model inside TRNSYS is presented in Aongya (2010).

In this study, the conventional gypsum boards of the external walls in Zone 1 were replaced with PCM wallboards. The sequent layers in the external wall section in Zone 1 from outside toward inside are brick, air gap (thermal resistance equivalent to 0.12 [$m^2.K.W^{-1}$]), fiberboard, insulation, and gypsum board, respectively. Their thickness and thermal properties are presented in Table 5.1.

Table 5.1 Layers in external wall section of zone 1

Name of layer	**Thickness [mm]**	**Thermal heat capacity [$J.kg^{-1}.K^{-1}$]**	**Thermal conductivity [$W.kg^{-1}.K^{-1}$]**	**Density [$kg.m^{-3}$]**
Gypsum board	13	1090	0.16	800
Insulation	140	944	0.05	49
Fiberboard	13	1300	0.07	350
Brick	102	840	0.42	1980

This zone has two external walls: one with the area of 8.64 m^2 and the other with the area of 13.53 m^2 oriented toward southwest and northwest, respectively. There is a steel door in the northwest wall with 1.256 [$m^2.K.W^{-1}$] equivalent heat transfer resistance. It has six adjacent zones. It shares walls with Zone 7 and Zone 2, the ceiling with the attic of the house and the floor with three zones; Zone 8, Zone 8A and Zone 13. The only interior opening of Zone 1 is a door located on the wall shared with zone 2. The details of the layers of the internal walls, the floor and the ceiling of Zone 1 are presented in Table 5.2 (Aongya, 2010).

Table 5.2 Layers in internal wall section, floor and ceiling of Zone 1: their thickness and thermo-physical properties

Position	Adjacent zones	Material	Thickness [mm]	Conductivity [$W.m^{-2}.K^{-1}$]	Thermal heat capacity [$J.kg^{-1}.K^{-1}$]	Density [$kg.m^{-3}$]
Wall	Zone 2, Zone 7	Gypsum board	13	0.16	1090	800
		Equivalent air gap	76	0.58	1088	41.08
		Gypsum board	13	0.16	1090	800
Floor	Zone 8, Zone 8A, Zone 13	Hardwood	10	0.16	1630	670
		Plywood	13	0.12	1210	540
		Equivalent insulation	140	0.05	940	49
		Air gap	-	-	-	-
		Gypsum board	13	0.16	1090	800
Ceiling	Attic	Gypsum board	13	0.16	1090	800
		Equivalent insulation	152	0.04	1430	76.09
		Insulation	191	0.04	1380	40.1

All zones were conditioned by baseboard heaters except the attic, Zone 5 (the corridor) and Zone 8A (the wardrobe in basement). The baseboard heaters were controlled by thermostats in each zone with their own zone temperature set point. Considering the simulation carried out in the TRNSYS, the source and sink of the heat occur in a single point inside a zone. Therefore, the exact location of the heater inside a zone is not specified, and the entire zone is thermally characterized as one node, well mixed assumption. For Zone 1 which is investigated in detail in this study, the heater has a measured full capacity of 1890 W (Aongya, 2010).

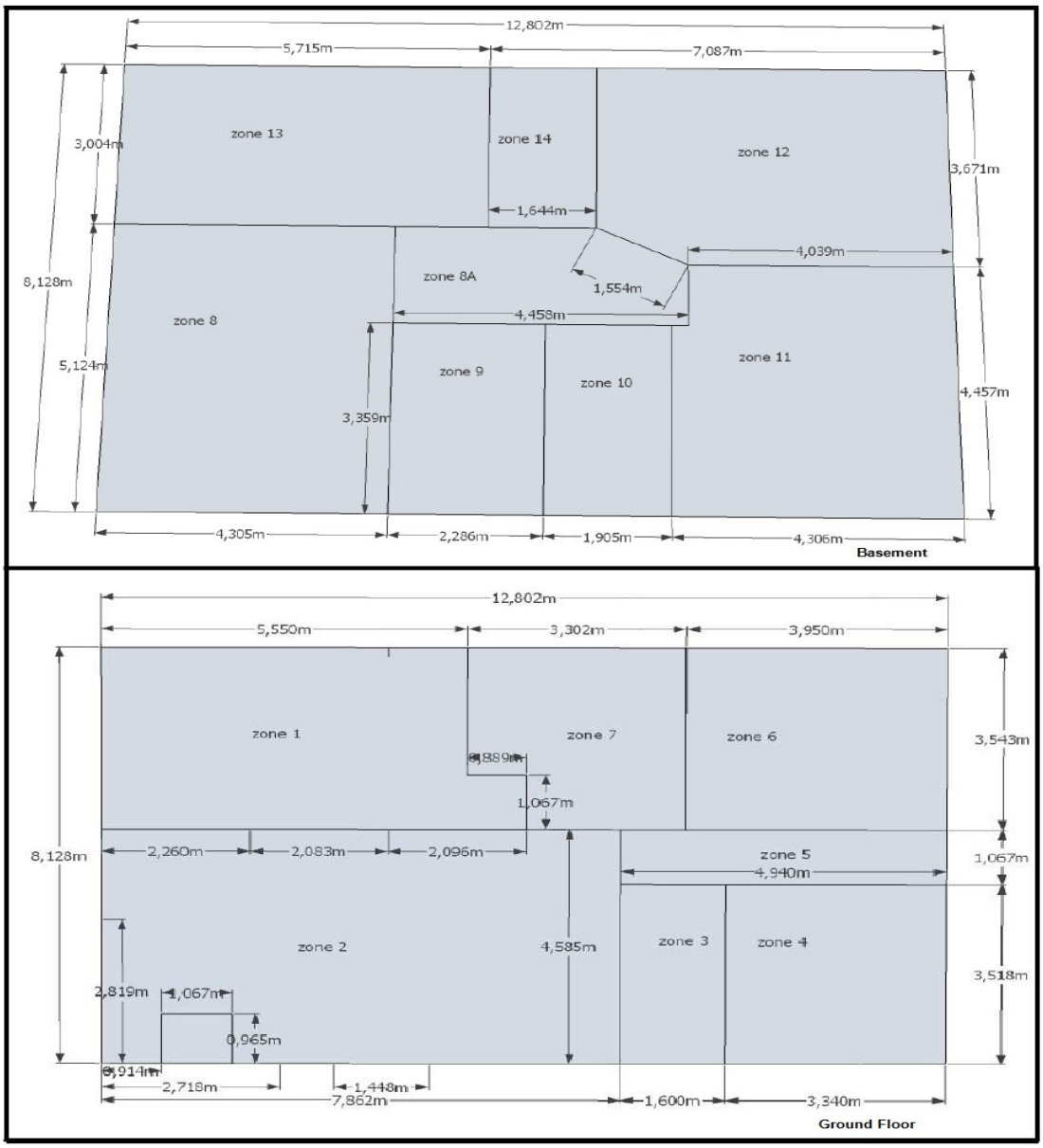

Figure 5.1 Plan of the zones in the simulated residential building from Aongya (2010)

To simulate the house, type 56 as the multi-zone building-component is accompanied by the other components required to provide the weather data, sky and soil temperatures, the set-point temperature of the rooms, and the baseboard heaters specifications. Those components are placed in Simulation Studio and linked together to

simulate the thermal performance of the building. The TRNSYS interface with all these components presented in Figure 5.2.

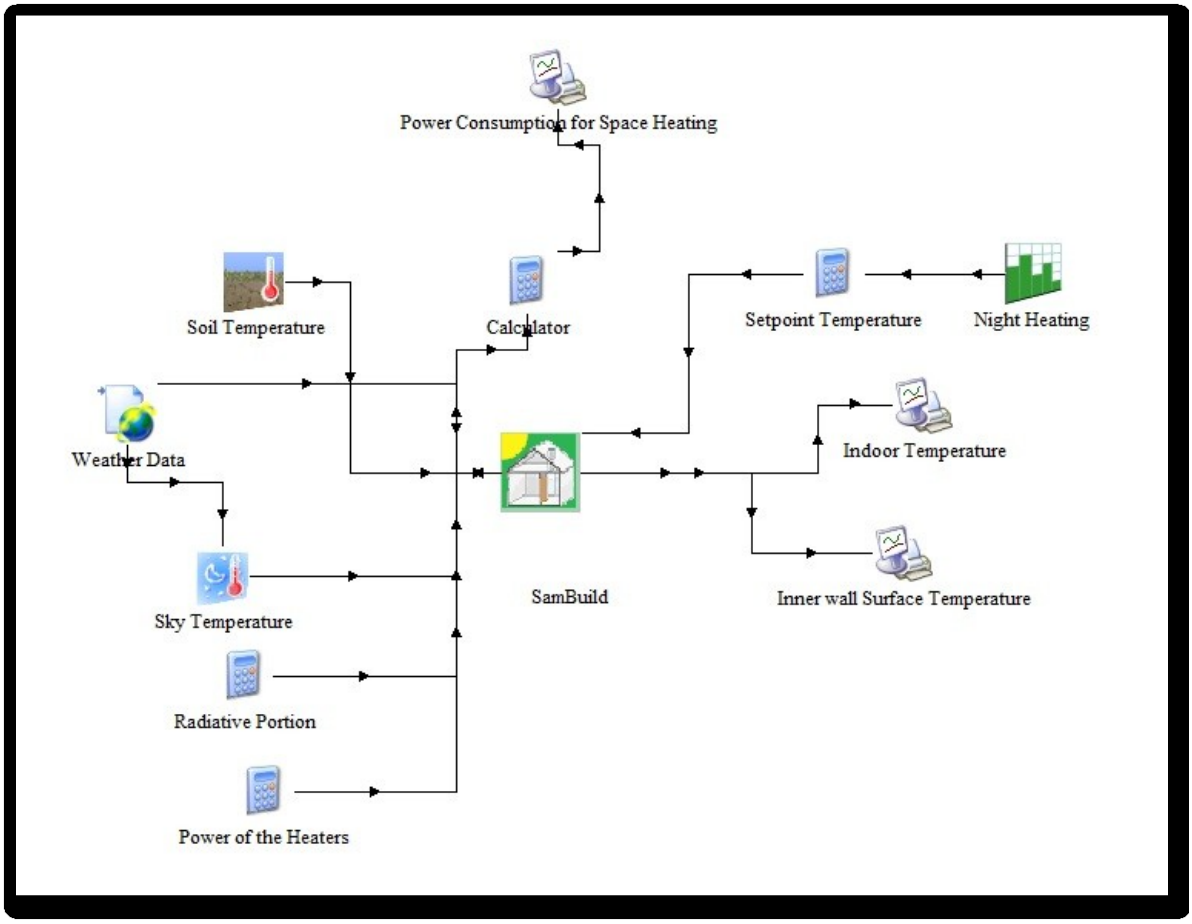

Figure 5.2 Simulation Studio of the TRNSYS simulation of SamBuild without PCM wallboard

5.2.2 PCM simulation component in TRNSYS

As explained in section 2.4.5, there are three different components developed in the platform of TRNSYS to simulate a PCM wallboard inside the building envelope. Among those components, only one, Type 255, has been validated by experimental data (Kuznik et al., 2010). The application of this component inside a TRNSYS simulation was validated using the experimental data of the pilot-scale cubicle with a PCM layer

(Kuznik and Virgone, 2009a) which is the same data employed to validate the developed finite difference model for simulating the heat transfer inside a PCM wallboard in this dissertation.

To simulate the PCM layer in TRNSYS, the component needs to be added to the Simulation Studio and linked with Type 56 for multi-zone building simulation. The PCM component is utilized to simulate the heat transfer through the whole wall section which includes the PCM layer. As an output, the inner surface temperature of the wall section is provided for type 56.

Herein, to render the application of the PCM component reliable, the experimental case of the pilot-scale cubicle with internal PCM layer in (Kuznik and Virgone, 2009a) was simulated in TRNSYS using the PCM component (Type 255). The details of the experiment were explained in section 2.4.5. The simulation of the cubicle was built in the Simulation Studio as the interface of TRNSYS software. The employed components including the PCM component are linked together as presented in Figure 5.3. The figure shows that type 56 was used to build the cubicle while the three wall sections with the PCM layer were prepared by the PCM component connected to type 56.

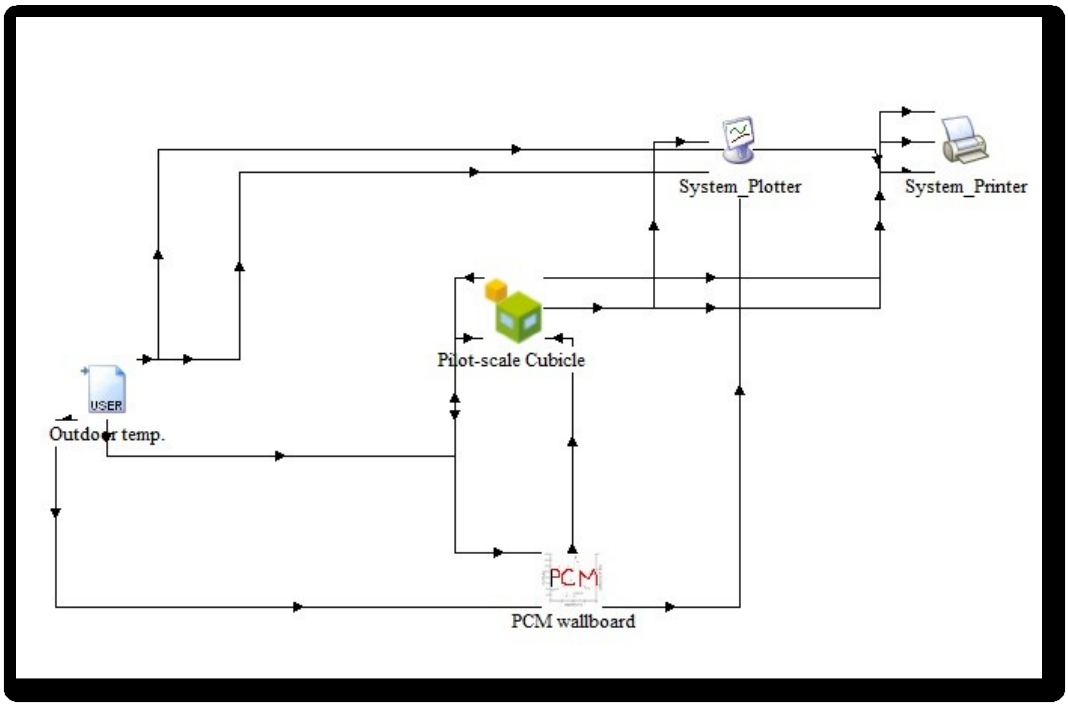

Figure 5.3 Validation of PCM component in TRNSYS simulation

Figure 5.4 shows the simulation results and the experiments for the step change of the outdoor temperature. Except for the starting part of the simulation, there is a good agreement between the experimental and simulation results. There is a deviation from the experimental data in the beginning of the simulation which can be associated with the initialization procedure in the transient simulations.

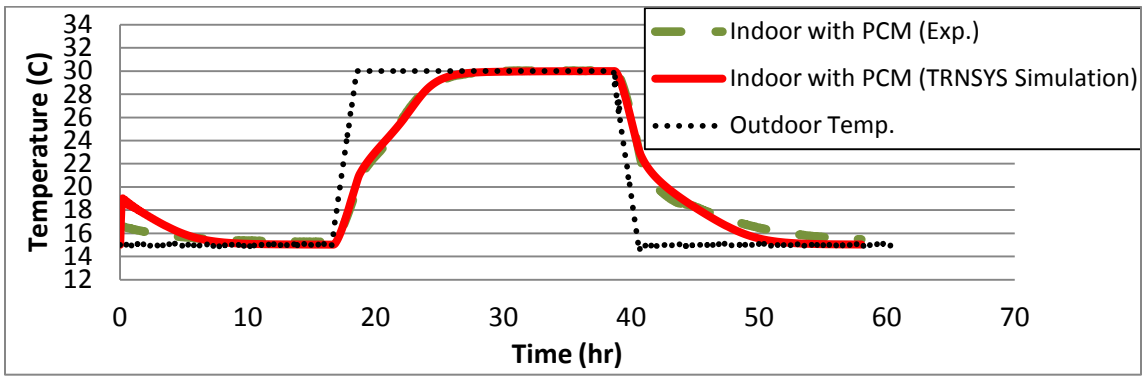

Figure 5.4 Validation of PCM component in TRNSYS simulation

Considering the cubicle simulation in TRNSYS, the application of the PCM component in TRNSYS was validated to simulate a PCM layer inside the TRNSYS software. In the following section, the validated component is employed to model the PCM wallboard in the real house.

5.3 Simulation of Refurbished Real House with PCM Wallboard

5.3.1 PCM wallboard selection and control strategy characterization

To investigate the application of the design framework of PCM wallboard in a real scenario, three PCM wallboards were sized using the framework presented in Figure 4.30 and implemented inside the TRNSYS simulation of Zone 1 of the house. The sized PCM layer is employed to replace the gypsum wallboard of the external wall. To conduct the simulation with the PCM layer, the related component, accompanied by the other components in Figure 5.2 was added to the Simulation Studio. For each external wall, a single PCM component (type 255) was designated: one for the northwest wall and one for the southwest wall. Each PCM component consisted of the materials presented in Table 5.1 except the gypsum board which was replaced by the PCM wallboard. Those PCM wallboards were selected from the collection of commercial materials in IEA ANNEX 23 (2013). The thermo-physical properties of these selected materials are tabulated in Table 5.3.

Each of these materials can be sized for Zone 1 to be fully melted in a predetermined time utilizing the developed design framework described in chapter 4. The determined melting period is equivalent to the off-peak period starting from midnight

until 5:30 a.m. which then is the onset of the peak period that lasts for four hours. To shift the space conditioning to the off-peak period, the set-point temperature of the zone is increased to 25°C at midnight and then brought back to 20°C at 5:30 a.m. Thus, the excessive heat is stored in the PCM wallboard during the night time and used to condition the space during the peak-period. The set-point temperature of Zone 1 is presented in Figure 5.5.

Table 5.3 PCM wallboards specifications mounted in the real house

Material	Thermo-physical properties						
	ρ [kg.m^{-3}]	k [W. m^{-2}. K^{-1}]	C [J. kg^{-1}. K^{-1}]	L [J.kg^{-1}]	Ts [°C]	Tm [°C]	Ste^{-1}
PCM1	900	0.21	1340	28800	17	23	21.49
PCM2	785	0.18	2220	111700	18	22	50.32
PCM3	1170	0.19	2100	127200	20	22	60.57

k: Thermal Conductivity, ρ: Density, C: Specific Heat Capacity, L: Latent Heat, Ts: Solidification Temperature, Tm: Melting Temperature

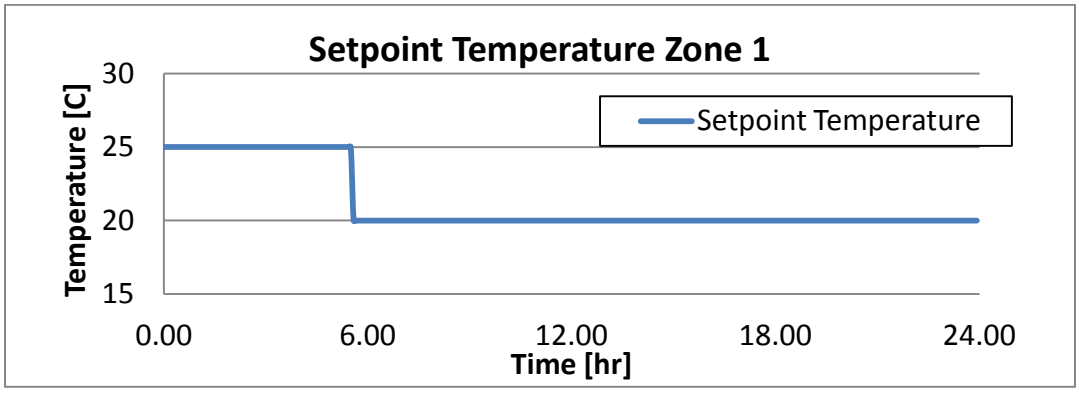

Figure 5.5 Zone 1 Set-point temperature trajectory in a day

Based on this control strategy, the idea is to fully charge the PCM wallboard in 5.5 hours. Therefore, it is the time employed as the charging period in the design framework. The next required information is the room temperature time lag (Γ_{RTL}) which

identifies the time needed for the room temperature of the Zone 1 to increase to 25°C from 20°C. Γ_{RTL} is applied to correct the charging time of the PCM wallboard.

To calculate Γ_{RTL}, the room temperature was simulated for three consecutive days with the set-point temperature profile presented in Figure 5.5. The time took for the room temperature to reach 25°C was calculated and averaged for the three days to compute Γ_{RTL} in Zone 1. The room temperature profile in those three days is illustrated in Figure 5.6; the average time lag was three hours. Γ_{RTL} was therefore set to 3.

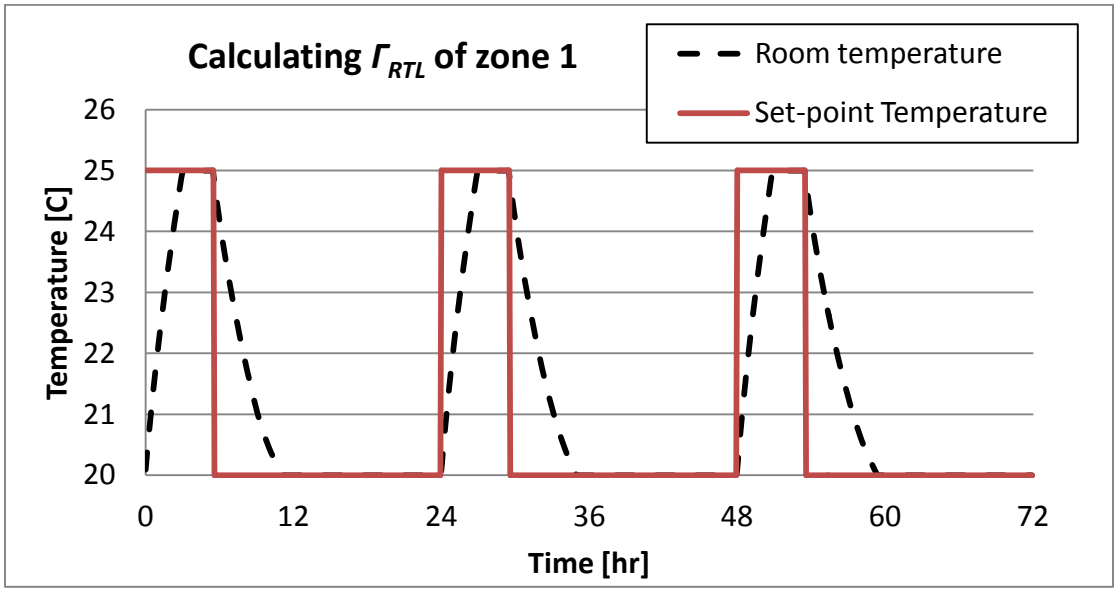

Figure 5.6 Calculating Γ_{RTL} of zone 1 in the real residential house

Considering the correlations developed in Figure 4.29 and the slope of 0.55, the corrected charging time required to fully melt the PCM wallboard in Zone 1 is 3.85 hr (3 hr and 51 min.). This time-length was utilized as the input parameter of Fo_{fl} in the framework to size the PCM wallboard.

5.3.2 Design and sizing of the PCM wallboards

To size the PCM wallboards, regarding their fusion temperature and melting range, different correlations are needed to be applied. Following the framework flowchart explained in Figure 4.30, each PCM wallboard was sized for Zone 1 as explained in Figure 5.7, Figure 5.8, and Figure 5.9, respectively. The chart in Figure 4.10 is set as the base chart in the framework. The heat transfer film coefficient of the inner side of the wallboards was set as 10 [$W.m^{-2}.K^{-1}$] like in the original simulation project of the real house with the gypsum wallboard.

5.3.2.1 PCM 1:

This component has a melting range of 6°C and a fusion temperature of 20°C. Thus, it has similar Ψ and Ψ_{pc} as the base chart (with $\Psi_{ref.}$ and $\Psi_{pc,\ ref}$). Therefore, the base chart presented in Figure 4.10 can be applied and no correction is required regarding the effect of Ψ and Ψ_{pc} to size PCM 1 in a way to have it fully melted after 5.5 hours in Zone 1.

Following the flow chart illustrated in Figure 5.7, the design thickness of this wallboard was calculated, equaling to 0.02 m.

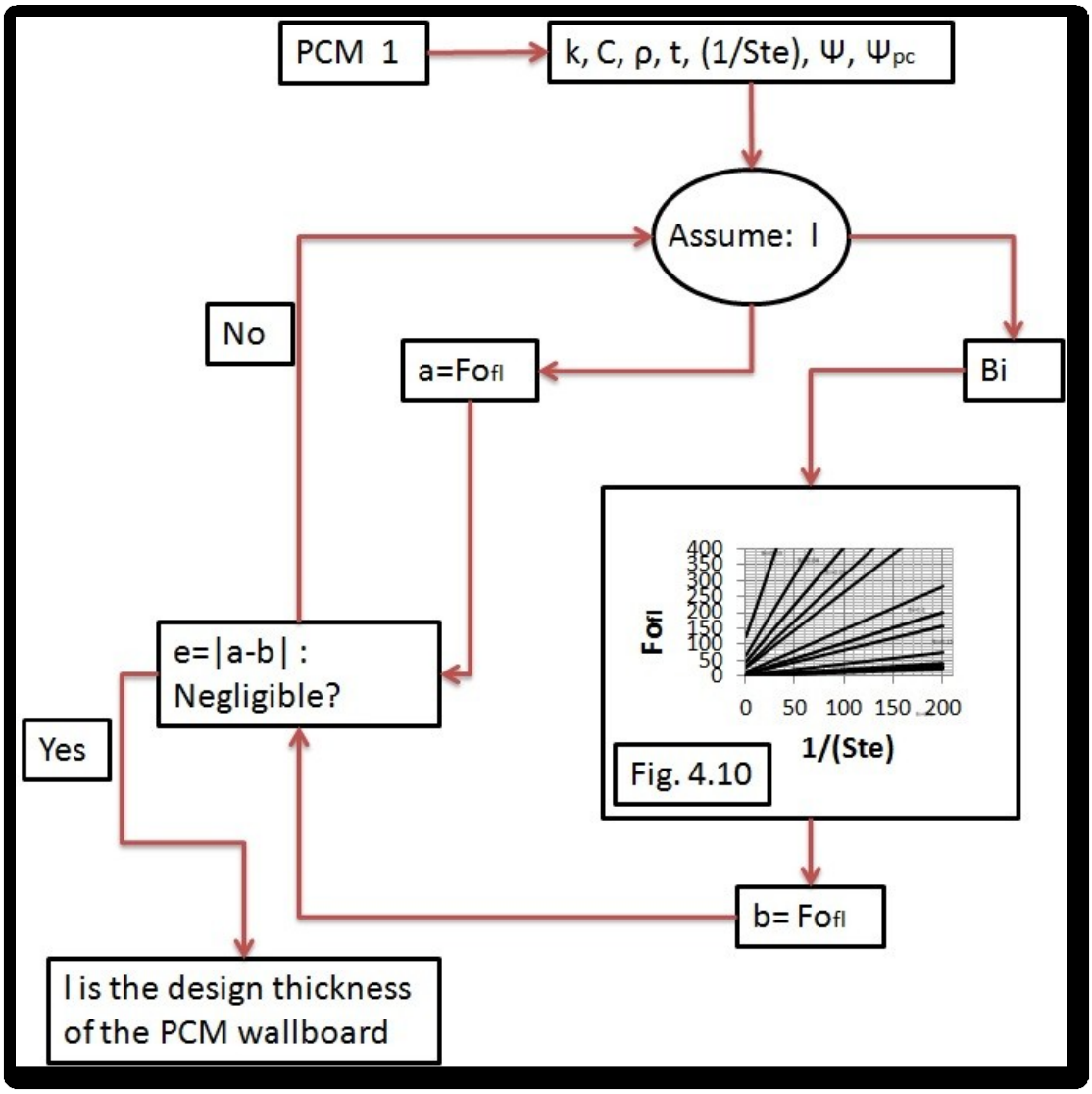

Figure 5.7 Design flowchart for PCM1

5.3.2.2 PCM 2:

This material, unlike PCM 1, has a melting range of 4°C, while its fusion temperature is the same as the first wallboard. Therefore, its Ψ is different from Ψ_{ref}, and the base chart in Figure 4.10 needs to be corrected using the slope of -0.4, as explained in section 4.4.1.

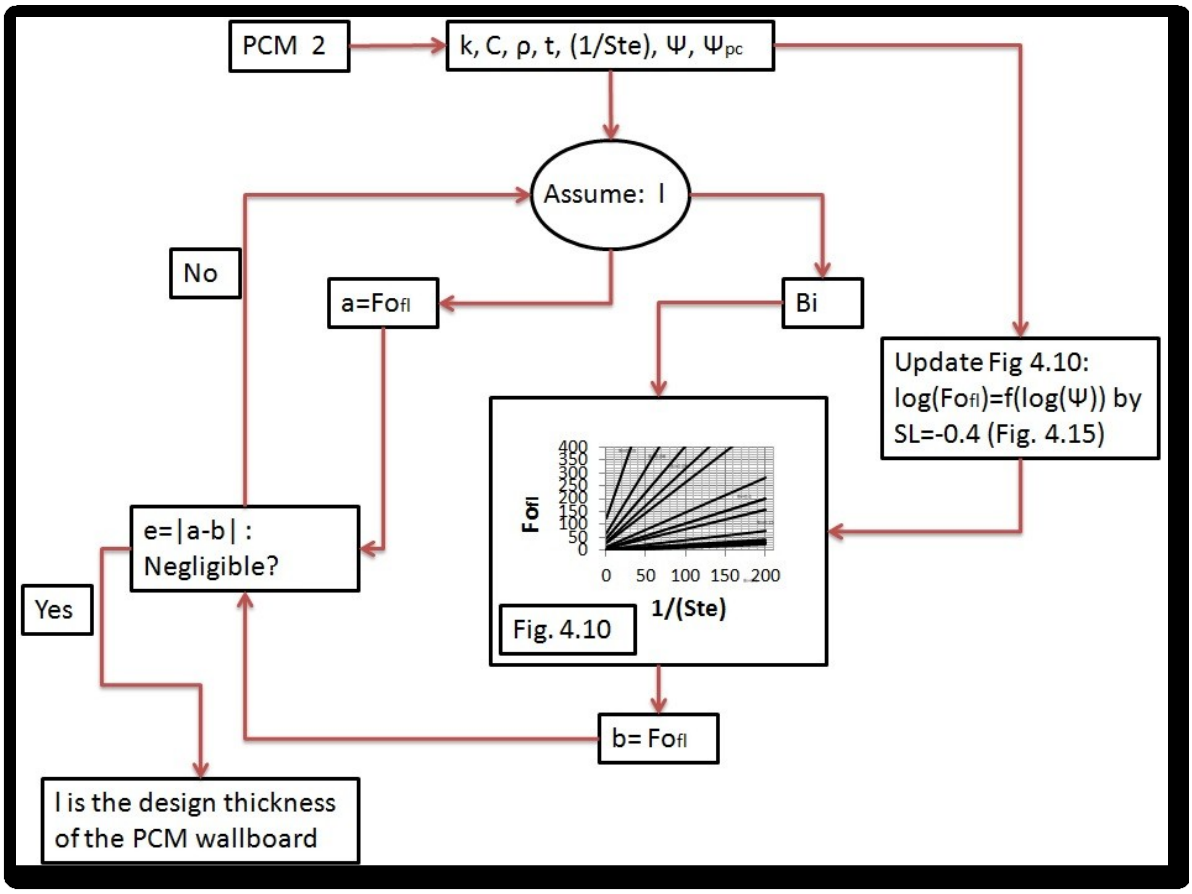

Figure 5.8 Design flowchart for PCM 2

Following the procedure illustrated in Figure 5.8, the sized design thickness of PCM 2 was 0.007 m.

5.3.2.3 PCM 3:

The third medium has different Ψ and Ψ_{pc} than the base chart in Figure 4.10. Therefore, the chart requires to be corrected for the effect of both Ψ and Ψ_{pc}. Taking into consideration the impact of the melting range and fusion temperature, the chart in Figure 4.10 needs to be modified employing the slope -0.4 (see section 4.4.1) for the effect of Ψ.

Also, it has to be corrected for the effect of Ψ_{pc} employing the slope calculated in Figure 4.27 (see section 4.4.2.)

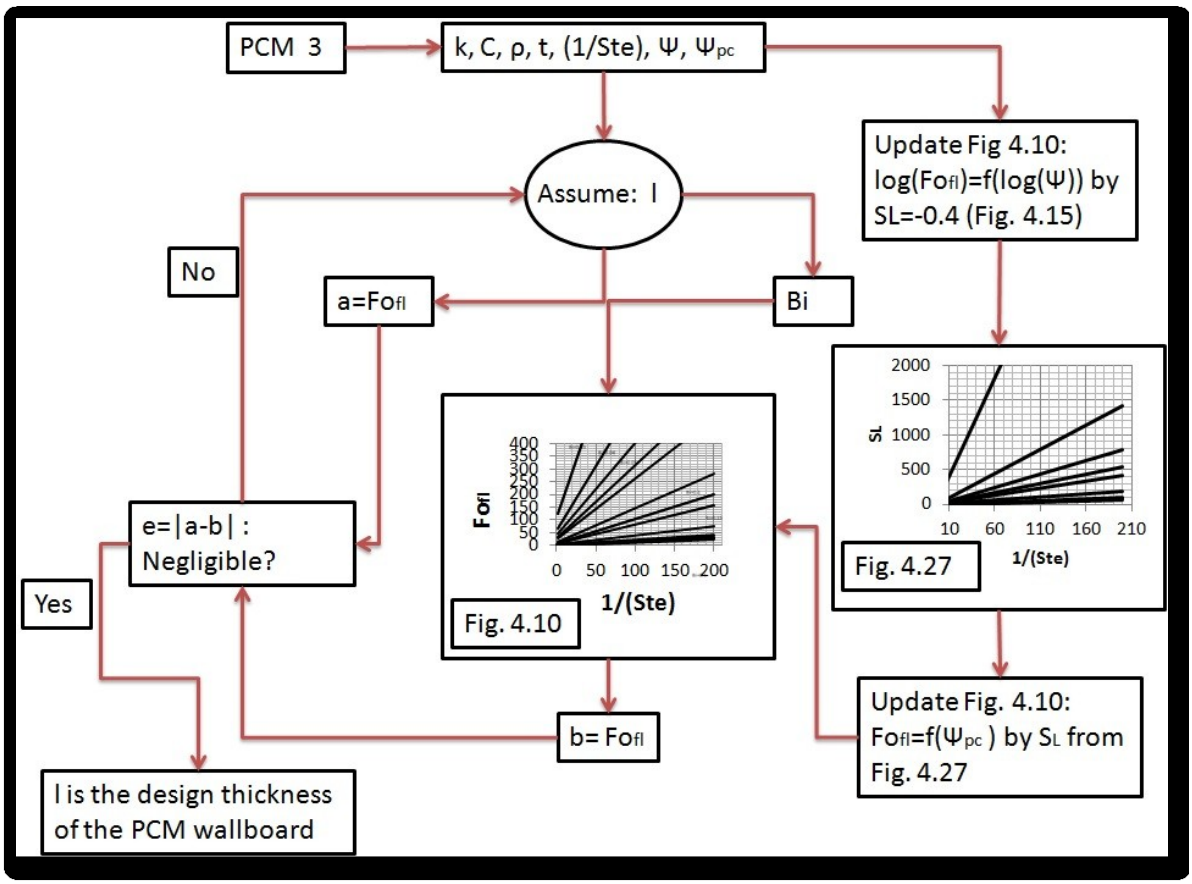

Figure 5.9 Design flowchart for PCM 3

Following the procedure illustrated in Figure 5.9, the sized design thickness of PCM 3 was 0.003 m.

5.3.3 Charging period characterization

Regarding the design objective, the thickness of the PCM wallboards was determined to result in the complete melting of the PCM at the end of the off-peak period. While the sizing of the materials was conducted through the application of the

framework developed in this study, the accuracy of the design was evaluated by measuring the outer surface temperature of the PCM wallboards. Also, the energy consumption for the space heating of Zone 1 was predicted using the TRNSYS simulating the house. To conduct the simulation of the house with a PCM wallboard, its original project built in Simulation Studio (Figure 5.2) needs to be modified to include the PCM wallboard by employing the PCM component. In the component, the thermo-physical properties of the PCM layer were set as tabulated in Table 5.3. The thickness was also set based on the calculation of the framework for each PCM wallboard (see section 5.3.2). The new simulation project was built in the Simulation Studio of TRNSYS to account for the PCM wallboard. The interface of the Simulation Project in Simulation Studio with PCM component is presented in Figure 5.10.

For each PCM wallboard, the simulation was conducted for nine days consisting of three separate periods of three consecutive days. Here, each set of consecutive three days was selected in a way to have one set with average outdoor temperature between 0°C to -10°C, another set between -10°C to -20°C, and the last set between -20°C to -30°C. Therefore, the outdoor temperature and its effect on the room thermal performance can be categorized in three groups: cold, very cold, and extremely cold. The average outdoor temperature for each set is -8.56°C, -13.9°C, and -21.93°C, respectively. The average temperature was calculated along the entire day and night of the three days in each category. The outdoor temperature profiles of those categorized conditions are illustrated in Figure 5.11.

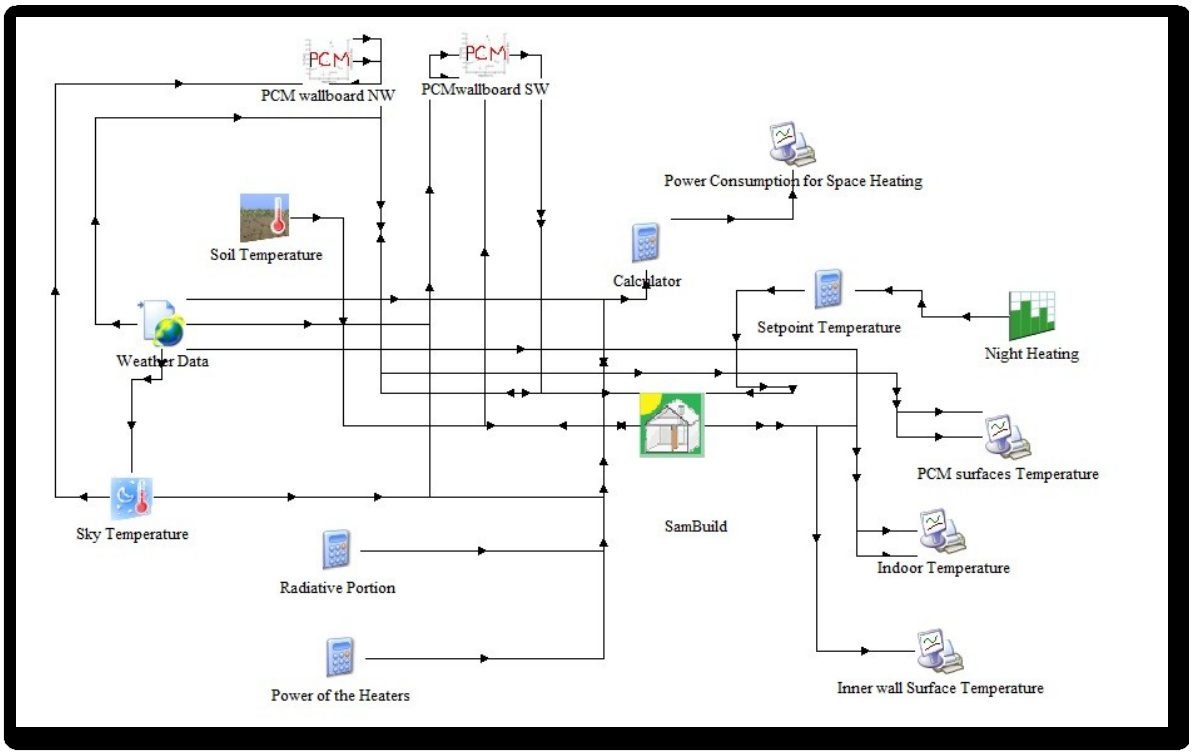

Figure 5.10 Simulation Studio of the TRNSYS simulation of the real house with PCM wallboard

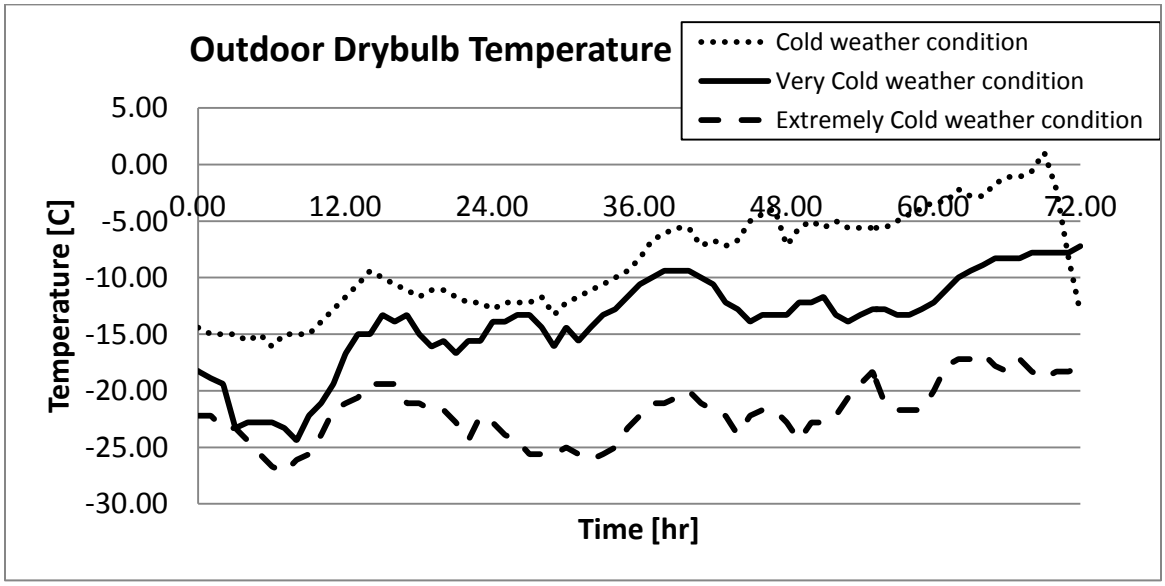

Figure 5.11 Outdoor temperature profile of three categorized outdoor temperature conditions

Figure 5.12 and Figure 5.13 show the inner and outer surface temperature profiles of all three PCM wallboards, respectively. As a means to evaluate the design framework, the wallboard temperature at the end of the charging period was compared with its melting temperature, and its deviation from the fully melted status of PCM was quantified. The temperatures for all the wallboards are tabulated in Table 5.4.

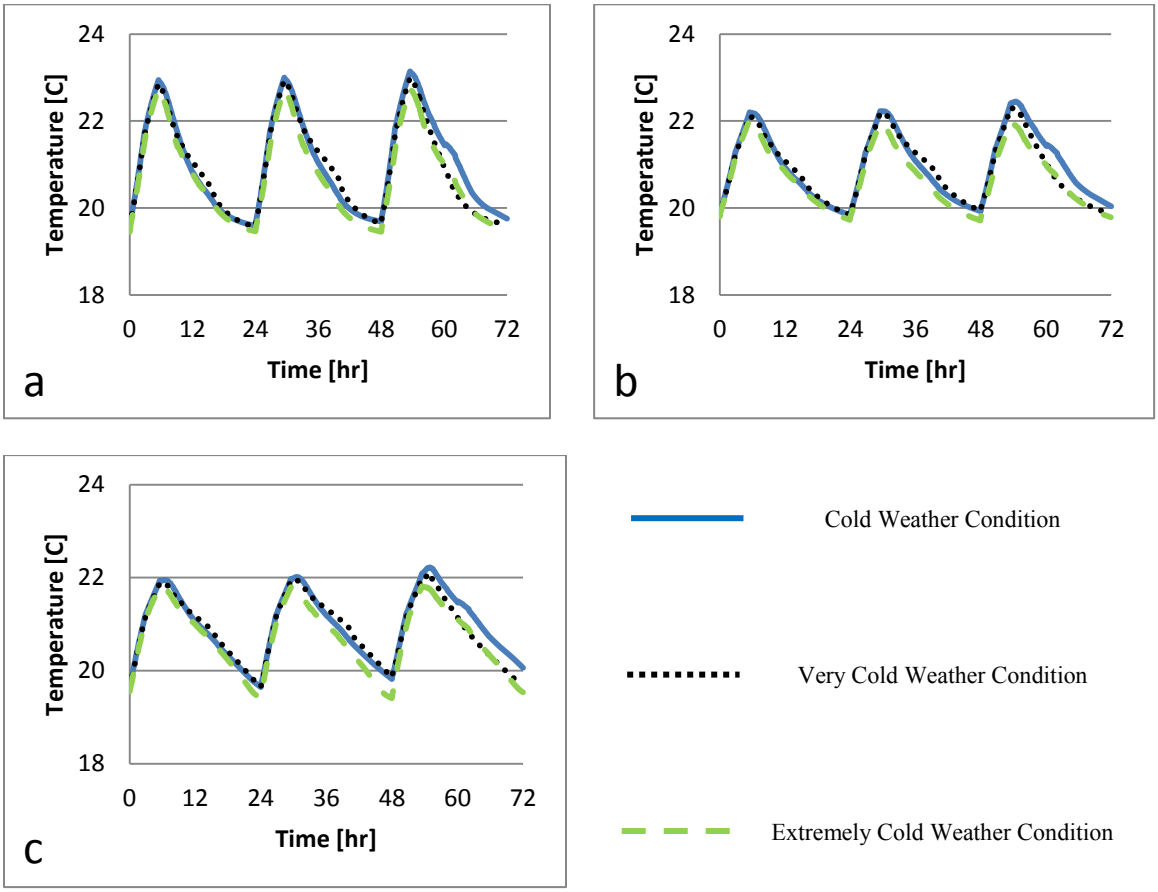

Figure 5.12 Inner surface temperature of PCM wallboards in zone 1 of the real house a) PCM 1 b) PCM 2 c) PCM 3

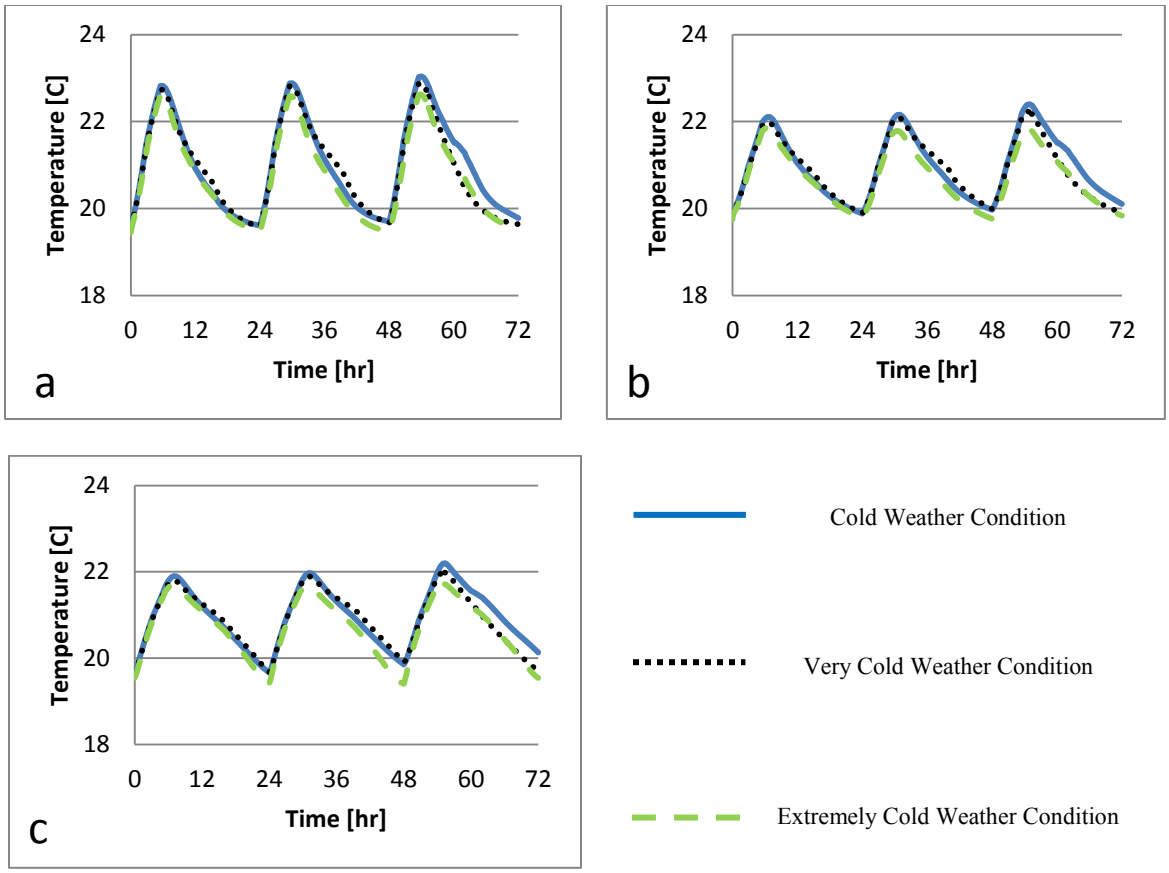

Figure 5.13 Outer surface temperature of PCM wallboards in zone 1 of the real house a) PCM 1 b) PCM 2 c) PCM 3

Although, the design framework was developed and employed with the assumption of complete insulation on the outer side of the PCM wallboard, in a real scenario the wallboard has some heat losses to the outdoor. Obviously, the proximity of the wall status to its complete liquefaction depends on the outdoor condition which governs the heat loss through the wall beside the U-value of the envelope. Table 5.4 shows that the wallboard has lower temperature at the end of the charging period during extremely cold days. Considering the average temperature of the wallboards in three days of extremely cold condition, none of the PCMs was fully melted at the end of the off-peak period with the design thickness calculated by the charts. For the cases with higher

outdoor temperature, the wallboard is much closer to its fully melted status, which means more thermal energy is stored as latent heat; it can be inferred that the design framework has higher accuracy in sizing the wallboard for cold and very cold outdoor conditions.

Table 5.4 PCM wallboard temperature at the end of charging period (off-peak period)

		PCM wallboard 1				**PCM wallboard 2**				**PCM wallboard 3**			
Day	**Weather condition**	**In. Surf. Temp.**	**Out. Surf. Temp.**	**Ave. In. Surf. Temp.**	**Ave. Out. Surf. Temp.**	**In. Surf. Temp.**	**Out. Surf. Temp.**	**Ave. In. Surf. Temp.**	**Ave. Out. Surf. Temp.**	**In. Surf. Temp.**	**Out. Surf. Temp.**	**Ave. In. Surf. Temp.**	**Ave. Out. Surf. Temp.**
1	**Cold**	22.91	22.82	**23.02**	**22.91**	22.27	22.06	**22.27**	**22.06**	21.92	21.70	**21.99**	**21.75**
2		23.00	22.88			22.23	22.00			21.97	21.71		
3		23.14	23.03			22.41	22.19			22.09	21.83		
1	**Very Cold**	22.86	22.74	**22.93**	**22.81**	22.12	21.89	**22.20**	**21.98**	21.88	21.62	**21.94**	**21.68**
2		22.93	22.81			22.19	21.96			21.93	21.67		
3		23.00	22.88			22.3	22.09			22.00	21.74		
1	**Extremely Cold**	22.75	22.62	**22.75**	**22.61**	22.02	21.78	**21.98**	**21.74**	21.82	21.56	**21.81**	**21.55**
2		22.73	22.59			21.95	21.71			21.79	21.53		
3		22.76	22.63			21.97	21.72			21.82	21.55		

In addition to the temperature status of the wallboards, the energy consumed to condition the space during the off-peak hours (charging period) was measured in all three simulation cases with different PCM wallboards and compared with the base case of the

real house without PCM. The heating energy was utilized to increase the room temperature to 25°C during the off-peak hours, which resulted in melting and charging the wallboard with latent heat thermal energy. The heating energy consumption of Zone 1 with every single PCM wallboard during the charging time was measured and averaged over each weather condition. These magnitudes are presented in Table 5.5 in addition to the results of the base case without PCM.

Table 5.5 Heating energy consumption of zone 1 during charging period with different wallboards

	Material specifications		**Weather condition**		
			Heating energy consumption [kWh]		
Wallboard	***Bi***	$(Ste)^{-1}$	**Cold**	**Very cold**	**Extremely cold**
PCM1	0.95	21.49	7.78	8.01	8.42
PCM2	0.39	50.32	7.97	8.18	8.59
PCM3	0.16	60.57	8.06	8.26	8.64
Gypsum (No PCM)	0.81	0.00	7.08	7.39	7.95

The consumed energy in cases with PCM wallboards was almost the same with a trivial difference due to their different *Bi*. In the case of wallboard with lower *Bi*, the required energy was higher due to its lower resistance against conduction heat transfer. Also, the average consumed energy inside the zone was higher in days with colder outdoor temperature. Moreover, the base case with conventional gypsum wallboard had the lowest energy consumption during the charging period which is understandable (no energy is required for fusion). In other words, the PCM wallboards need extra heating energy as their phase transition occurs in the operational temperature of the room.

5.3.4 Discharging period (Peak hour) Characterization

Another design achievement which needs to be evaluated is the impact of the PCM wallboard on the heating energy consumption and thermal performance of the

building during peak hours. Indeed, the objective of the night heating was to avoid energy consumption during peak hours and shift it to a later time. Therefore, the results of the simulations with designed PCM wallboards were investigated during peak hours and the rest of the day to quantify the energy consumption of the zone and the shift of space heating. To quantify the shift of energy consumption, the period from the time that the heater was turned off until it restarted the heating of the space was measured. Considering the shift of energy consumption as the main objective, the best design-thickness of the PCM wallboard is the one with the longest shift which is claimed to be obtained using the framework presented earlier. Therefore, for the purpose of comparison, the same measurements were carried out for each PCM with a different thickness than the one estimated using the framework as the best design thickness.

To conduct the simulations, each PCM wallboard with the new thickness was built inside the TRNSYS simulation Studio like the one in Figure 5.10 with thermo-physical properties tabulated in Table 5.3.

The house without the PCM wallboard, which served as a reference, was simulated with the same night heating control strategy. The time-shift of energy consumption and the total day heating energy consumption were calculated and averaged during three consecutive days in each weather condition and tabulated in Table 5.6.

Table 5.6 The average time-shift and the total heating energy consumption of three days in different weather conditions in Zone 1 without PCM wallboard

Weather condition	Cold	Very Cold	Extremely Cold
Time-shift [hr]	5.61	4.91	4.08
Whole day energy consumption [kWh]	11.19	12.34	14.73

5.3.4.1 PCM 1 discharging characterization:

The thickness of the first PCM wallboard in Table 5.3 (PCM 1) was sized to 0.020 m for the application in Zone 1 of the house using the framework (see Figure 5.7). For the purpose of evaluating this design thickness, four more simulations were conducted with the same wallboard and different thicknesses as; 0.010 m, 0.015 m, 0.025 m and 0.030 m. These various thicknesses are provided in Table 5.7.

Table 5.7 PCM 1 : The various simulated thickness of the wallboard

Name	**Thickness [m]**	***Bi***	Ste^{-1}
PCM 1	0.020	0.95	21.49
PCM 1-a	0.010	0.48	21.49
PCM 1-b	0.015	0.71	21.49
PCM 1-c	0.025	1.19	21.49
PCM 1-d	0.030	1.43	21.49

Any change in the thickness of the PCM wallboard changes the mass of the wall and consequently the latent heat storage capacity. The U-value of the wall section is also altered when the thickness of the wallboard is modified. Considering the similar film coefficient between the room air and the wall surface in all cases, a thicker wallboard has higher Bi. Thus, the wall section has lower U-value resulting in less heat loss to the outdoor. Moreover, its ratio of heat diffusion vs. heat storage is smaller. Therefore, it takes longer for the wall to become fully melted. Hence, during 5.5 hours of a similar charging period, the PCM wall cannot store the latent heat in its full capacity. On the other hand, having a thicker PCM wallboard means a larger capacity of latent heat storage due to the bigger mass of the wallboard. Therefore, there should be a balance between the capacity of storage and charging rate for the PCM wallboard to achieve the highest performance.

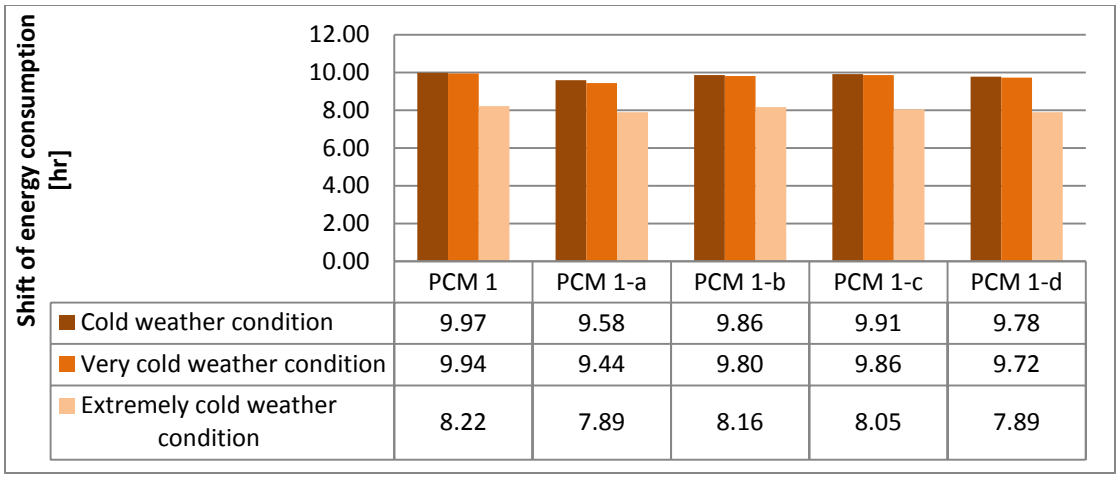

	PCM 1	PCM 1-a	PCM 1-b	PCM 1-c	PCM 1-d
Cold weather condition	9.97	9.58	9.86	9.91	9.78
Very cold weather condition	9.94	9.44	9.80	9.86	9.72
Extremely cold weather condition	8.22	7.89	8.16	8.05	7.89

Figure 5.14 PCM 1: The average shift of energy consumption in three days in different weather conditions

Conducting the simulations with PCM 1 mounted in Zone 1, the time duration in which the heater was off after the charging period was calculated for the selected thicknesses provided in Table 5.7 The average values of these time-shifts of energy consumption in three days of each weather condition are presented and compared in Figure 5.14. The figure shows that the wall with the thickness sized using the design framework has the longest time-shift of energy consumption. Also, the thicknesses closer to the size of PCM 1 (PCM 1-b and PCM 1-c) have a longer time-shift than PCM 1-a and PCM 1-d. Deduced from those simulation results, the wallboard which has both the highest melting percentage at the end of charging and the largest latent heat storage capacity presents the longest time-shift of energy consumption. Moreover, the time-shift is longer for all the scales of thickness when the outdoor temperature is higher.

In addition to the time-shift, the heating energy consumption of Zone 1 was measured during the charging period and the entire day. For all of the five thicknesses of PCM 1 and the conventional gypsum wallboard, the heating power of Zone 1 was

calculated during three days of each outdoor condition, and they are presented in Figure 5.15 to Figure 5.17. The average of those measurements for all the selected thicknesses of the PCM wallboard in three consecutive days in each weather condition is illustrated in Figure 5.18.

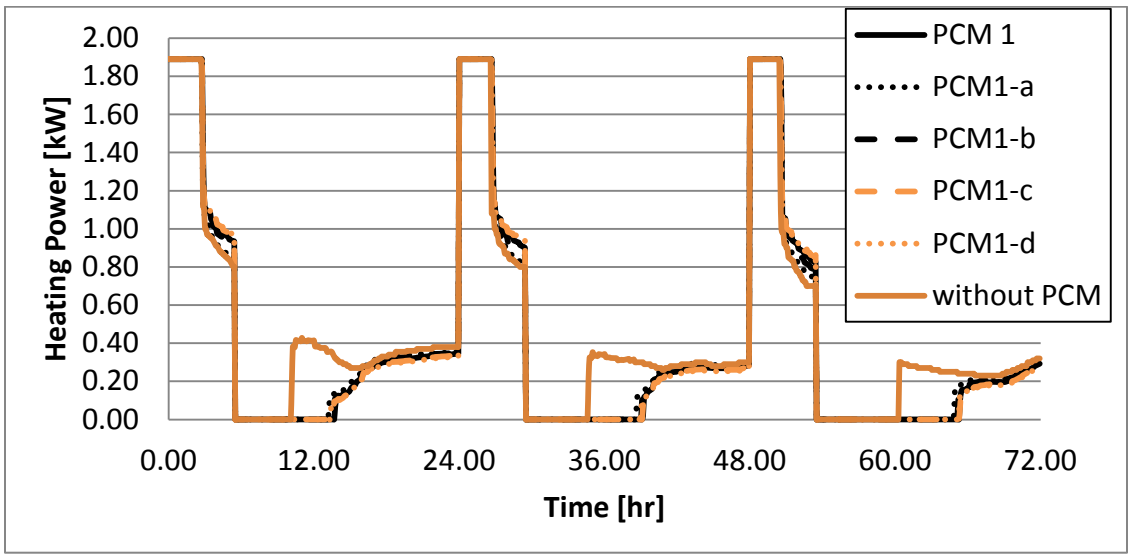

Figure 5.15 Heating power profile of Zone1 for cold outdoor weather condition

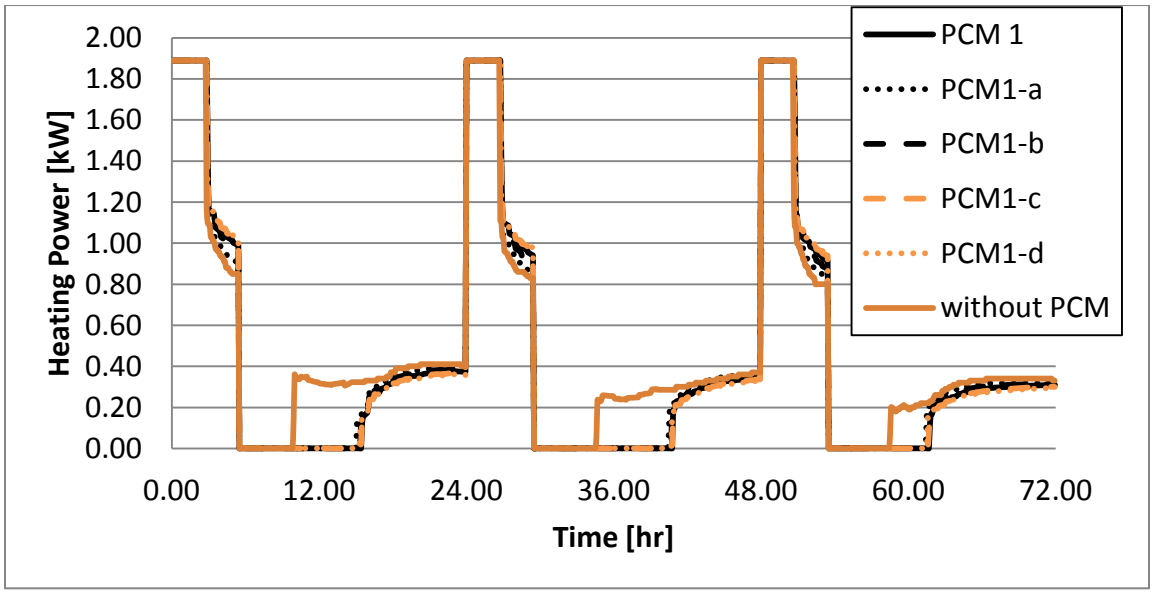

Figure 5.16 Heating power profile of Zone1 for very cold outdoor weather condition

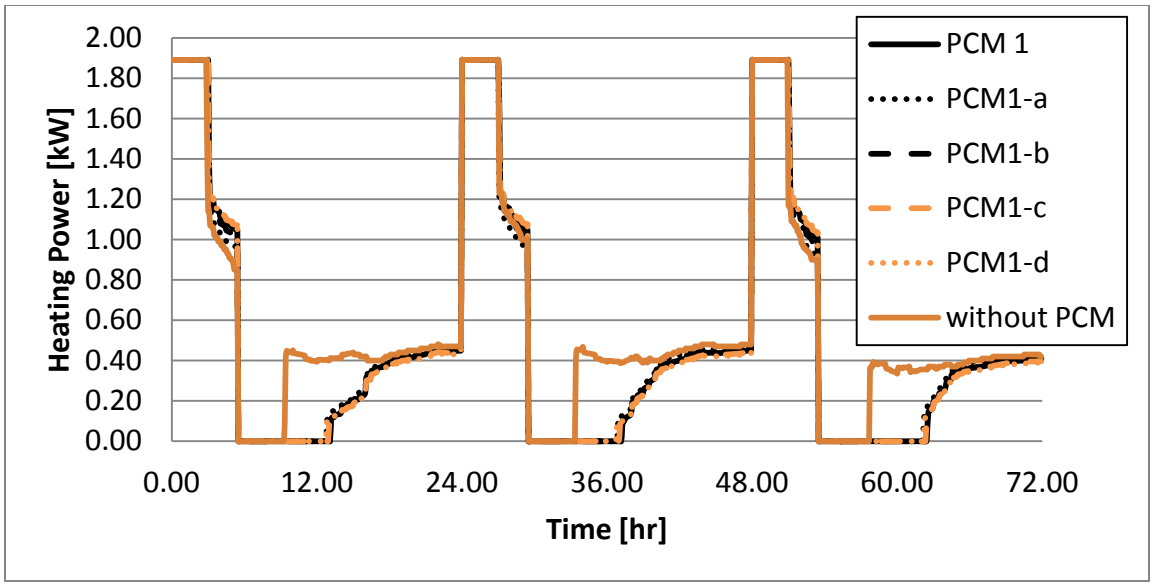

Figure 5.17 Heating power profile of Zone1 for extremely cold outdoor weather condition

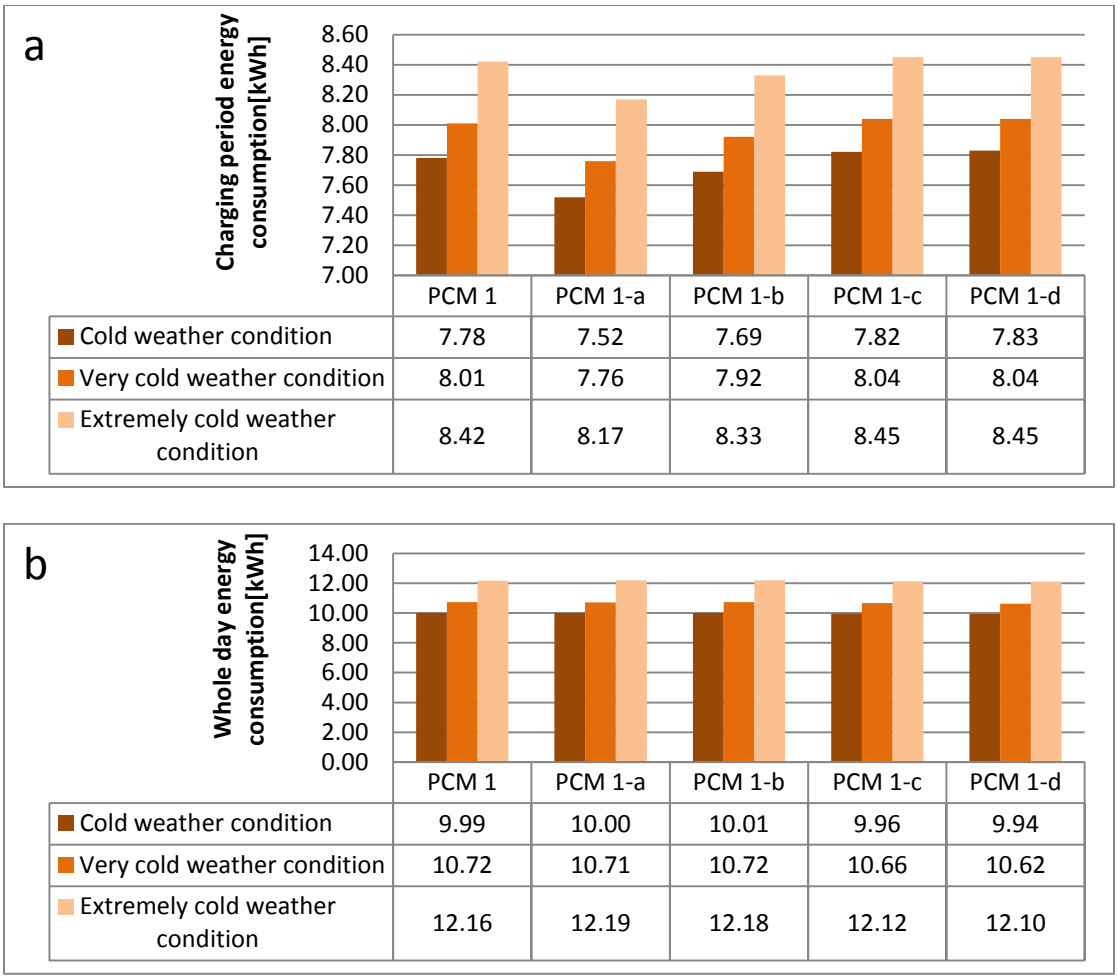

	PCM 1	PCM 1-a	PCM 1-b	PCM 1-c	PCM 1-d
Cold weather condition	7.78	7.52	7.69	7.82	7.83
Very cold weather condition	8.01	7.76	7.92	8.04	8.04
Extremely cold weather condition	8.42	8.17	8.33	8.45	8.45

	PCM 1	PCM 1-a	PCM 1-b	PCM 1-c	PCM 1-d
Cold weather condition	9.99	10.00	10.01	9.96	9.94
Very cold weather condition	10.72	10.71	10.72	10.66	10.62
Extremely cold weather condition	12.16	12.19	12.18	12.12	12.10

Figure 5.18 PCM 1: The average energy consumption of Zone 1 in three days in different weather conditions a) During charging period (off-peak hours) b) During the entire day (24 hours)

As expected, the wallboard with greater thickness had higher energy consumption during the charging time due to the bigger mass of the medium to be melted and higher latent heat to be provided. However, the difference of the consumed energy in different sizes of the wallboard was trivial. The colder the outdoor temperature, the higher the energy required for heating the zone either during the off-peak hours or the entire day.

As in the charging period, the difference of the heating energy consumption during the entire day with different sizes of the PCM wallboard was not significant.

However, it showed lower consumption in the simulation with the thicker wallboard. The lowest amount of energy consumption was observed for the case of PCM 1-d due to its low U-value.

5.3.4.2 PCM 2 discharging characterization:

The thickness of the second PCM wallboard in Table 5.3 (PCM 2) was sized to 0.007 m for the application in zone 1 using the framework (see Figure 5.8). For the purpose of evaluating this design thickness, three more simulations were conducted with the same wallboard and different thicknesses as; 0.005 m, 0.009 m and 0.015 m. These various thicknesses are provided in Table 5.8.

Conducting the simulations with PCM 2 mounted in Zone 1, the duration in which the heater was off after the charging period was calculated for the selected thicknesses provided in Table 5.8. The average values of these time-shifts of energy consumption in three days of each weather condition are presented and compared in Figure 5.19.

Table 5.8 PCM 2 : The various simulated thickness of the wallboard

Name	**Thickness [m]**	***Bi***	***Ste*$^{-1}$**
PCM 2	0.007	0.39	50.32
PCM 2-a	0.005	0.28	50.32
PCM 2-b	0.009	0.50	50.32
PCM 2-c	0.015	0.83	50.32

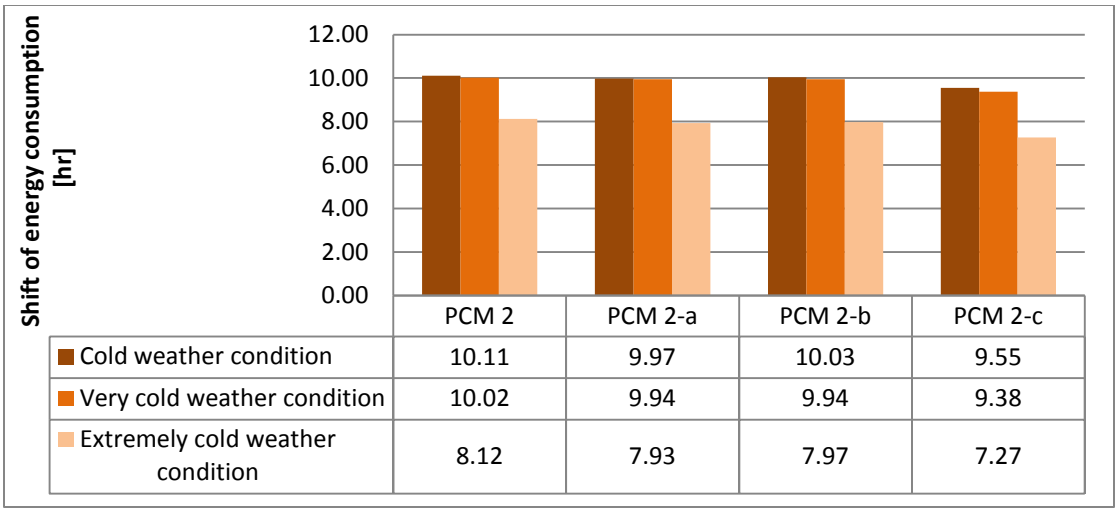

	PCM 2	PCM 2-a	PCM 2-b	PCM 2-c
Cold weather condition	10.11	9.97	10.03	9.55
Very cold weather condition	10.02	9.94	9.94	9.38
Extremely cold weather condition	8.12	7.93	7.97	7.27

Figure 5.19 PCM 2: The average shift of energy consumption in three days in different weather conditions

Figure 5.19 shows that the wall with the thickness sized using the framework shifted the demand for a longer period of time. It also shows the PCM layers with thicknesses closer to the size of PCM 2 (PCM 2-a and PCM 2-b) have a longer time-shift than PCM 2-c. Like PCM 1, the wallboard which has both the highest melting percentage at the end of charging and the larger latent heat storage capacity has been able to shift the load for a longer period of time. Similar to the simulations conducted for PCM 1, the time-shift is longer for all the thicknesses of PCM 2 when the outdoor temperature is higher; this indicates that the results make sense.

In addition to the time-shift, the heating energy consumption (heating power profile of the heater) of Zone 1 was measured during the charging period and the entire day (similar to the simulation cases conducted for PCM 1 and profiles in Figure 5.15 to Figure 5.17). The average values of the measurements for all the selected thicknesses of the PCM wallboard in three consecutive days for each weather condition are illustrated in Figure 5.20.

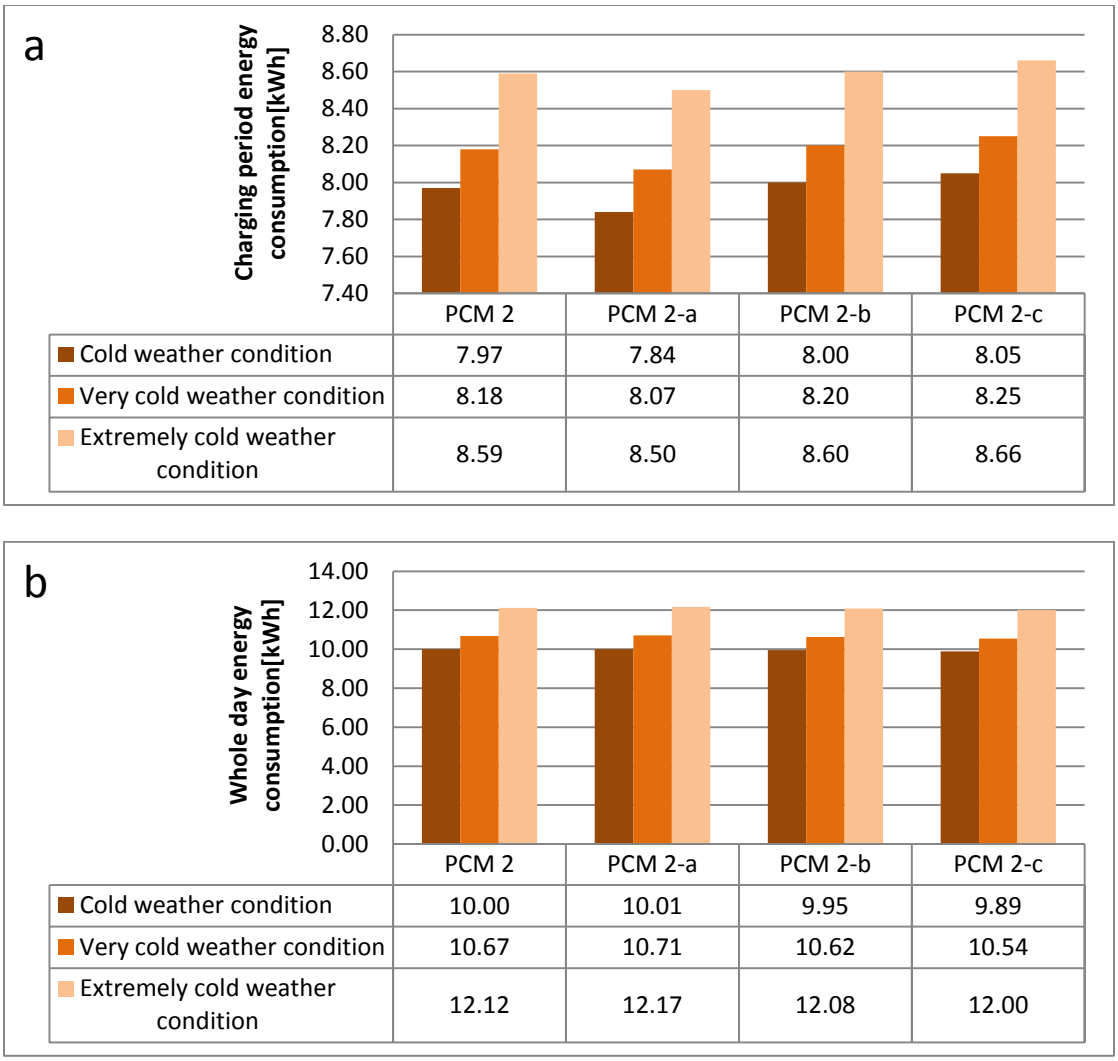

Figure 5.20 PCM 2: The average energy consumption of Zone 1 in three days in different weather conditions a) During charging period (off-peak hours) b) During the entire day (24 hours)

As induced by the analysis of PCM 1, the energy consumption for heating the zone during the charging time is higher in the case of the wallboard with greater thickness due to the higher sensible and latent heat required. Also, the colder the outdoor temperature got, the more energy was required for heating the zone both during the off-peak hours and the entire day.

Similar to the simulation cases conducted for PCM 1, the difference of the heating energy consumption inside Zone 1 either during charging time or the entire day was insignificant in cases with different PCM wallboard sizes. However, it showed lower consumption in the simulation with thicker wallboards. The same phenomenon was seen in PCM 1, and the least energy consumption was acquired in the simulation with the thickest PCM 2 wallboard (PCM 2-c) which has the lowest heat loss during the day due to its lower U-value.

5.3.4.3 PCM 3 discharging characterization:

The thickness of the third PCM wallboard in Table 5.3 (PCM 3) was sized to 0.003 m for the application in Zone 1 of the house using the framework (see Figure 5.9). For the purpose of evaluating this design thickness, three more simulations were conducted with the same wallboard and different thicknesses as 0.001 m, 0.005 m and 0.010 m. These various thicknesses are named as presented in Table 5.9.

Table 5.9 PCM 3 : The various simulated thickness of the wallboard

Name	**Thickness [m]**	***Bi***	Ste^{-1}
PCM 3	0.003	0.19	60.57
PCM 3-a	0.001	0.06	60.57
PCM 3-b	0.005	0.31	60.57
PCM 3-c	0.010	0.62	60.57

While conducting the simulations with PCM 3, the time duration in which the heater was off after the charging period was calculated for the selected thicknesses in Table 5.9. Figure 5.21 shows the average of these time-shifts of energy consumption in three days of each weather condition.

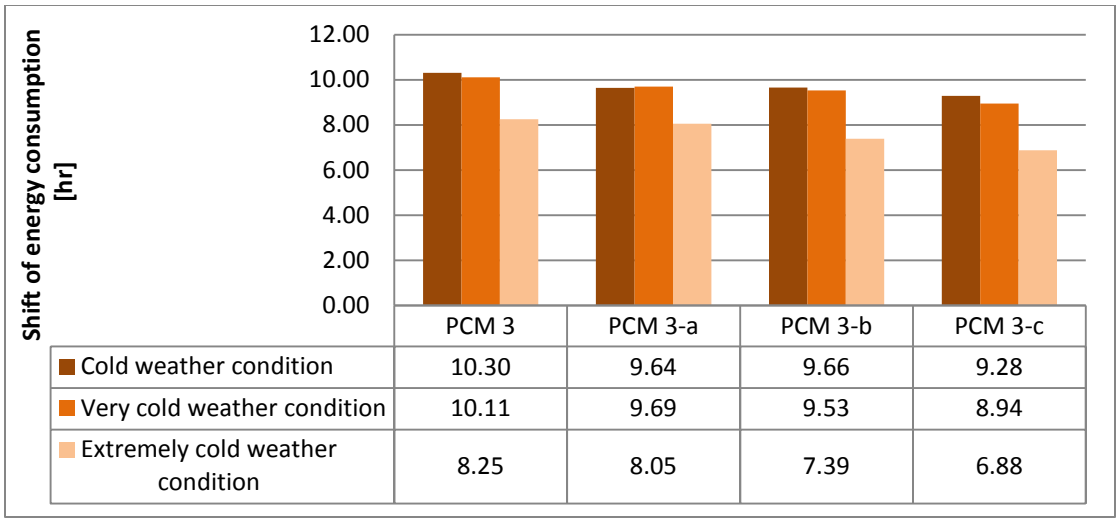

	PCM 3	PCM 3-a	PCM 3-b	PCM 3-c
Cold weather condition	10.30	9.64	9.66	9.28
Very cold weather condition	10.11	9.69	9.53	8.94
Extremely cold weather condition	8.25	8.05	7.39	6.88

Figure 5.21 PCM 3: The average shift of energy consumption in three days in different weather conditions

It was concluded that the wall with the thickness sized by the design framework has the longest time-shift of energy consumption. Also, the thicknesses closer to the size of PCM 3 (PCM 3-a and PCM 3-b) have longer time-shift than PCM 3-c. Like PCM 1 and PCM 2, the wallboard which has both the highest melting percentage at the end of charging and the largest latent heat storage capacity presents the longest time-shift of energy consumption. Again, similar to the cases for PCM 1 and PCM 2, the time-shift is longer for all the thicknesses when the outdoor temperature is higher.

In addition to the time-shift, the heating energy consumption of Zone 1 was measured for both charging period and the entire day. The average of those measurements for all the selected thicknesses of the PCM wallboard in three consecutive days in each weather condition is illustrated in Figure 5.22.

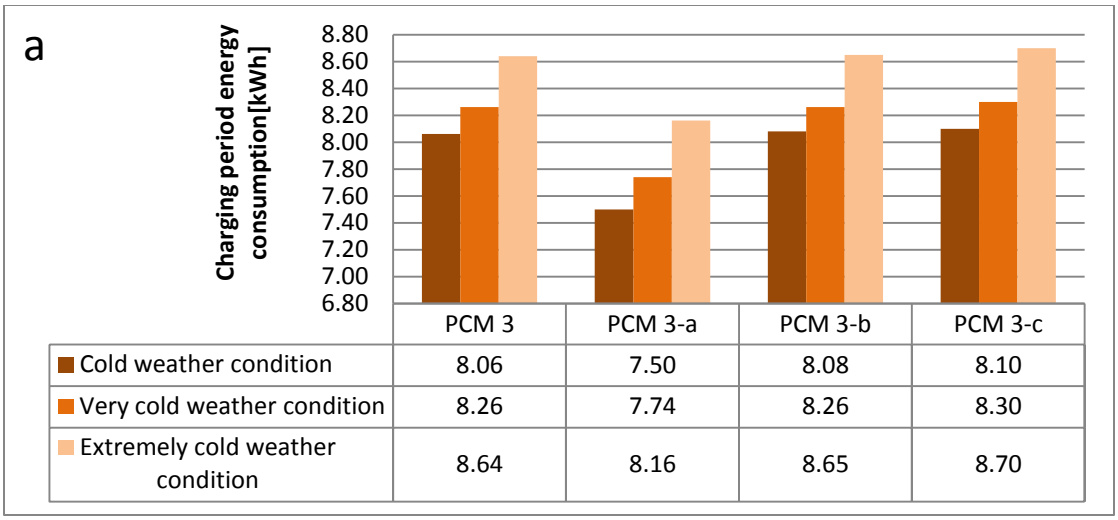

	PCM 3	PCM 3-a	PCM 3-b	PCM 3-c
Cold weather condition	8.06	7.50	8.08	8.10
Very cold weather condition	8.26	7.74	8.26	8.30
Extremely cold weather condition	8.64	8.16	8.65	8.70

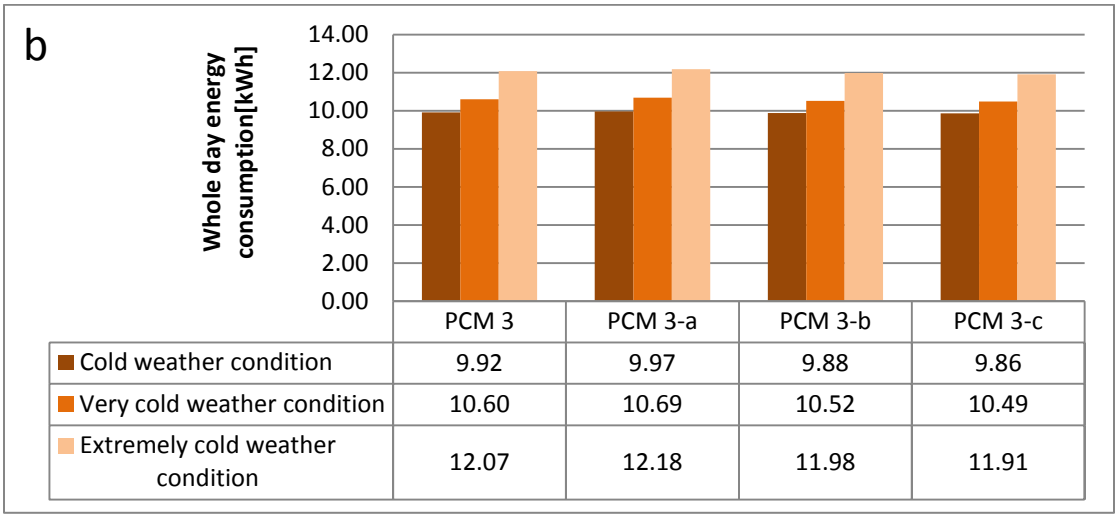

	PCM 3	PCM 3-a	PCM 3-b	PCM 3-c
Cold weather condition	9.92	9.97	9.88	9.86
Very cold weather condition	10.60	10.69	10.52	10.49
Extremely cold weather condition	12.07	12.18	11.98	11.91

Figure 5.22 PCM 3: The average energy consumption of Zone 1 in three days in different weather conditions a) During charging period (off-peak hours) b) During the entire day (24 hours)

As concluded in the simulation cases with PCM 1 and PCM 2, the room with thicker PCM wallboard has higher energy consumption during charging time due to the higher sensible and latent heat required. However, the difference in the consumed energy of the different wallboard sizes was trivial. Also, the colder the outdoor temperature was, the higher the energy was required for heating the zone either during the off-peak hours or the entire day.

As in the charging period, the difference in the heating energy consumption for different sizes of the PCM wallboard was insignificant. However, it showed lower consumption in the simulation with thicker wallboards. Similar to the scenarios with PCM 1 and PCM 2, the least heating energy consumption of Zone 1 was obtained in the simulation with the thickest PCM 3 wallboard (PCM 3-c) which has the lowest heat loss during the day due to its lower U-value.

5.3.4.4 Discussion and comparison between the PCMs

Regarding the time-shift of the required heating load, although the difference was trivial, PCM 3 had the longest shifting period. The latent heat storage capacity and the phase transition temperature range mainly influenced the performance of the PCM wallboard in shifting the energy demand. PCM 3 has the highest latent heat, while it has the lowest latent heat storage capacity based on its applied thickness (the least wall mass). Presented in Table 5.10, considering the design thickness, PCM 2 has the highest latent heat storage capacity. PCM 1 also has higher capacity than PCM 3. However, both PCM 1 and PCM 2 have a solidification temperature less than 20°C: the lowest operational temperature in the house. Therefore, these two PCM wallboards would never go through a full cycle of charging and discharging of their stored latent heat as their temperatures barely drop less than 20°C. On the other hand, PCM 3 faces the complete cycle of melting and solidification during the operational temperature of Zone 1 as it is solidified and liquefied at 20°C and 22°C, respectively. Thus, its full latent heat storage capacity is utilized in conditioning the space unlike the other two PCMs which yield a percentage of their capacity.

Table 5.10 Design Specifications of the wallboards, average time-shift and consumption of energy in three days

		PCM 1	PCM 2	PCM 3	Gypsum Board
Density [kg.m^{-3}]		900	785	1170	800
Specific heat capacity [J.kg^{-1}.K^{-1}]		1340	2220	2100	1090
Thermal conductivity [W.m^{-1}.K^{-1}]		0.21	0.18	0.19	0.16
Latent heat [J.kg^{-1}]		28800	111700	127200	-
Solidification temp. [°C]		17	18	20	-
Melting temp. [°C]		23	22	22	-
Thickness [m]		0.020	0.007	0.003	0.013
Ste^{-1}		21.49	50.32	60.57	-
Bi		0.95	0.39	0.19	0.81
Latent heat capacity [kJ]		11493	13608	9898	-
Energy consumption (Charging) [kWh]	Cold	7.78	7.97	8.06	7.08
	Very Cold	8.01	8.18	8.26	7.39
	Ext. Cold	8.42	8.59	8.64	7.95
Energy consumption (whole day) [kWh]	Cold	9.99	10.00	9.92	11.19
	Very Cold	10.72	10.67	10.6	12.34
	Ext. Cold	12.16	12.12	12.07	14.73
Time-Shift energy consumption [hr]	Cold	9.97	10.11	10.30	5.61
	Very Cold	9.94	10.02	10.11	4.91
	Ext. Cold	8.22	8.12	8.25	4.08

Compared to the PCM wallboards, conventional gypsum boards had the least time-shift and the highest energy demand in a full day. In the absence of latent heat

storage in conventional gypsum boards, higher frequency of heater usage for space heating and higher fluctuation of room temperature was expected.

5.6 SUMMARY

In this chapter, a real house was simulated using TRNSYS software while one of its zones was furnished with the PCM wallboard. Three different PCMs were selected and mounted in this building; each was sized employing the proposed design framework. The application of the PCM wallboard was characterized for both charging and discharging periods.

At the end of the charging period (off-peak hours), the final state of the PCM wallboard with respect to its melting percentage was evaluated. Considering the inner and outer surface temperature of the wallboards at the end of charging time, the thicknesses of the PCMs were sufficient to have them fully melted just before the onset of the peak-hour. Therefore, the proposed design framework could successfully determine the thickness of the PCM wallboard so that the medium was fully melted at a predetermined period.

Analyzing the discharging period, the thickness of PCMs determined by the framework presented the longest time-shift of energy consumption as the objective of this design framework.

CHAPTER 6 CONCLUSION AND RECOMMENDATION FOR FUTURE WORK

6.1 SUMMARY AND CONCLUSIONS:

As the interest for both supply and demand sides is to shave the load during peak hours, the application of TES is a promising way to store thermal energy during off-peak periods and utilize it during peak hours. Conventionally, a building envelope provides the thermal mass as the sensible heat storage, and its capacity can be enhanced by integrating PCM wallboards. Taking into account the advantages of latent heat over sensible heat, PCM wallboards provide larger storage capacity in a smaller mass and volume due to its high energy storage density. Therefore, it particularly offers a longer shift of energy consumption for space conditioning and a longer period of energy-free and thermally comfortable indoor environment. Eventually, selecting the most appropriate PCM wallboard (thickness, thermo-physical properties) was the main design goal. Accordingly, this dissertation focused on the development of a design framework to quantify and qualify the application of PCM wallboards in a building envelope.

To achieve this objective, the thermal behavior of a PCM wallboard was mathematically modeled, and the governing equations were non-dimensionalized. A numerical model was developed and validated using available measured data. Regarding the numerical modeling and dimensionless analysis:

- Adding a source term to the heat equation to govern the adsorption and release of latent heat is an alternative to using the apparent specific heat capacity in the enthalpy method.

- The assumption of the linear rate of change of the liquid fraction between the solidification temperature and melting temperature to characterize the rate of absorption and release of latent heat was validated. Consecutively, the model assuming the linear change of liquid fraction can simulate the dynamics thermal behavior of a PCM wallboard with high accuracy.

- While the design parameters of a PCM wallboard including its thermo-physical properties and thickness influence the thermal performance of the medium, all those parameters can be grouped in the following dimensionless parameters: Fo, Bi, Ste, Ψ, and Ψ_{pc}. These parameters were introduced as the effective dimensionless parameters and employed to conduct the parametric study in order to characterize the impact of the design parameters on the performance of the PCM wallboard as a latent heat TES to shift the load to off-peak hours.

The validated model was used to conduct the parametric study to identify the correlations between the dimensionless parameters and the performance of the PCM wallboard. These correlations were presented as the design framework for selecting and sizing an appropriate PCM wallboard. The performance of the wallboard was evaluated based on the strategy to have it fully melted at the end of charging time. When the PCM fully melts, it provides latent heat storage in its full capacity. Knowing the time length for the charging process, Fo_{fl} was presented as the indicator of design. Based on the parametric studies the following results were concluded:

- The changes of thermo-physical properties and the thickness of a PCM wallboard have no significant impact on its Fo_{fl}, as long as *Bi*, *Ste*, Ψ and Ψ_{pc} are kept constant. This conclusion is applied for different wallboards in the market with similar dimensionless parameters.

- *Fo* increases linearly by decreasing *Ste* when the remaining dimensionless parameters are kept constant. Lower magnitude of *Ste* means lower ratio of sensible over latent heat storage which infers domination of the latent over the sensible heat. Thus, a higher *Fo* of a fully melted PCM is expected for the lower magnitude of *Ste.*

- Logarithmic magnitude of *Fo* is a linear function of logarithmic magnitude of *Bi*, while the rest of dimensionless parameters remain constant. By increasing *Bi, Fo* decreases. The reduction in *Fo* is expected for higher magnitude of *Bi*. The wallboard with larger *Bi* has stronger resistance against conduction heat transfer. Therefore, the reduction in *Fo* as the ratio of heat conduction rate to the sensible thermal storage would be observed.

- Utilizing the correlations between Fo_{fl}, *Ste* and *Bi* in $\Psi_{ref.}$ and $\Psi_{pc,\ ref.}$ a base chart was developed. For the wallboards with Ψ and Ψ_{pc} equal to $\Psi_{ref.}$ and $\Psi_{pc,ref.}$, the base chart is employed to size the PCM wallboard for a building envelope.

- The developed chart is the extension of Heisler chart for materials that undergo the phase transition. As the y-intercepts of the correlations are the calculated *Fo*

for materials with $(Ste)^{-1}=0$, they were compared with the analytical calculation of *Fo* and were in good agreement.

- Similar to the analytical results of the Heisler Chart, *Fo* calculated by the design framework in $(Ste)^{-1}=0$ is only a function of the temperature and *Bi* of the wallboard.

- The precision of the base chart of the framework to calculate Fo_{fl} for a PCM wallboard with $\Psi_{ref.}$ and $\Psi_{pc,\ ref.}$ was evaluated for ten testing cases; the mean average error was less than 3%.

- The effect of the melting range and the fusion temperature were studied by characterizing the change of Fo_{fl} as a function of Ψ and Ψ_{pc}. As the essential elements in the proposed design framework, the correlations regarding these two dimensionless parameters are required to map the base chart from $\Psi_{ref.}$ and $\Psi_{pc,\ ref.}$ to another Ψ and Ψ_{pc}. This transformation helps take into account all the physical properties and characteristics of PCM wallboards and develop a universal chart.

- Based on the parametric study of the impact of Ψ, it was found that the log (Fo_{fl}) is a linear function of log (Ψ) with the slope of (-0.40), and it is independent of *Bi* and *Ste*. Therefore, Fo_{fl} calculated by the base chart for all PCM wallboards can be extrapolated to another Ψ than $\Psi_{ref.}$.

- The effect of fusion temperature and its relationship to the operational temperature were characterized by conducting a parametric study on the effect of Ψ_{pc} on Fo_{fl}. The conducted parametric study provided an auxiliary chart in the design framework to calculate the required slope to map the base chart to another Ψ_{pc} than $\Psi_{pc,\,ref.}$. The slope depends on the *Bi* and *Ste* of the PCM wallboard.

- As the base chart needs to be mapped to another Ψ and Ψ_{pc} than $\Psi_{ref.}$ and $\Psi_{pc,\,ref.}$, the precision of the mapped chart to calculate Fo_{fl} in PCM wallboard was evaluated for ten testing cases, and the mean average error was less than 5%.

- As an influential parameter in the design framework, the effect of room air temperature time lag was investigated on the time required to fully melt a PCM wallboard. The result of this stage of the framework is employed to correct the charging time of the medium. It was observed that the charging time is a linear function of Γ_{RTL} (room air temperature time lag). The precision of the corrected time was also evaluated for ten testing cases, and the mean average error was less than 1%.

- Accordingly, the set of a base chart for $\Psi_{ref.}$ and $\Psi_{pc,\,ref.}$, the calculated slopes and auxiliary chart to map the base chart for another Ψ and Ψ_{pc} created the design framework with which to select and size a PCM wallboard in order to shift the peak load to off-peak hours. The complete procedures and steps in the framework were presented as a flowchart in Figure 4.30.

The developed design framework was applied to select and size three PCM wallboards for an existing residential house. To characterize the thermal performance of the house furnished with a PCM wallboard, TRNSYS simulation software was used. The application of PCM wallboards was evaluated for both charging and discharging periods of the house at three outdoor conditions: cold, very cold, extremely cold. The simulation study over the charging period concluded:

- Although the thickness of the PCM wallboard is overestimated in the design framework due to the assumption of complete insulation on the outer side of the board, the wallboard with the thickness measured by the framework reaches an almost fully melted state at the end of the charging period.

- The error of the framework in calculating the appropriate thickness of the wallboard increases for colder outdoor conditions. While the wallboard was almost fully melted by the end of the charging period during the cold and very cold outdoor conditions, during extremely cold outdoor conditions, the wallboards yet needed time to become fully melted.

- The consumed energy for charging the PCM wallboards was almost the same with a trivial difference due to their differing *Bi*. In the case of wallboards with lower *Bi*, the energy required was higher as a result of lower resistance against heat losses through the building envelope. Also, the energy consumed to charge the PCM depends on the outdoor condition as the consumption was the highest during extremely cold weather conditions.

- The PCM wallboards need extra heating energy compared to the conventional gypsum board due to the fact that their phase transition occurs in the operational temperature of the room. Therefore, in the cases where PCM wallboards were utilized, the zone had higher heating energy consumption during the charging hours in comparison with the case where gypsum board was used.

For the discharge period, each PCM wallboard was simulated with varying magnitude of thickness using TRNSYS software, and they were compared based on the time-shift of the house load and heating energy consumption. As one of the selected thicknesses was the one calculated by the design framework, the effectiveness of the framework was evaluated by comparing the time shift of load of the design thickness and the other possible sizes of the PCM wallboard. The investigation over discharge period concluded:

- In aiming for the longest possible shift of load, a balance between *Bi* and the latent heat mass needs to be considered. Although having a thicker PCM wallboard provides a larger mass of latent heat storage, the possibility of having a fully melted and fully functional latent heat storage at the end of the charging period diminishes. Therefore, aiming for a fully melted wallboard is the best criterion for designing a PCM wallboard.

- The comparisons between different sizes of a PCM wallboard reflected that the size calculated using the developed design framework provides the longest load-shift for each selected wallboard.

- As the thickness was closer to the designed magnitude of the framework, the longer shift load was observed for all three simulated PCMs.

- Although the difference in the consumed heating energy for different sizes of the wallboard was trivial, the case regarding the wallboard with larger thickness had higher heating energy consumption during the charging time due to the larger mass of the medium to be melted and larger latent heat to be stored.

- As in the charging period, the difference in the heating energy demand for different sizes of the PCM wallboard was insignificant during the entire day. However, it was demonstrated that the lower energy demand corresponds to the case with the thicker wallboard with a lower U-value.

- The best performance was observed for PCM 3 as its total latent heat capacity is employed during charging and discharging periods although it had the lowest latent heat capacity among the simulated wallboards. Having the total melting range inside the operational temperature, PCM 3 was able to undergo a complete phase transition. Meanwhile the other two materials were not able to do so as their solidification temperature, T_s, was less than the lowest operational temperature. As a result, the materials which have their total melting range inside the operational temperature of the building are recommended.

- In comparing the PCM wallboards, the house with conventional gypsum board presented the least time-shift and the highest heating energy demand for an entire day. In the absence of latent heat storage in a conventional gypsum board, a

higher frequency of heater usage for space heating and a higher fluctuation of room temperature can be expected.

6.2 FUTURE WORKS RECOMMENDATIONS:

The recommended future research work on the developed design framework of PCM wallboards follows from the advancements and limitations of the present study:

- According to the dimensionless analysis conducted in this study, one of the effective dimensionless parameters was Ψ_{op} presenting the impact of the operational temperature on the performance of a PCM wallboard. Here, only one single control strategy was selected based on (Leduc et al., 2011). A parametric study on the effect of Ψ_{op} is required to improve the proposed design framework for other control strategies and operational temperatures.

- Based on the simulations carried out for the house, the framework overestimates the thickness of a PCM wallboard due to the assumption of complete insulation on the outer side of the wallboard. Specifically, in extremely cold outdoor conditions, the assumption negatively impacts the sizing and selection of the PCM wallboard. Therefore, the effects of the U-value of the other layers accompanying the PCM wallboard inside a wall section need to be investigated.

- Beside PCM wallboards charging passively, they can be employed as an active layer accompanied by auxiliary heaters, i.e., electrical heater or heating water flow which needs a similar framework for appropriately sizing them.

Additionally, the application of transparent wallboards, i.e., glass brick filled with PCM is investigated (Miranda Fuentes et al., 2013) and requires a related design framework to be sized for building applications.

CHAPTER 7 REFERENCES

Ahmad M., Bontemps A., Sallée H., Quenard D. (2006a) Thermal testing and numerical simulation of a prototype cell using light wallboards coupling vacuum isolation panels and phase change material. Energy and Buildings 38:673-681. DOI: http://dx.doi.org/10.1016/j.enbuild.2005.11.002.

Ahmad M., Bontemps A., Sallée H., Quenard D. (2006b) Experimental investigation and computer simulation of thermal behaviour of wallboards containing a phase change material. Energy and Buildings 38:357-366.

Alawadhi E.M. (2008) Thermal analysis of a building brick containing phase change material. Energy and Buildings 40:351-357. DOI: http://dx.doi.org/10.1016/j.enbuild.2007.03.001.

Aongya S. (2010) Contrôle du chauffage pour la gestion de la demande résidentielle, Rapport technique sur la création d'un modèle résidentiel fonctionnel. Laboratoire des technologies de l'énergie (LTE), Shawinigan.

Baetens R., Jelle B.P., Gustavsen A. (2010) Phase change materials for building applications: A state-of-the-art review. Energy and Buildings 42:1361-1368. DOI: http://dx.doi.org/10.1016/j.enbuild.2010.03.026.

Braun J.E., Lee K.H. (2006a) Assessment of Demand Limiting Using Building Thermal Mass in Small Commercial Buildings. ASHRAE Transactions 112:547-558.

Braun J.E., Lee K.H. (2006b) An Experimental Evaluation of Demand Limiting Using Building Thermal Mass in a Small Commercial Building. ASHRAE Transactions 112:559-571.

Cabeza L.F., Castellón C., Nogués M., Medrano M., Leppers R., Zubillaga O. (2007) Use of microencapsulated PCM in concrete walls for energy savings. Energy and Buildings 39:113-119.

Carbonari A., De Grassi M., Di Perna C., Principi P. (2006) Numerical and experimental analyses of PCM containing sandwich panels for prefabricated walls. Energy and Buildings 38:472-483. DOI: http://dx.doi.org/10.1016/j.enbuild.2005.08.007.

Castell A., Martorell I., Medrano M., Pérez G., Cabeza L.F. (2010) Experimental study of using PCM in brick constructive solutions for passive cooling. Energy and Buildings 42:534-540.

Cengel Y.A., Ghajar A.J. (2011) Heat and mass transfer; Fundamentals and applications. The McGraw-Hill Companies, Inc., New York, NY 4th edition.

Cerón I., Neila J., Khayet M. (2011) Experimental tile with phase change materials (PCM) for building use. Energy and Buildings 43:1869-1874.

Darkwa K., Kim J.S. (2005) Dynamics of energy storage in phase change drywall systems. International Journal of Energy Research 29:335-343. DOI: 10.1002/er.1062.

Darkwa K., O'Callaghan P.W. (2006) Simulation of phase change drywalls in a passive solar building. Applied Thermal Engineering 26:853-858. DOI: http://dx.doi.org/10.1016/j.applthermaleng.2005.10.007.

Diaconu B.M., Cruceru M. (2010) Novel concept of composite phase change material wall system for year-round thermal energy savings. Energy and Buildings 42:1759-1772.

Dutil Y., Rousse D.R., Salah N.B., Lassue S., Zalewski L. (2011) A review on phase-change materials: Mathematical modeling and simulations. Renewable and Sustainable Energy Reviews 15:112-130.

El-Sawi A., Haghighat F., Akbari H. (2014) Assessing long-term performance of centralized thermal energy storage system. Applied Thermal Engineering 62:313-321. DOI: http://dx.doi.org/10.1016/j.applthermaleng.2013.09.047.

Ettouney H., El-Dessouky H., Al-Kandari E. (2004) Heat Transfer Characteristics during Melting and Solidification of Phase Change Energy Storage Process. Industrial & Engineering Chemistry Research 43:5350-5357. DOI: 10.1021/ie030495b.

Ettouney H., El-Dessouky H., Al-Ali A. (2005) Heat Transfer During Phase Change of Paraffin Wax Stored in Spherical Shells. Journal of Solar Energy Engineering 127:357-365.

Farid M., Chen W.J. (2001) Underfloor heating with latent heat storage. Proceedings of the Institution of Mechanical Engineers, Part A: Journal of Power and Energy 215(A5):601-609.

Farid M.M., Chen X.D. (1999) Domestic electrical space heating with heat storage. Proceedings of the Institution of Mechanical Engineers, Part A: Journal of Power and Energy 213(A2):83-92.

Farid M.M., Khudhair A.M., Razack S.A.K., Al-Hallaj S. (2004) A review on phase change energy storage: materials and applications. Energy Conversion and Management 45:1597-1615.

Feldman D., Banu D., Hawes D., Ghanbari E. (1991) Obtaining an energy storing building material by direct incorporation of an organic phase change material in gypsum wallboard. Solar Energy Materials 22:231-242.

Gwerder M., Lehmann B., Tödtli J., Dorer V., Renggli F. (2008) Control of thermally-activated building systems (TABS). Applied Energy 85:565-581. DOI: http://dx.doi.org/10.1016/j.apenergy.2007.08.001.

Halford C.K., Boehm R.F. (2007) Modeling of phase change material peak load shifting. Energy and Buildings 39:298-305.

Hawes D.W. (1991) Latent heat storage in concrete. Doctoral Dissertation Concordia University, Montreal, Quebec, Canada.

Hawlader M.N.A., Uddin M.S., Khin M.M. (2003) Microencapsulated PCM thermal-energy storage system. Applied Energy 74:195-202.

Heim D. (2010) Isothermal storage of solar energy in building construction. Renewable Energy 35:788-796. DOI: http://dx.doi.org/10.1016/j.renene.2009.09.005.

Heim D., Clarke J.A. (2004) Numerical modelling and thermal simulation of PCM-gypsum composites with ESP-r. Energy and Buildings 36:795-805.

Herter K., McAuliffe P., Rosenfeld A. (2007) An exploratory analysis of California residential customer response to critical peak pricing of electricity. Energy 32:25-34. DOI: http://dx.doi.org/10.1016/j.energy.2006.01.014.

HydroQuebec. (2007) Demande R-3648-2007. Hydro Quebec Distribution-1.

HydroQuebec. (2011) Demande R-3776-2011. Hydro Quebec Distribution-2.

IEA ANNEX 23. (2013) Apply energy storage in ultra-low energy building. Final report, Edited by F.Haghighat.

IEA ANNEX 44. (2009) Expert Guide: Part 1 Responsive Building Concepts. Per Heiselberg, Aalborg University, Denmark.

Jokisalo J., Lamberg P., Siren K. (2000) Thermal simulation of PCM structures with TRNSYS. 8th International Conference on Thermal Energy Storage, Stuttgart, Germany.

Kaasinen H. (1992) The absorption of phase change substances into commonly used building materials. Solar Energy Materials and Solar Cells 27:173-179.

Khudhair A.M., Farid M.M. (2004) A review on energy conservation in building applications with thermal storage by latent heat using phase change materials. Energy Conversion and Management 45:263-275.

Kondo T., Ibamoto T., Yuuji T. (2000) Research on thermal storage of PCM wallboard. 10, Workshop for International Energy Agency, Annex (Japan).

Koschenz M., Lehmann B. (2004) Development of a thermally activated ceiling panel with PCM for application in lightweight and retrofitted buildings. Energy and Buildings 36:567-578.

Kuznik F., Virgone J. (2009a) Experimental investigation of wallboard containing phase change material: Data for validation of numerical modeling. Energy and Buildings 41:561-570.

Kuznik F., Virgone J. (2009b) Experimental assessment of a phase change material for wall building use. Applied Energy 86:2038-2046.

Kuznik F., Virgone J., Roux J.-J. (2008a) Energetic efficiency of room wall containing PCM wallboard: A full-scale experimental investigation. Energy and Buildings 40:148-156.

Kuznik F., Virgone J., Noel J. (2008b) Optimization of a phase change material wallboard for building use. Applied Thermal Engineering 28:1291-1298.

Kuznik F., Virgone J., Johannes K. (2010) Development and validation of a new TRNSYS type for the simulation of external building walls containing PCM. Energy and Buildings 42:1004-1009.

Kuznik F., David D., Johannes K., Roux J.-J. (2011) A review on phase change materials integrated in building walls. Renewable and Sustainable Energy Reviews 15:379-391.

Leduc M.-A., Daoud A., Celyn L.B. (2011) Developing winter residential demand response strategies forelectric space heating. Proceedings of Building Simulation 2011 12th conference of international building performance simulation association, Sydney, 14-16 November.

Lee K.-H., Braun J.E. (2008a) Evaluation of methods for determining demand-limiting setpoint trajectories in buildings using short-term measurements. Building and Environment 43:1769-1783.

Lee K.-h., Braun J.E. (2008b) Development of methods for determining demand-limiting setpoint trajectories in buildings using short-term measurements. Building and Environment 43:1755-1768.

Lehmann B., Dorer V., Koschenz M. (2007) Application range of thermally activated building systems tabs. Energy and Buildings 39:593-598. DOI: http://dx.doi.org/10.1016/j.enbuild.2006.09.009.

Lin K., Zhang Y., Xu X., Di H., Yang R., Qin P. (2004) Modeling and simulation of under-floor electric heating system with shape-stabilized PCM plates. Building and Environment 39:1427-1434.

Lin K., Zhang Y., Xu X., Di H., Yang R., Qin P. (2005) Experimental study of under-floor electric heating system with shape-stabilized PCM plates. Energy and Buildings 37:215-220.

Liu S., Henze G.P. (2006a) Experimental analysis of simulated reinforcement learning control for active and passive building thermal storage inventory: Part 2: Results and analysis. Energy and Buildings 38:148-161.

Liu S., Henze G.P. (2006b) Experimental analysis of simulated reinforcement learning control for active and passive building thermal storage inventory: Part 1. Theoretical foundation. Energy and Buildings 38:142-147.

Marín J.M., Zalba B., Cabeza L.F., Mehling H. (2003) Determination of enthalpy–temperature curves of phase change materials with the temperature-history method: improvement to temperature dependent properties. Measurement Science and Technology 14:184.

Mathieu-Potvin F., Gosselin L. (2009) Thermal shielding of multilayer walls with phase change materials under different transient boundary conditions. International Journal of Thermal Sciences 48:1707-1717. DOI: http://dx.doi.org/10.1016/j.ijthermalsci.2009.01.010.

Matlab. (2010) R2010b Math Work Documentation. Math Works Inc.

Mehling H., Cabeza L.F. (2008) Heat and cold storage with PCM; An up to date introduction into basics and applications. Springer-Verlag Berlin Heidelberg.

Miranda Fuentes J., Johannes K., Kuznik F., Cosnier M., Virgone J. (2013) Melting with convection and radiation in a participating phase change material. Applied Energy 109:454-461. DOI: http://dx.doi.org/10.1016/j.apenergy.2012.11.031.

Mirzaei P.A., Haghighat F. (2012) Modeling of phase change materials for applications in whole building simulation. Renewable and Sustainable Energy Reviews 16:5355-5362. DOI: http://dx.doi.org/10.1016/j.rser.2012.04.053.

Natural Resources CANADA. (2011) Energy Efficiency Trends in Canada 1990 to 2009. Cat. No. M141-1/2009E-PDF (Online), Online Available: HTTP://OEE.NRCAN.GC.CA/CORPORATE/STATISTICS/PUBLICATIONS ISSN 1926-8254.

Neeper D.A. (2000) Thermal dynamics of wallboard with latent heat storage. Solar Energy 68:393-403.

Nkwetta D.N., Vouillamoz P.-E., Haghighat F., El-Mankibi M., Moreau A., Daoud A. (2014) Impact of phase change materials types and positioning on hot water tank thermal performance: Using measured water demand profile. Applied Thermal

Engineering 67:460-468. DOI: http://dx.doi.org/10.1016/j.applthermaleng.2014.03.051.

Pasupathy A., Velraj R. (2008) Effect of double layer phase change material in building roof for year round thermal management. Energy and Buildings 40:193-203.

Pasupathy A., Athanasius L., Velraj R., Seeniraj R.V. (2008) Experimental investigation and numerical simulation analysis on the thermal performance of a building roof incorporating phase change material (PCM) for thermal management. Applied Thermal Engineering 28:556-565.

Peng X., Haves P. (2006) Case Study of Demand Shifting with Thermal Mass in Two Large Commercial Buildings. ASHRAE Transactions 112:572-580.

Pérez-Lombard L., Ortiz J., Pout C. (2008) A review on buildings energy consumption information. Energy and Buildings 40:394-398. DOI: http://dx.doi.org/10.1016/j.enbuild.2007.03.007.

Russell M.B., Surendran P.N. (2001) Influence of active heat sinks on fabric thermal storage in building mass. Applied Energy 70:17-33. DOI: http://dx.doi.org/10.1016/S0306-2619(01)00023-X.

Schossig P., Henning H.M., Gschwander S., Haussmann T. (2005) Micro-encapsulated phase-change materials integrated into construction materials. Solar Energy Materials and Solar Cells 89:297-306.

Schranzhofer H., Heinz A., Puschnig P., Streicher W. (2006) Validation of a TRNSYS simulation model for PCM energy storages and PCM wall construction elements. Ecostock Conference, 31th May – 2nd June 2006, Pomona, USA.

Shilei L., Guohui F., Neng Z., Li D. (2007) Experimental study and evaluation of latent heat storage in phase change materials wallboards. Energy and Buildings 39:1088-1091.

Verma P., Varun, Singal S.K. (2008) Review of mathematical modeling on latent heat thermal energy storage systems using phase-change material. Renewable and Sustainable Energy Reviews 12:999-1031.

Voelker C., Kornadt O., Ostry M. (2008) Temperature reduction due to the application of phase change materials. Energy and Buildings 40:937-944. DOI: http://dx.doi.org/10.1016/j.enbuild.2007.07.008.

Weinläder H., Beck A., Fricke J. (2005) PCM-facade-panel for daylighting and room heating. Solar Energy 78:177-186. DOI: http://dx.doi.org/10.1016/j.solener.2004.04.013.

Xu X., Zhang Y., Lin K., Di H., Yang R. (2005) Modeling and simulation on the thermal performance of shape-stabilized phase change material floor used in passive solar buildings. Energy and Buildings 37:1084-1091.

Yang L., Li Y. (2008) Cooling load reduction by using thermal mass and night ventilation. Energy and Buildings 40:2052-2058. DOI: http://dx.doi.org/10.1016/j.enbuild.2008.05.014.

Zalba B., Marín J.M., Cabeza L.F., Mehling H. (2003) Review on thermal energy storage with phase change: materials, heat transfer analysis and applications. Applied Thermal Engineering 23:251-283.

Zhang Y., Zhou G., Lin K., Zhang Q., Di H. (2007) Application of latent heat thermal energy storage in buildings: State-of-the-art and outlook. Building and Environment 42:2197-2209.

Zhou G., Zhang Y., Wang X., Lin K., Xiao W. (2007) An assessment of mixed type PCM-gypsum and shape-stabilized PCM plates in a building for passive solar heating. Solar Energy 81:1351-1360.